**Mariana Côrte-Real Marques Pedro**

Licenciada em Engenharia Electrotécnica e de Computadores

# Modelling of Shading Effects in Photovoltaic Optimization

Dissertação para obtenção do Grau de
Mestre em Engenharia Electrotécnica e de Computadores

Orientador: João Murta Pina, Professor Doutor, FCT-UNL

| Júri: | |
|---|---|
| Presidente: | Prof. Doutor João Rosas |
| Arguente: | Prof. Doutor Pedro Pereira |
| Vogal: | Prof. Doutor João Murta Pina |

FACULDADE DE
CIÊNCIAS E TECNOLOGIA
UNIVERSIDADE NOVA DE LISBOA

**Março, 2016**

*To my family*

# Acknowledgements

First of all, I would like to express my gratitude to my supervisor, Professor João Murta Pina, for all his support and availability during the elaboration of this dissertation. His opinions provided me with direction, motivating me to pursue the best possible outcome.

I would also like to thank the Faculty of Sciences and Technology of Nova University of Lisbon, in particular to the Department of Electrical Engineering, for providing me with the relevant conditions (equipment, infrastructure, etc.) necessary to develop the work that lead to this dissertation. I would also like to take the chance to thank all my lecturers from whom I learned and ultimately grew during the past years.

I would also like to thank my family for the support they provided through my entire life. In particular, I must mention my father who patiently provided me with guidance on how to structure my thought and my writing in order to produce an important document as this one.

Last, but not least, I would like to thank my colleges, most of whom became friends, for joining me during this journey. I would also like to thank all of my close friends who always provided support and encouragement, pushing me to believe myself.

# Abstract

The use of photovoltaic systems as a source of power supply has entered a maturity phase. Nevertheless, there is still some room for improvement in certain areas, such as the accurate estimation of power output production during the project stage.

There are different types of shading with distinct effects on photovoltaic energy production. These differences need to be taken into account when projecting a PV installation. The ECEN2026 is a PV module model, that enables the simulation of any existent solar panel, according to a set of parameters, which can be compared with real world installations, providing a mean to study the feasibility of hypothetical installation.

The implementation and simulation of this model generates several outputs. In the presented context, an expression can be obtained, which correlates the annual power production with the severity of shading and the number of shaded panels. It also allows the plot of the IV and PV characteristic curves, aiming to optimize the maximum output power and, using different shading situations, to validate the model. R

The model validation is possible due to the comparison between the obtained simulation results and practical implementations. One limitation of this model is the impossibility to simulate partly shaded modules.

**Keywords:** Shading Influence; ECEN2026 Model; Modelling of Shading Effects; PV Optimization; Sun Path Chart Model; PV Installation Simulation; Energy Production Estimation ...

# RESUMO

A utilização de sistemas fotovoltaicos como fonte de fornecimento de energia encontra-se atualmente numa fase desenvolvida. No entanto há espaço para melhoria em determinadas áreas, como a precisão na estimativa de potência produzida aquando do projeto de uma instalação.

Existem diferentes tipos de sombreamento que afetam de diferente forma a produção de energia fotovoltaica. Estes devem ser tidos em conta na fase de projeto. O ECEN2026 é um modelo de módulo fotovoltaico que permite a simulação de qualquer painel solar existente, com base num grupo de parâmetros, que pode ser comparado com instalações reais, fornecendo uma forma de estudar a viabilidade de instalações hipotéticos.

A implementação e simulação deste modelo gera vários resultados possíveis. Neste contexto, uma expressão é gerada, correlacionando a produção energética anual com a severidade de sombreamento e número de módulos sombreados. Este permite também o desenho de curvas corrente-tensão e potência-tensão, com o objetivo de otimizar em tempo real a potência produzida e, usando diferentes situações de sombreamento, validar o modelo em si.

A validação do modelo é possível devido à comparação entre os resultados de simulação obtidos e implementações práticas. Uma limitação do mesmo é a impossibilidade de simular painéis parcialmente sombreados.

**Palavras-chave:** Influência de Sombreamentos; Modelo ECEN2026; Modelização de Efeitos de Sombreamento; Otimização Fotovoltaica; Diagrama do Percurso Solar; Simulação de Instalações Fotovoltaicas; Estimativa de Produção de Energia ...

# CONTENTS

**Contents** xi

**List of Figures** xiii

**List of Tables** xvii

**1 Introduction** 1
- 1.1 Motivation . . . 1
- 1.2 Objectives . . . 2
- 1.3 Contribution to the Domain . . . 2
- 1.4 Structure of the Thesis . . . 3

**2 State of the Art** 5
- 2.1 Shading Influence on Photovoltaic Systems . . . 5
  - 2.1.1 Types of Shading Effects on the Photovoltaic System . . . 5
  - 2.1.2 Effects of Shading on Photovoltaic Systems . . . 6
- 2.2 Modelling Solar Systems . . . 10
  - 2.2.1 PN Juntion . . . 10
  - 2.2.2 Mathematical Model and Equivalent Circuit of a PV Cell . . . 11
- 2.3 Strategies to Optimize the Shading Effect on Solar Panels . . . 16
  - 2.3.1 Evolution in Optimization in the Past Decades . . . 16
  - 2.3.2 Use of Diodes to Compensate the Shading Effect on Solar Panels . . . 22
- 2.4 Methods for Calculating the Shade Factor for a Photovoltaic System . . . 24
  - 2.4.1 Calculations Based on Observation . . . 25
  - 2.4.2 Computer Aided Calculations and Software . . . 28
  - 2.4.3 Shading Simulation Software Review . . . 31

**3 Implementation Simulations in Simulink** 37
- 3.1 Introduction to the ECEN2026 Model . . . 37
  - 3.1.1 Specifications of the Model . . . 38
  - 3.1.2 Simulink Implementation . . . 38
- 3.2 Simulations . . . 41
  - 3.2.1 Designing and Testing Theoretic Photovoltaic Installations . . . 41

3.2.2 Simulation and Study of IV and PV Characteristic Curves for Different Cases of Shading . . . 43
3.2.3 Development of the Power Output Expression of a Specific PV Installation According to Shade Variation . . . 45
3.2.4 Determination of the Annual Energy Production of a Single PV Module Assuming a Previously Defined Shade . . . 50
3.2.5 Comparison between the impact of a calculated Shade Factor on the production of an installation with the one simulated . . . 57

**4 Experimental Results**
**Testing Shadings on Photovoltaic Panels** **67**
4.1 Test of Isolated Modules . . . 67
4.1.1 Evaluation of IV and PV Curves on Photovoltaic Modules . . . 67
4.1.2 Experiment 1 . . . 69
4.1.3 Experiment 2 . . . 74
4.1.4 Remarks on the Outputs of Experiments 1 and 2 . . . 76
4.2 Test of Grid-connected Modules . . . 77
4.2.1 Study of the Power Production on a two Module Installation . . . 77
4.2.2 Experiment 3 - No Shade Cast on the Installation: . . . 81
4.2.3 Experiment 4 - A Single Module With Soft Shading cast upon it: . . . 82
4.2.4 Experiment 5 - One Module Partly Soft Shaded: . . . 84
4.2.5 Experiment 6 - One Module Partly Hard Shaded: . . . 85
4.2.6 Remarks on the Outputs of Experiments 3 to 6 . . . 86

**5 Conclusions and Future Work** **87**
5.1 Conclusions . . . 87
5.2 Future Work . . . 89

**Bibliography** **91**

**A Appendix** **97**

# List of Figures


2.1 Cell hard shading examples. Source: Sargosis Solar & Electric, 2014. . . . . 6
2.2 Hot spot heating. Source: Honsberg and Bowden, 2011. . . . . 7
2.3 Effects on IV characteristic curves on solar systems taking into account the type of shade suffered. Source: Sargosis Solar & Electric, 2014. . . . . 8
2.4 Effects on PV characteristic curves on solar systems taking into account the type of shade suffered. Source: Sargosis Solar & Electric, 2014. . . . . 10
2.5 PN junction of a solar cell. Source: Masters, 2004. . . . . 11
2.6 Circuit linking a solar cell to a load. Source: Masters, 2004. . . . . 11
2.7 Equivalent circuit of a PV cell. Source: Masters, 2004. . . . . 12
2.8 PV cell model examples drawn using a circuit simulator software. . . . . 12
2.9 Single-diode model - equivalent circuit of a PV cell. Source: Marnoto, Sopian, Daud, Algoul, and Zaharim, 2007. . . . . 13
2.10 Short-circuit current and open-circuit voltage. Source: Masters, 2004. . . . . 15
2.11 Photovoltaic IV relationship for "dark" (no sunlight) and "light" (illuminated cell). Source: Masters, 2004. . . . . 16
2.12 Conventional grid-tie PV system with central inverter. Source: Tsao, 2010. . . 17
2.13 Micro-inverters application and power saving example. Source: Canterbury Power Solutions, 2012. . . . . 18
2.14 Power optimizers installation examples. Source: Tsao, 2010. . . . . 19
2.15 Solar dual-axis tracker application example. Source: Queensland Windmill & Solar, 2008. . . . . 20
2.16 Example of installation without backtracking technology. Source: Sistemas Digitales de Control 2002, S.L., 2014. . . . . 21
2.17 Installation using backtracking technology. Source: Sistemas Digitales de Control 2002, S.L., 2014. . . . . 21
2.18 Bypass and blocking diode application. Source: Storr, 2014. . . . . 23
2.19 Sun path diagram of shading from objects over 10 m away. Source: (MCS), 2012. 26
2.20 Sun path diagram of shading from objects within 10 m of distance from the away. Source: (MCS), 2012. . . . . 27
2.21 3D editing tool on PVSYST. Source: *Solar PV System Shading Calculation with PVSYST - YouTube* 2009. . . . . 33

2.22 Module positioning analysis on PVCad. Source: *Controlling software for photovoltaics - PVCAD* 2015. . . . . 33
2.23 Archelios report on shadow analysis. Source: *Archelios PRO*. . . . . 34
2.24 Simulation with power optimizers in 3D mode. Source: Zipp, 2014. . . . . 35
2.25 Solmetric Suneye solar reading. Source: Home Power Inc., 2015. . . . . 35
2.26 Easy solar app - PV designing tool. Source: Zipp, 2014. . . . . 36

3.1 Equivalent circuit of a PV cell used on the ECEN2026 model. Source: Marnoto, Sopian, Daud, Algoul, and Zaharim, 2007. . . . . 38
3.2 Current and voltage module inputs designed using Simulink . . . . . 38
3.3 Parameters of the PV current and voltage input modules designed. . . . . 39
3.4 Parameters of the PV current-input module mask designed. . . . . 40
3.5 Voltage-input module undermask subsystem design. . . . . 40
3.6 PV installation with seven modules designed using Simulink. . . . . 42
3.7 PV installation with a single module designed using Simulink. . . . . 43
3.8 PV installation with two PV modules designed using Simulink. . . . . 43
3.9 Case 1: Simulink XY plot of the IV and PV curves for a PV installation with two modules. . . . . 44
3.10 Case 2: Simulink XY plot of the IV and PV curves for a PV installation with seven modules. . . . . 44
3.11 Explanatory diagram of the process used on scrip A.2 (steps 1 to 4). . . . . 46
3.12 Correlation between maximum power produced, number of shaded modules and shade severity plotted using MATLAB. . . . . 47
3.13 Fit of the correlation between maximum power produced, number of shaded modules and shade severity plotted using MATLAB'c fitting tool - Cftoll. . . 48
3.14 Sun path chart of Lisbon 2015 designed using *University of Oregon Sun Path Chart Program* available online. Source: University of Oregon, Solar Radiation Monitoring Laboratory, 2007. . . . . 52
3.15 Sun path chart of Lisbon 2015 with shade cast by *object 1*. . . . . 53
3.16 Parameters of the PV voltage-input module mask designed. Source: University of Oregon, Solar Radiation Monitoring Laboratory, 2007. . . . . 53
3.17 Power production from January for diffuse or zero irradiance cast upon the module when shaded by *object 1*. . . . . 54
3.18 Monthly power production estimation without shade - simulated using Simulink and plotted using MATLAB. . . . . 55
3.19 Monthly power production estimation considering diffuse or zero irradiation is input on the installation when shaded by *object 1*. . . . . 55
3.20 Comparison between Images (a) and (b) to design a new sun path diagram with 84 segments, essential to the calculus of the SF. . . . . 58
3.21 New solar path chart created by comparison of figures 3.20a and 3.20b. . . . . 59
3.22 SF calculus of *Object 1* using the solar path chart developed for this propose. . 60

3.23 Display of *Object 2* on the sun path chart. . . . . 61
3.24 Display of *Object 3* on the sun path chart. . . . . 62
3.25 SF calculus of *Object 2* using the solar path chart developed for this propose. . 63
3.26 SF calculus of *Object 3* using the solar path chart developed for this propose. . 64

4.1 Diagram of the circuit composed of a photovoltaic module, designed using Simulink. . . . . 69
4.2 IV characteristic curve plotted using the values input to an Excel spreadsheet. 70
4.3 IV curve family for module, for a 25°C cell temperature, as a function of irradiace. 71
4.4 IV Curve family for Module HIP-215NHE5 for a 1000 W/m$^2$ irradiance as a function of temperature. . . . . 71
4.5 PV characteristic curve resulting from the values input to the Excel spreadsheet. 72
4.6 Nominal electrical data for the SANYO HIP-xxxNHE5 module family (relevant data for the tested model contained in the "215" column). . . . . 73
4.7 IV characteristic curve plotted using the values input to an Excel spreadsheet. 75
4.8 PV characteristic curve plotted using the values input to an Excel spreadsheet. 75
4.9 Shaded experiment 3 - Two module installation configuration with Micro-inverter. 77
4.10 Illustrations of shaded cases B to D, where different shading situations are simulated. . . . . 78
4.11 Diagram of the setup used to gather information from the installation to the APS EMA. Source: CivicSolar, 2015 . . . . . 79
4.12 Layout of experiment 3 - Installation with two PV panels and a micro-inverter with no shade cast upon them. . . . . 81
4.13 EMA real-time data screen production for experiment 3. . . . . 81
4.14 Simulink simulation of experience 3. . . . . 82
4.15 Layout of experiment 4 - Photovoltaic installation with a translucent fabric casting soft shade on totality of one module surface. . . . . 83
4.16 EMA real-time data screen production for experiment 4. . . . . 83
4.17 Layout of experiment 5 - Installation with a translucent fabric casting soft shade on half of the surface of one module. . . . . 84
4.18 EMA real-time data screen production for experiment 5. . . . . 84
4.19 Layout of experiment 6 - Installation with an opaque fabric casting soft shade on half of the surface of a module. . . . . 85
4.20 EMA real-time data screen production for experiment 6. . . . . 85

# List of Tables


2.1 Examples of photovoltaic software per category. . . . . 30
2.2 Shading software chart. . . . . 32

3.1 Data gathered using PGVIS-CMSAF database report for a daily profile of the month June for the location Lisbon. . . . . 51
3.2 Interval of solar time where the installation is suffering from the presence of shade from object 2. . . . . 54
3.3 Power and energy production for simulations 1, 2 and 3 . . . . . 57
3.4 Percentage of energy loss due to shading for simulations 2 and 3. . . . . 60
3.5 Interval of solar time where the installation is suffering for the presence of shade from object 3. . . . . 62
3.6 Interval of solar time where the installation is suffering for the presence of shade. 62
3.7 Simulation results. . . . . 63
3.8 Power and energy production for simulations 1, 2 and 3 . . . . . 64

4.1 External Conditions for Experiment 1. . . . . 69
4.2 Experiment 1 - Results obtained. . . . . 72
4.3 Realized adjustments for the obtained maximum power current and voltage values. . . . . 74
4.4 External conditions for experiment 2. . . . . 74
4.5 Experiment 2 - Results obtained. . . . . 76
4.6 External conditions for experiment 1. . . . . 80
4.7 Experiment 3 - Simulink simulation input and output values. . . . . 82
4.8 Experiment 4 - Simulink simulation input and output values. . . . . 83

# LISTINGS

A.1 Initialization code for PV module in Simulink. . . . . 97
A.2 MATLAB script in-charged of running Simulink seven module design. . . 98
A.3 MATLAB script in-charged of running Simulink seven module design. . . 100

CHAPTER 1

# INTRODUCTION

In this chapter a brief summary of the contents of the thesis is presented. It is divided in four sections including, the motivation to study this particular field of renewable energy, the main objectives of the work held, its contribution to the domain and a short summary of the thesis structure.

## 1.1 Motivation

In the past decades the global concern with energetic sustainability experienced a rapid growth due to the social awareness of a few very important aspects such as the increasing global demand for energy and the reduction of damage to the environment (BBC - GCSE Bitesize, 2014). This brought public enthusiasm for an environmentally benign energy source and with it many favourable conditions to the adoption of the solar energy as a general source of energy. Conditions relevant for this matter were the improvement of technology, lowering of the cost, creation of government subsidies, standardized interconnection to the electric utility grid, etc., conditions which, prompted this photovoltaic industry rapid growth (Sera and Baghzouz, 2008).

The main motivation to this dissertation is therefore to improve the estimation appraised by PV planners, providing solar energy possible adherents all over the world with the chance to have a more reliable generation prevision when designing photovoltaic installations.

## 1.2 Objectives

The main objectives of the dissertation can be summarized in the following topics:

- Survey of the different shading styles or situations and their effects on photovoltaic energy production;
- Validate the chosen model trough comparison with practical experiments;
- Complement the facts stated in the state of the art with experiments;
- Modelling of shading effects for photovoltaic optimization;
- Development of an expression that estimates power production according to the presence of shading;

## 1.3 Contribution to the Domain

The work performed in this dissertation produced new tools that can be used in the planning phase of photovoltaic installations.

One contribution to the domain is the validation, through the comparison of results, of the ECEN2026 Model[1], developed by the Electrical & Computer Energy Engineering department of the University of Colorado (*ECEN2060 Renewable Sources and Efficient Electrical Energy Systems*) and allows a reliable estimate of output power of a PV installation during the project phase, although it requires a working knowledge of the Simulink software.

Another contribution to the renewable energies domain is the development of a generic expression that correlates the number of shaded modules and severity of the shading, with the power production value for a particular photovoltaic installation. This equation, if generalized for variables such as the number of panels in the installation and the type of connection, can be used as a general purpose method to evaluate the losses due to shading and also to estimate power production under different shading conditions.

At last, another interesting development contributing to the domain is the development of a sun path chart, used to obtain Shade Factor values based on solar time instead of solar elevation as on the existing general one, presented in *Guide to the Installation of Photovoltaic Systems*[2] Manual. This chart allows users to calculate more easily the losses due to shading resulting from the presence of different objects in the vicinity of a PV installation. On this matter, there are also conclusions drawn through simulation analysis about the segments sizing accordingly to their position on the chart.

[1]This tool is available on ECEN2026 website: `http://ecee.colorado.edu/~ecen2060/matlab.html`.

[2]This methodology is provided by the British certification entity Microgeneration Certification Scheme(MCS) Source: (MCS), 2012.

## 1.4 Structure of the Thesis

This dissertation is organized in the following five chapters:

- **Chapter 1 - Introduction** sets the motivation, objectives and contribution to the domain provided by this work;
- **Chapter 2 - State of the Art** presents the fundamental concepts and state of the art of the understating of shading influence on photovoltaic systems;
- **Chapter 3 - Implementation** covers the theoretical implementations performed using Matlab to process data generated with a the help of a Simulink Block Model;
- **Chapter 4 - Experimental Results** describes the practical implementations performed using different types of photovoltaic panels, sets a comparison between theoretical simulation outputs and measured values and performs an analysis on the obtained data;
- **Chapter 5 - Conclusions and Future Work** presents the main conclusions of this work, as well as directions for future developments related to the effects of shading on solar modules.

CHAPTER 2

# STATE OF THE ART

In this chapter, a framework of the thesis theme is presented, addressing important topics such as the shading influence on photovoltaic systems according to the type of shading experienced, the mathematical model used to study photovoltaic (PV) cells, the known strategies to optimize solar systems, the methods for calculating the shading suffered by the solar models and the existing software used nowadays for modelling shading effects.

## 2.1 Shading Influence on Photovoltaic Systems

### 2.1.1 Types of Shading Effects on the Photovoltaic System

When a shadow from any object is cast on a solar module, the photovoltaic system in question is considered to be under the influence of shading.

Shading in solar modules interferes with the IV characteristic curve[1] of the system causing losses in performance. If these losses are not taken into account, the power output of a photovoltaic system is often severely lower than expected (Quaschning and Hanitsch, 1995).

In general, shades that affect photovoltaic systems can be categorized into soft and hard, according to the shade characteristics and the amount of light blocked.

A soft shade occurs when the intensity of solar irradiance on the modules is reduced due to dust, haze or smog and causes the current flow to drop proportionally to the intensity of the light. This affects the IV curve of the system because there is a decrease in irradiance and consequently less current will flow from the module.

[1] IV characteristic curve, short for current-voltage characteristic curve, is a graphical curve which shows the relationship between the current generated by a solar module and its output voltage. It is usually used to obtain information regarding the input or output operation ranges of a device.

This object of study of this project is mainly focused on hard shading. A shade can be considered a hard shade when it is provoked by an object that blocks the light, completely obscuring the affected area. See figure 2.1 for examples of hard shading in cells.

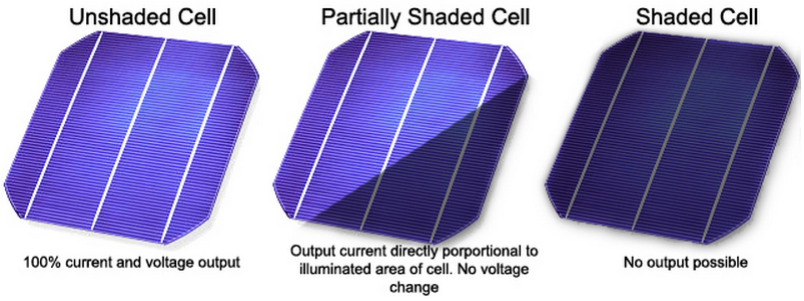


Figure 2.1: Cell hard shading examples. Source: Sargosis Solar & Electric, 2014.

As we can see in figure 2.1, unshaded cells are in the optimized situation for current and voltage output. In a partially shaded cell, only a portion of the area of the cell is affected. For example if a leaf lays on a solar module or if the moving shade from a building is cast on part of a module. This type of shading leads to a current production drop, since only the irradiated percentage of the cell is producing current, although there is no impact on the voltage, that remains constant. Finally, totally hard shaded cells have absolutely no current production.

### 2.1.2 Effects of Shading on Photovoltaic Systems

In cases of partially shaded modules, the chances of damage of the cells are much higher since this can lead to hot-spot heating. In a solar panel, several solar cells are connected in series, called strings, in order to increase the overall output voltage. Hot-spot heating occurs when within a string, the operating current of the module exceeds the short circuit current of at least one shaded, low-current-producing cell.

A string of 10 cells is presented in figure 2.2, where one of them is shaded. If the string current approaches the short-circuit current of the shaded cell, then the overall current becomes limited by this cell. In this situation, the extra current produced by the unshaded cells is forward biased along the string, reverse biasing the shaded cell (Hong Yang, He Wang, and Minqiang Wang, 2012; Honsberg and Bowden, 2011).

The more cells in the string, the higher the reverse current bias across the shaded cell and the higher the power dissipation in it. These factors combined with the fact that the affected area of the string is small, result in the increase of local surface temperature or, as mentioned before, hot-spot heating. The effects of this overheating process are usually, glass cracking, melting of solder or degradation of the solar cell (Honsberg and Bowden, 2011).

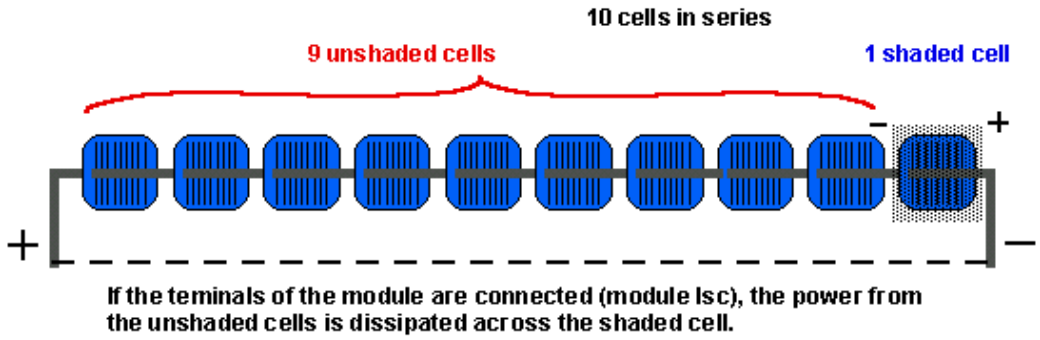


Figure 2.2: Hot spot heating. Source: Honsberg and Bowden, 2011.

Nowadays, to prevent hot-spot heating or to circumvent the problem caused by open-circuited cells, bypass diodes are connected in anti-parallel with a few solar modules, providing an alternative current path around the cell blocks. The optimised way to limit the current in a system can be to install one, or possibly two, bypass diodes per solar cell. In this case, the only current that is lost is the one produced by the shaded part of the cell.

As modules in strings are series connected, the current is the same through all the components. The presence of a bypass diode linked in parallel with a cell block allows the current from other modules in the string to continue flowing when the current production of some cells is at stake, instead of wasting the power production of the whole string (Sargosis Solar & Electric, 2014; Solar-Facts, 2012).

Thanks to the bypass diodes and the inverter[2], the current output typically remains the same unless all modules are affected. However, when two or more strings connected in parallel have an unevenly shade cast on them, an effect called **voltage mismatch** occurs. Voltage mismatch is the condition in which two parallel strings are outputting different voltages when measured independently. This can have a adverse effect on the inverter, which may not be able to operate at the most efficient power point (see discussion about the Maximum Power Point ahead in this section) (Sargosis Solar & Electric, 2014).

Casting a hard shade on a single string will drop its output voltage, but the inverter will detect this voltage decrease and adjust, compensating for the drop. A solar array consisting of only one string of modules cannot suffer from voltage-mismatch (Sargosis Solar & Electric, 2014).

A soft shade applied to some modules in a string and not evenly to others will cause an effect called **current mismatch**, where the current output of each module is varied. Since the laws of electricity dictate that all components connected in series must have the same current, what typically happens is that the string settles on the output of the lowest-performing module, reducing the entire string output to the one of the most heavily-shaded cell in the string. As strings are connected in parallel, this same effect

[2]Photovoltaic Inverter, is an electronic device, critical to the photovoltaic balance of the system, able to convert the variable direct current (DC) produced into alternating current (AC) to inject on the commercial electrical grid or be used in a local off-grid electrical network. It is its function to track the maximum point of power.

occurs independently for all strings in an array. Despite being independent to each string, current imbalance in one string can still negatively affect other strings, through interaction with the inverter (Sargosis Solar & Electric, 2014).

Through the analysis of the IV characteristics of a module, we can visualize how its output is affected by different types of shade. In the figure below 2.3, we can verify the effects on a IV curve of a system in case of soft, hard and partially hard shaded cells.

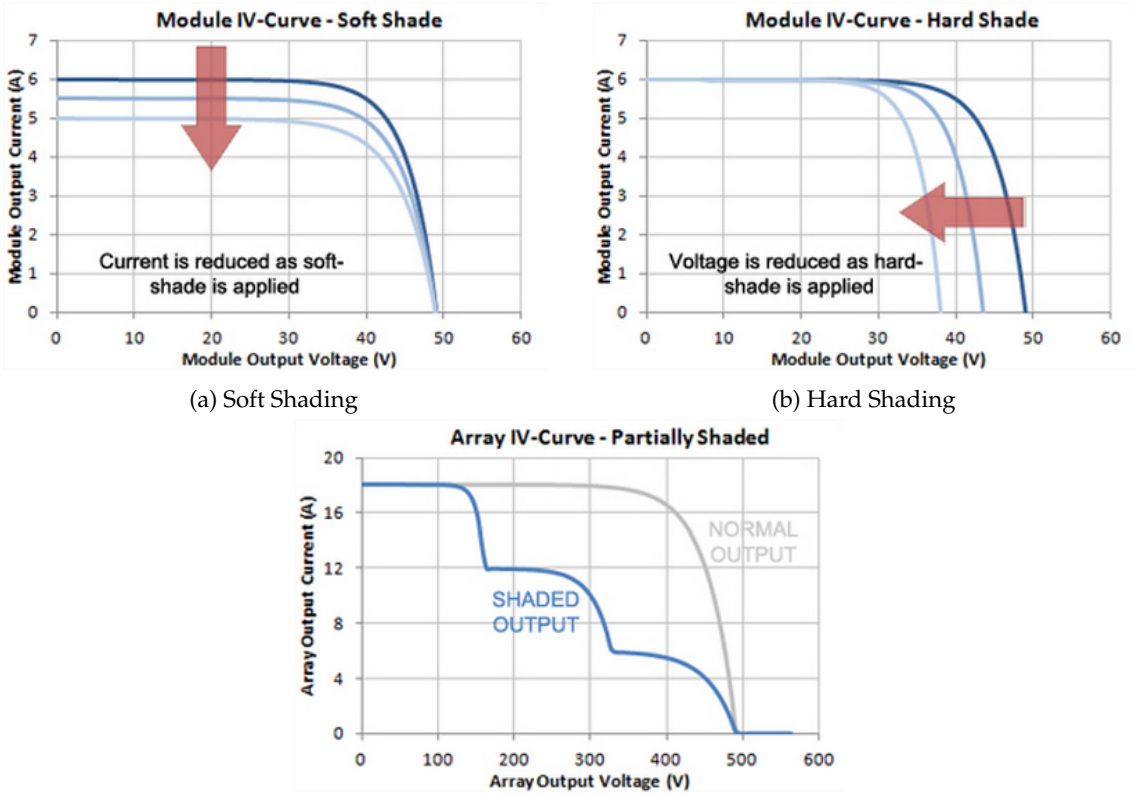


(a) Soft Shading

(b) Hard Shading

(c) Partial Hard Shading

Figure 2.3: Effects on IV characteristic curves on solar systems taking into account the type of shade suffered. Source: Sargosis Solar & Electric, 2014.

Figure 2.3 summarises the impact of shading in the IV characteristics curve:

- IV Curve a) Soft Shade: Output voltage remains unaffected but less current will flow from the module.
- IV Curve b) Hard Shade: Output current remains unaffected but the voltage generated by the module drops.
- IV Curve c) Partial Hard Shade (systems with at least two strings): a voltage-mismatch occurs causing the IV characteristics to become bumpy. This behaviour is due to the presence of the bypass diodes and the action of the inverter, which is constantly trying to adjust its load, seeking the optimal output.

If a system is working at its best performance, as the output voltage increases, the current of the module remains constant while the power is below the maximum power point. This point will be discussed later on. When reaching this point, the output current starts to drop. The way to verify this is by evaluating the IV curve sides, as these tend do get more sloped if the system is faulty. The measure of this effect is called the fill factor (Ff). It is calculated using the formula (2.1), shown below.

$$Ff = \frac{I_{pp} \cdot V_{pp}}{I_{sc} \cdot V_{oc}} \tag{2.1}$$

where:

$I_{pp}$ is the peak power current (A)

$V_{pp}$ is the peak power voltage (V)

$I_{sc}$ is the short circuit current, where the voltage is zero (A)

$V_{oc}$ is the open circuit voltage, where the current is zero (V)

If the fill factor is roughly below 70%, depending on the type of cells, this means there can be faulty modules or loose wires.

For every module, there is a point on its PV curve that is higher than any other point, at a specific voltage. This is called the Maximum Power Point[3], which the solar inverter is designed to seek, in order to most effectively deliver the most power to the grid. However, the effects of shade cause this point to shift around as can be observed in figure 2.4.

Whenever shade is applied to a solar array, the inverter loses the ability to deliver the optimal amount of power, and must begin shifting its power-tracking point around, trying to find the new maximum. This behaviour on the part of the inverter can drastically reduce the power output of the array for a few minutes.

Figure 2.4 summarises the impact of shading in the PV characteristic curve[4] depicting the behaviour of the inverter tracking the MPP.

- PV Curve a) Soft Shade: The current drop induces a lower peak but maintaining a similar shaped curve. tracking the new MPP is easy.
- PV Curve b) Hard Shade: The voltage drop induces a lower peak, but causing a larger variation in the curve. Even though tracking the new MPP is not particularly difficult.

[3]Maximum Power Point (MPP), refers to the highest power output value the inverter can find in the PV curve. The Maximum Power Point Tracking of a photovoltaic panel is performed in order to optimize its efficiency.

[4]PV Characteristic Curve, short for Power-Voltage Characteristic Curve, is a graphical curve which shows the relationship between the power output of solar module and its output voltage. It is usually used to see how a system is operating.

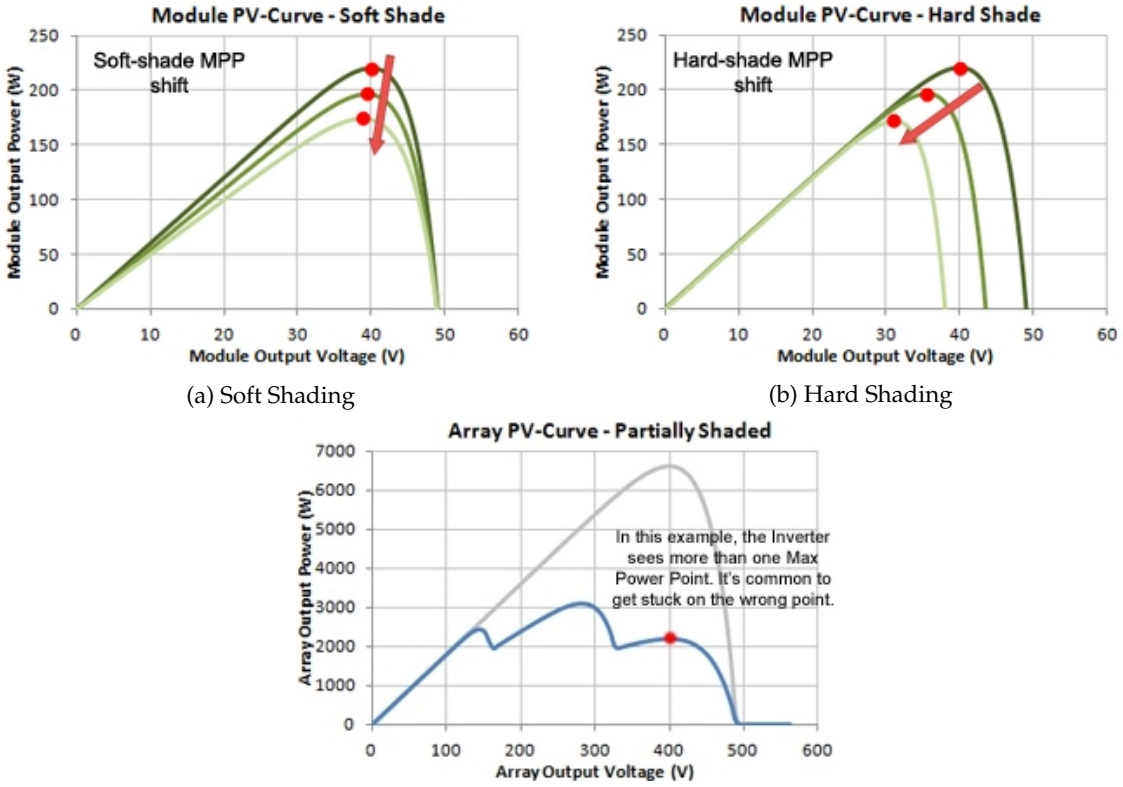


(a) Soft Shading

(b) Hard Shading

(c) Partial Hard Shading

Figure 2.4: Effects on PV characteristic curves on solar systems taking into account the type of shade suffered. Source: Sargosis Solar & Electric, 2014.

- PV Curve c) Partial Hard Shade: A shadow moving over the surface of several modules over time has the effect of changing the PV curve from having a well defined maximum to a multi peaked shape. It is hard for the inverter to find the real MPP often setting for a lower power point.

## 2.2 Modelling Solar Systems

After seeing the importance of installations' electric output prediction and the relevance of understanding its characteristics, this section details important aspects such as how a solar cell generates current and its mathematical model and equivalent circuit.

### 2.2.1 PN Juntion

A solar cell is essentially a PN junction with a large surface area is known, light travels in packets of energy called photons. The generation of electric current happens inside the depletion region of the PN junction forming the solar photocells. The depletion region is the area around the PN junction where the electrons from the N-type semiconductor material which is kept thin to allow light to pass through, are diffused into the holes of the

P-type material. When a photon of light is absorbed by one of these atoms in the N-Type layer it will dislodge an electron, creating a free electron and a hole (Images SI Inc., 2007).

As this process happens, photons will create hole–electron pairs near the junction, causing the electric field in the depletion region to sweep holes into the P-side and sweep electrons into the N-side of the cell (Masters, 2004).

The process described above can be visualized in figure 2.5.

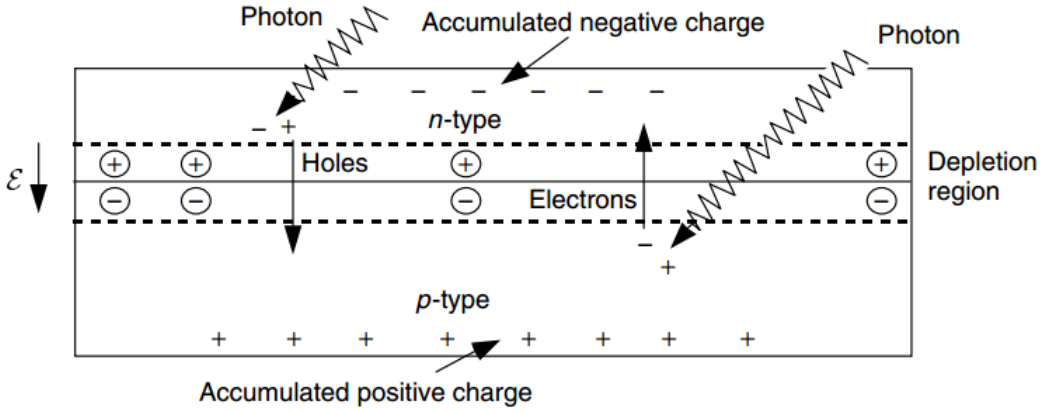


Figure 2.5: PN junction of a solar cell. Source: Masters, 2004.

If an external load is placed between the cathode (N-type silicon) to the anode (P-type silicon) electrons will be attracted to the positive charge of the P-type material travelling from the N-type material and back to the P-side creating a flow of electric current (Images SI Inc., 2007; Masters, 2004).

The hole created by the dislodged electron is attracted to the negative charge of N-type material and migrates to the back electrical contact. As the electron enters the P-type silicon from the back electrical contact it combines with the hole restoring the electrical neutrality (Images SI Inc., 2007).

The circuit described can be seen in figure 2.6.

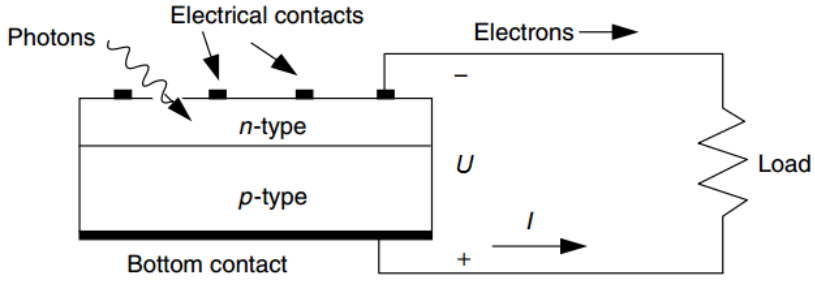


Figure 2.6: Circuit linking a solar cell to a load. Source: Masters, 2004.

### 2.2.2 Mathematical Model and Equivalent Circuit of a PV Cell

The equivalent circuit model for a photovoltaic cell is depicted below. This model consists of a real diode in parallel with an ideal current source as can be seen in figure

2.7. The ideal current source delivers current in proportion to the solar flux to which it is exposed (Masters, 2004).

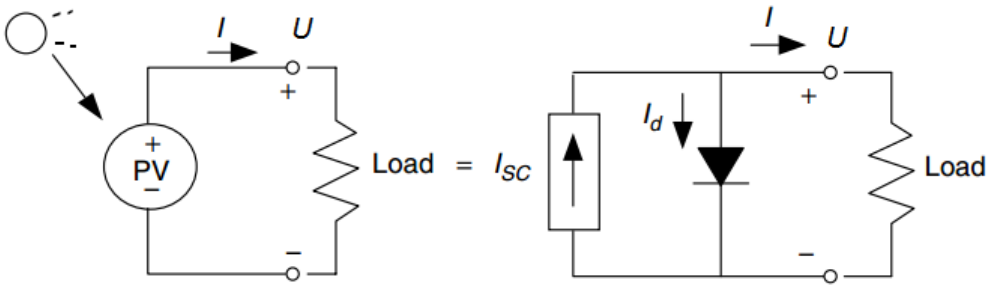


Figure 2.7: Equivalent circuit of a PV cell. Source: Masters, 2004.

There are several other models for the equivalent circuit of a solar cell as can been seen in figure 2.8, such as:

- Figure 2.8a) Ideal single diode model (ISDM), in which despite their simplicity, these do not guarantee an accurate characteristic at the MPP.
- Figure 2.8b) Simplified single diode with a series resistance (SSDM).
- Figure 2.8c) Two-diode circuits are more accurate as they allows the system to keep working under more cases than the other, accordingly the saturation current value of each diode.

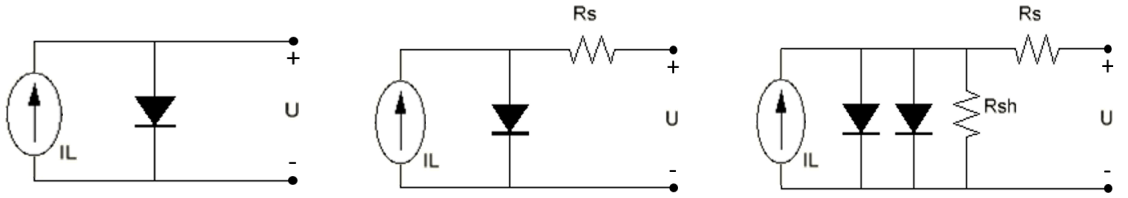


(a) PV cell using the ideal single-diode model.

(b) PV cell using the Series resistance single-diode model.

(c) PV cell circuit using one extra diode.

Figure 2.8: PV cell model examples drawn using a circuit simulator software.

The equivalent circuit of a PV cell is an adaptation to the single-diode model. It uses four components: photo-current source, diode parallel to source, series of resistor $R_S$, and shunt resistor $R_{SH}$. This model is represented in figure 2.9 and is the most commonly used model for conducting PV studies due to its accuracy (Krismadinata, Rahim, Ping, and Selvaraj, 2013).

The current source represents the electron flow produced by photon collisions in the semiconductor material, and the non-linear behaviour of the PN junction is modelled through a diode in parallel. The losses caused by leakage current are represented by the parallel resistor and the resistance associated to the electric contacts is modelled with the series resistor (Rodríguez, Ramos-Paja, and Mejia, 2012).

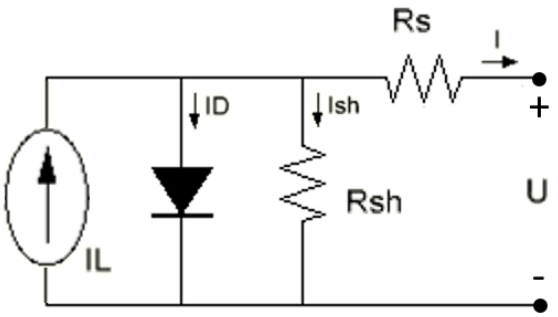


Figure 2.9: Single-diode model - equivalent circuit of a PV cell. Source: Marnoto, Sopian, Daud, Algoul, and Zaharim, 2007.

where:

$I$ is the output current (A)

$I_L$ is the photo-generated current (A)

$I_D$ is the diode current (A)

$I_{SH}$ is the shunt current (A)

$R_S$ is the series resistance ($\Omega$)

$R_{SH}$ is the shunt resistance ($\Omega$)

$U$ is the voltage across the output terminals (V)

In this model, detailed below, the diode IV charactheristic is described through a non linear equation, which adds to its complexity (Drif, Pérez, Aguilera, and Aguilar, 2008).

Using Kirchoff's Current Law (KCL), the current balance is given by equation 2.2.

$$I = I_L - I_D - I_{SH} \tag{2.2}$$

Considering the Shockley diode equation, the current diverted through the diode is given by equation 2.3.

$$I_D = I_0\left(e^{\frac{qU_j}{nkT}} - 1\right) \tag{2.3}$$

where:

$U_j$ is the voltage across both diode and resistor $R_{SH}$ and it is given by: $U_j = U + IR_S$ (V)

Using the Ohm's law, the current diverted through the shunt resistor is is given by equation 2.4.

$$I_{SH} = \frac{U_j}{R_{SH}} \tag{2.4}$$

Substituting equations 2.3 and 2.4 into the first equation, the characteristic equation of a solar cell, which relates solar cell parameters to the output current and voltage, can be obtained. This means equation 2.2 can also be expressed as the equation 2.5.

$$I = I_L - I_0\left(e^{\frac{qU_j}{mkT}} - 1\right) - \frac{U_j}{R_{SH}} \tag{2.5}$$

where:

$I_0$ is the reverse saturation current (A)

$q$ is the elementary charge carried by a single electron ($q = 1,602 \times 10^{-19}$ C)

$m$ is the diode ideality factor ($m = 1$ for an ideal diode and $m > 1$ for a real diode)

$k$ is the Boltzmann's constant ($k = 1,381 \times 10^{-23}$ J/K)

$T$ is the absolute temperature (K)

Since the parameters $I_0$, $n$, $R_S$, and $R_{SH}$ cannot be measured directly, the best way to tackle the characteristic equation of the PV cell is to apply a non-linear regression to extract the values of these parameters on the basis of their combined effect on the behaviour of the cell.

If the value of the shunt resistance $R_{SH}$ is much higher than the one of the series resistance $R_S$, then equation 2.5 can be simplified into the equation 2.9 shown below (Marnoto, Sopian, Daud, Algoul, and Zaharim, 2007):

$$I = I_L - I_0\left(e^{\frac{qU_j}{mkT}} - 1\right) \tag{2.6}$$

Finally, using Kirchoff's Voltage Law (KVL), the current balance is given by equation 2.7.

$$U = U_D - R_S I \tag{2.7}$$

These expressions are extremely important for the work developed further on the thesis, specifically on the design of theoretical models on MATLAB[5] presented in in section 3.1 of chapter 3, *Implementation*.

There are two conditions of particular interest for the equivalent circuit of a PV cell. As shown in figure 2.10 those are:

[5]MATLAB is a high-level language for numerical computation, visualization, and application development used worldwide. It offers the user an interactive environment for iterative exploration, design, and problem solving Mathworks, Inc., 2015.

- the current that flows when the terminals are short-circuited together, denominated the short-circuit current, $I_{SC}$;

- the voltage across the terminals when the leads are left open, denominated the open-circuit voltage, $U_{OC}$.

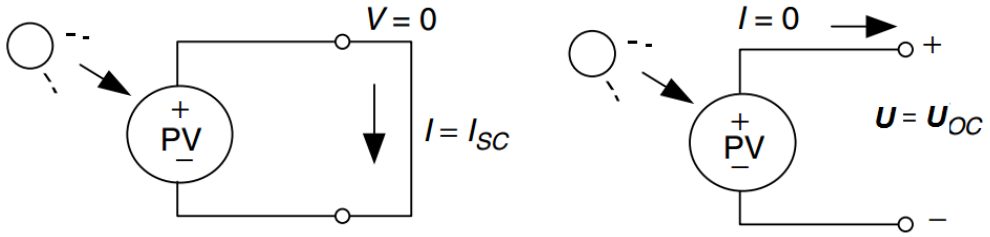


(a) Short-circuit current ($I_{SC}$)

(b) Open-circuit voltage ($V_{OC}$)

Figure 2.10: Short-circuit current and open-circuit voltage. Source: Masters, 2004.

When the connections of the equivalent circuit for the PV cell are short-circuited together, as demonstrated in figure 2.10a, no current flows in the diode since $U = 0$, so all of the current from the ideal source flows through the short-circuited leads (Masters, 2004). It can be shown that for a high-quality solar cell (low $R_S$ and $I_0$, and high $R_{SH}$) the short-circuit current $I_{SC}$ is expressed by the equation 2.8.

$$I_{SC} \approx I_L \tag{2.8}$$

So it is possible to assume that:

$$I = I_{SC} - I_0\left(e^{\frac{qU_j}{mkT}} - 1\right) \tag{2.9}$$

Similarly, as demonstrated in figure 2.10b, when the cell is operated at open circuit, i.e., when $I = 0$, the voltage across the output terminals is defined as the open-circuit voltage. Assuming the shunt resistance is high enough to neglect the final term of the characteristic equation, the open-circuit voltage $V_{OC}$ is given by the following equation, equation 2.10:

$$V_{OC} \approx \frac{mkT}{q} \ln\left(\frac{I_L}{I_0} + 1\right) \tag{2.10}$$

It is not possible to extract any power from the device when operating at either open-circuit or short-circuit conditions.

In both these equations, the short-circuit current, $I_{SC}$, is directly proportional to the solar insolation, which means that in this conditions it is easy to plot sets of photovoltaic current–voltage curves for varying sunlight, as the ones previously seen in section 2.1.2.

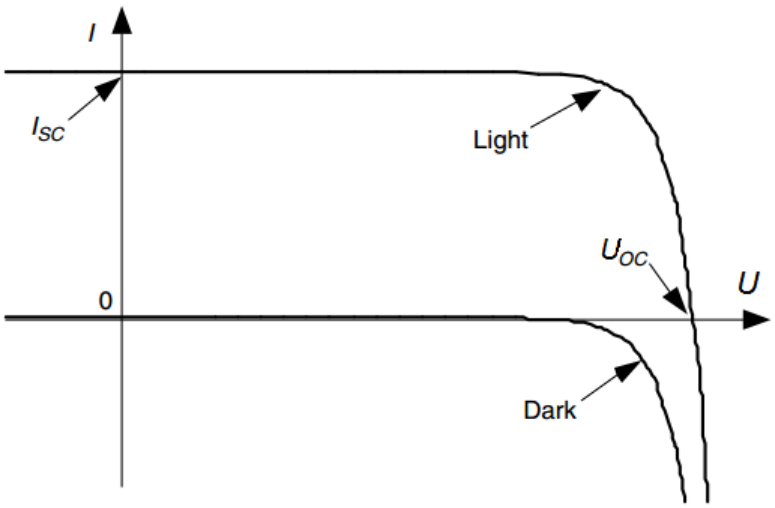


Figure 2.11: Photovoltaic IV relationship for "dark" (no sunlight) and "light" (illuminated cell). Source: Masters, 2004.

The dark curve is the curve of the diode shifted on the voltage axis. The light curve is the dark curve plus $I_{SC}$.

IV and PV characteristics of PV systems are popularly expressed in the form of IV curves that may be presented graphically or using non-linear equations (Marnoto, Sopian, Daud, Algoul, and Zaharim, 2007) as the output characteristics of a PV array vary non-linearly when temperature or irradiance conditions change (Kadri, Andrei, Gaubert, Ivanovici, Champenois, and Andrei, 2012).

## 2.3 Strategies to Optimize the Shading Effect on Solar Panels

### 2.3.1 Evolution in Optimization in the Past Decades

Complex designs and landscapes of PV systems usually necessary in urban environments may provoke non-uniform operating conditions within the arrays resulting, as seen above, from factors such as varied panel orientation, presence of soiling or shading on the modules, or mismatched electrical characteristics between PV cells. Non-uniforme operating conditions cause module sections to sacrifice their individual power production potential, bringing the system to not operate at its maximum efficiency (MacAlpine, Erickson, and Brandemuehl, 2013).

As seen, in installations such as the one schematically presented in figure 2.12, non-uniform operating conditions within the PV system, may cause the equipment to operate for long periods of time well outside the optimal output range, due to inverter errors in tracking the MPP in irregular PV characteristic curves. In order to deal with the complications brought on by shade, there have been introduced new technologies and notable advances in the methods and electronics of the inverters (Sargosis Solar & Electric, 2014; Tsao, 2010).

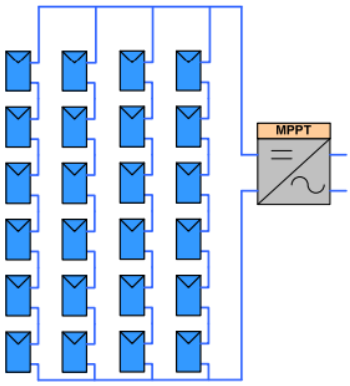


Figure 2.12: Conventional grid-tie PV system with central inverter. Source: Tsao, 2010.

Next a few revolutionary technologies in the photovoltaic field and their contribution to minimize shading effects, are introduced further down:

- Micro-Inverters
- Power Optimizers
- Solar Tracking
- Solar Backtracking

**Micro-Inverters**

Micro-inverters are inverters which are installed on single solar modules. This technology allows each module to independently generate AC current at its own optimal rate whether the other modules are shaded or not. The idea to design modules fitted with buit-in inverters, resulted from the conclusion that installation in domestic applications, even with string inverters, was not easy. This type of design was initiated in early 90's under the name of OK4 and is also termed as Micro-Inverter (MI), Module Integrated Converters (MIC) or AC module (Sher and Addoweesh, 2012).

Although the initial idea of MI is not new, the latest developments in this field classify it as a new concept. With the use of a micro inverter each PV module produces its own AC power, therefore in case of failure of any individual module, power can still be supplied without any interruption (Canterbury Power Solutions, 2012). For example, in fig. 2.13 a case of partial shading affecting a module is depicted. In the case of a shunt connection (left), performance degradation due to shading, lowers the overall power output and the input voltage to the converter, if the connection is in shunt. Adverse situations like this can have less impact if micro-inverter technology is used (right).

Unfortunately, there are downsides to the micro-inverter approach (Canterbury Power Solutions, 2012; Sargosis Solar & Electric, 2014):

- extreme higher cost of acquiring and installing the MIs needed for each PV system;

- lower efficiency of the micro-inverters compared to regular inverters, since they are directly exposed to adverse environmental conditions like humidity, temperature, light etc.;
- reducing Mean Time to Failure (MTTF), and higher difficulty of repairing in cause of faulty or malfunction

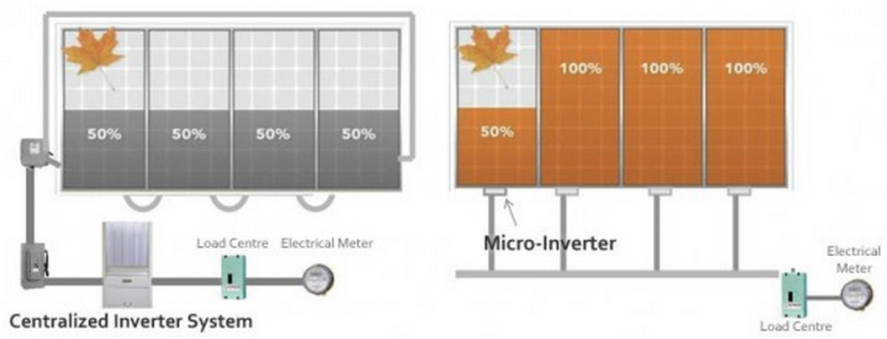


Figure 2.13: Micro-inverters application and power saving example. Source: Canterbury Power Solutions, 2012.

**Power Optimizers**

Although the discrete PV power generation solution provided by micro-inverters partially eliminates the shadow problem, its structure constrains the system energy harvesting efficiency and entails high costs. The solar power optimizer was developed as an alternative to maximize the energy generated by each individual PV module. A power optimizer is a DC–DC converter with Maximum Power Point Tracking (MPPT), which increases PV panel voltage to optimum voltage levels for a DC microgrid connection or for a DC–AC inverter (Chen, Liang, and Hu, 2013).

There are many different system configurations in which distributed power electronics can be deployed accordingly to the mechanical orientation and electrical connection of the solar modules and to the power electronics devices in the system.

Figure 2.14 summarises the possible installations using power optimizers in conventional PV systems.

- PV Installation 2.14a) Power electronic devices installed on all the modules.
- PV Installation 2.14b) Power optimizers are installed in parallel output.
- PV Installation 2.14c) String optimizers are installed in parallel rows of panels.

It should be noted that applications using power optimizers exactly like the ones shown in figure 2.14 are not the most typical. Systems are generally designed with power optimizers only on a portion of the system for financial reasons and also because the use

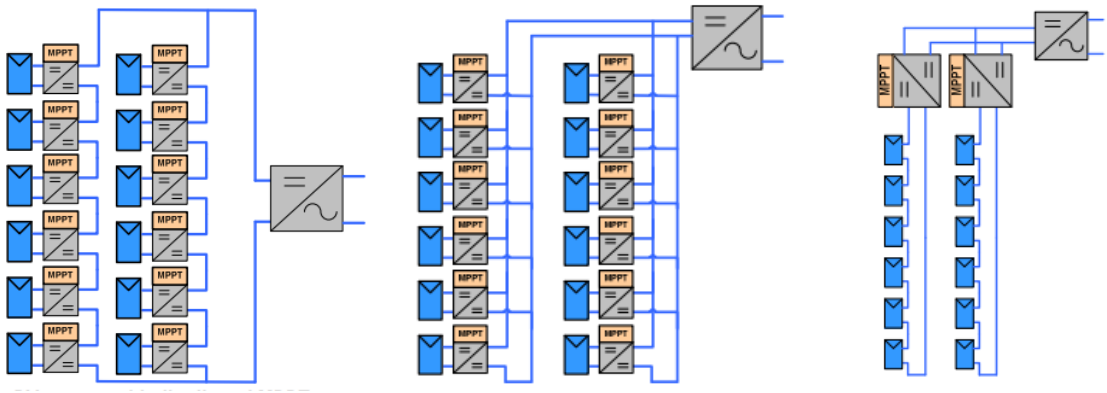


(a) Distributed MPPT power optimizers on each module.

(b) Parallel output DMPPT power optimizers.

(c) String DMPPT power optimizers.

Figure 2.14: Power optimizers installation examples. Source: Tsao, 2010.

of power optimizers allows the system to be designed in configurations that could not be used in conventional systems, offering options such as configurations with strings of different length connected using DMPPT[6] (MacAlpine, Erickson, and Brandemuehl, 2013; Tsao, 2010).

As with micro-inverters, power optimizers are an effective answer to the problems caused by shade, but their relative complexity raises their cost to a point that makes them economically unsuited most photovoltaic projects.

### Solar Tracking

Even though a fixed flat-panel can be set to collect a high proportion of available noon-time energy, significant power is also available in the early mornings and late afternoons when the misalignment with a fixed panel becomes excessive to collect a reasonable proportion of the available energy. For example, even when the Sun is only 10° above the horizon the available energy can be around half the noon-time energy levels depending on latitude, season, and atmospheric conditions. Having this in consideration, a technology, known as solar tracking with the primary benefit of collecting solar energy for the longest period of the day, and with the most accurate alignment as the position of the sun, was developed .

Tracking systems are therefore responsible for orienting photovoltaic panels towards the sun, minimizing the angle of incidence to the incoming sunlight with the objective of increasing the amount of energy produced compared to a similar fixed installation (Lorenzo, Pérez, Ezpeleta, and Acedo, 2002). There are two possible installations, single or dual axis. According to the possible energy gain in each particular case, one of the two is used.

Single axis trackers have one degree of freedom that acts as an axis of rotation aligned along a true North meridian. There are several common implementations of single axis

[6]DMPPT, short for Distributed Maximum Power Point Tracker, is the technology of distributing the MPP trackers by each PV panel instead of only covering the overall output of the system.

trackers, according to the orientation of the module, including: horizontal, horizontal with tilted modules, vertical, tilted and polar aligned.

Dual axis trackers, on the other hand, have two degrees of freedom that act as axes of rotation, which allows optimum solar energy levels due to their ability to follow the sun vertically and horizontally, the primary axis is fixed with respect to the ground and the secondary is typically perpendicular to primary. As happens with singles axis trackers, there are also several common implementations of dual axis trackers classified by the orientation of their primary axes to the ground such as: tip-tilt and azimuth-altitude. An example of this kind of installation is shown in figure 2.15.

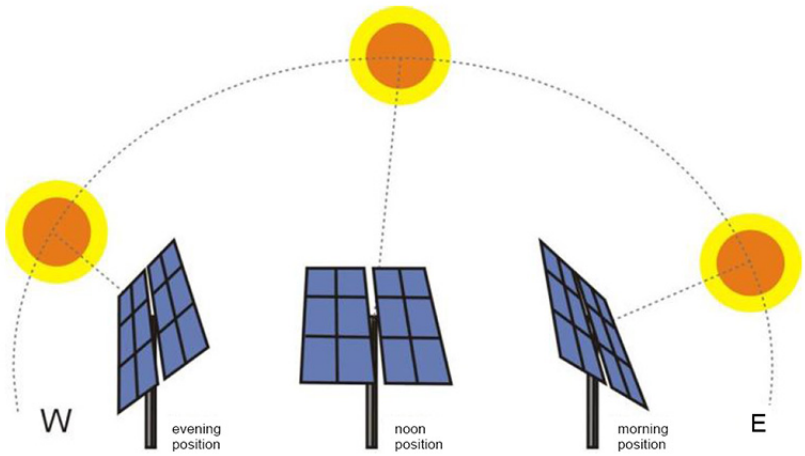


Figure 2.15: Solar dual-axis tracker application example. Source: Queensland Windmill & Solar, 2008.

On clear sunny days the direct sunshine represents up to 90% of the total solar energy, with the other 10% from diffuse solar irradiance. However, on cloudy conditions, almost all of the solar irradiance is diffuse and identically distributed over the whole sky. Tests show that during overcast periods a horizontal module orientation increases the solar energy capture by nearly 50% compared to 2-axis solar tracking during the same period. This led to an improved of the tracking algorithm in which a solar array tracks the sun during cloud-free periods using 2-axis tracking, and switches to horizontal configuration case the sky becomes overcast (Kelly and Gibson, 2009) making this technology a good asset for solar energy harvesting on shading situations.

Solar trackers are highly reliable and have low maintenance requirements. Although it is proven that solar tracking is an excellent technology when it comes to improving the produced energy levels of a PV installation, its safe to assume that they can, depending on the algorithm used, introduce or not an improvement when dealing with soft or hard shade.

**Solar Backtracking**

When simple PV systems with more than one row of panels or arrays using single or dual axis solar tracker panels are receiving solar light at low angles, one panel may shade the panel behind it, rendering it less efficient, as can be seen in figure 2.16. This effect is more pronounced in winter when the solar angles are lower. A way of maximizing efficiency of the system in this cases is by the use of a technology called backtracking (Lauritzen Inc., 2011).

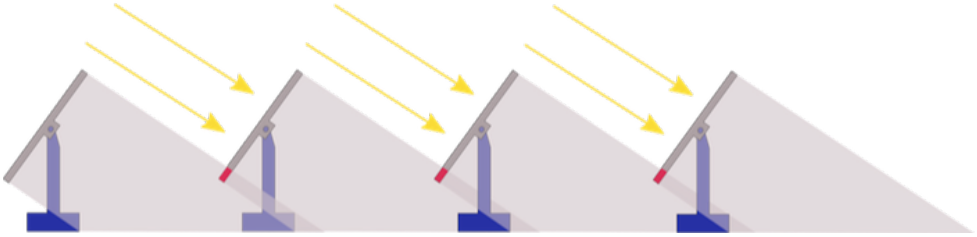

Figure 2.16: Example of installation without backtracking technology. Source: Sistemas Digitales de Control 2002, S.L., 2014.

As seen previously, shade reduces the electric output power and increases the risk of hot spots. Hence, the interest of the so called backtracking strategy as a mean of reducing shadowing impact (Lorenzo, Pérez, Ezpeleta, and Acedo, 2002). This is achieved by moving the surface angles away from then ideal values, just enough to get the shadow borderline to pass outside the border of the adjacent tracker. This way, first, shade is fully avoided and, second, the loss due to the angle of incidence is minimised (Lorenzo, Narvarte, and Muñoz, 2011). This is accomplished by flattening out the arrays in the morning and afternoon hours (i.e., zero tilt angle), using the precise control achievable with a microprocessor-based system (Panico, Garvison, Wenger, and Shugar, 1991).

The backtracking algorithm takes into account the topography of the site, position of the sun and the spacing, size and shape of the panels in the array to minimize shading and maximize orthogonality, so that the maximum amount of solar energy can be harvested (Lauritzen Inc., 2011). The system in figure 2.16 is re-shown in figure 2.17 illustrating the behaviour if backtrackers were installed.

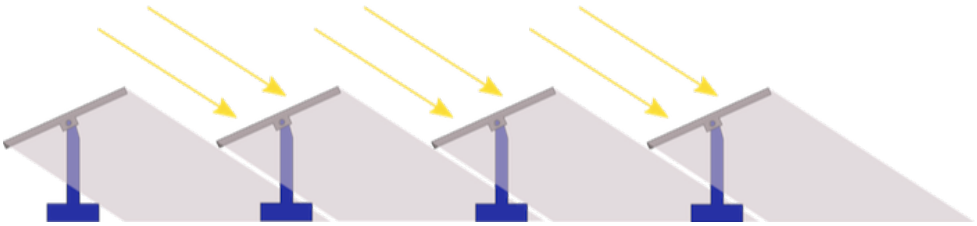

Figure 2.17: Installation using backtracking technology. Source: Sistemas Digitales de Control 2002, S.L., 2014.

Tests made before indicate that backtracking actually increases the solar energy collection as compared to conventional single-axis tracking with shading losses. Further, since direct shading is eliminated, backtracking allows the use of series-configured panels,

which offers benefits of flexibility, optimum fault tolerance, and cost savings associated with bypass and blocking diodes. The elimination of shading could result in increased system reliability via reduced reverse-bias conditions (Panico, Garvison, Wenger, and Shugar, 1991).

The use of backtracking can provide four main types of benefits:

**Area-related benefits** - Because backtracking systems permit smaller row-to-row spacing without penalty of shading, arrays can be closer-packed.

**Performance-related benefits** - Energy losses due to increased incidence angles, introduced by the elimination of inter-array shading, are lower than those resulting from shading. To this adds the fact that motor energy requirements are not relevant next to the gain of the system.

**Reliability-related benefits** - In addition to the benefits of reducing capital cost and enhancing energy production, backtracking can potentially improve PV installations reliability and variable operation and maintenance costs by significantly reducing the duration of reversed bias operating conditions in the array field.

**Design-related benefits** - The elimination of inter-array shadowing through backtracking allows systems to utilize series-configured panels. Tests showed that single series strings of cells with bypass diodes have the greatest fault tolerance to short circuit and open circuit component failures. The series string design provided the least life-cycle cost, based on repair and replacement of failed cells and modules.

The concept of backtracking was developed to lower balance of system costs, improve array performance, and increase long-term system reliability and has proven to be extremely successful overcoming shading losses of conventional tracking and reducing the balance of system costs (Panico, Garvison, Wenger, and Shugar, 1991).

### 2.3.2 Use of Diodes to Compensate the Shading Effect on Solar Panels

Previously it was shown that diodes can be used to compensate the effect of shading on solar panels. In this section is described in detail how this process works.

As it is known, a diode is a semiconductor two-terminal device with the varying ability to conduct electrical current, i.e., to allow electrical current to pass in one direction but not the other.

In photovoltaic systems, there two types of diode installations used:

- Blocking Diodes
- Bypass Diodes

Both use the same model of diode but installed in a different way, as it can be seen in figure 2.18.

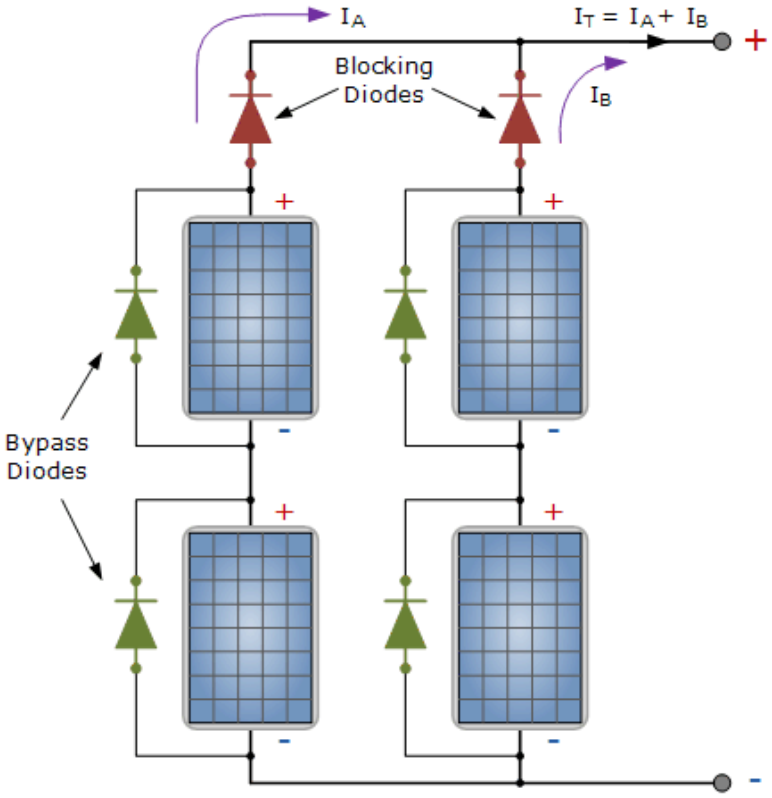


Figure 2.18: Bypass and blocking diode application. Source: Storr, 2014.

**Blocking Diodes**

Blocking diodes are usually connected at the end of a string or a series of panels and are used in photovoltaic installations equipped with batteries. These devices work as charge controllers, mainly to maintain isolation of power supplies, preventing reverse electrical currents from flowing back from the battery through the panels causing it do discharge (Prontes, 2013).

This type of diode assembly is also used as protective measure, protecting panels against other panels in cases of breakdown, ground fault issues and shading (Prontes, 2013).

Summarizing, blocking diodes are used in PV installations fitted with batteries isolating panel strings in order to prevent reverse currents from flowing through the panels in shading or other situations. (Prontes, 2013; Solar-Facts, 2012).

**Bypass Diodes**

Bypass diodes are connected in parallel with a string of panels or a single panel, providing an alternative current path around the cell block, if by chance, it becomes faulty or open-circuited due to overheating, per example. This prevents large voltages from building up across the solar cells in the reverse-biased direction, protecting the solar cells. (Deutsche Gesellschaft für Sonnenenergie, 2008; Sargosis Solar & Electric, 2014).

In the case of shading, a panel not only produces very low power but also presents

resistance. In these cases, the largest shading tolerance would be attained if bypass diodes were connected across every cell. In practice, however, bypass diodes are usually connected for manufacturing reasons across 18 to 20 solar cells. Consequently, modules with 36 to 40 cells have two bypass diodes, and modules with 72 solar cells have four bypass diodes (Deutsche Gesellschaft für Sonnenenergie, 2008). By creating an alternative current path through the shaded panel, bypass diodes also avoid wasting the power produced by the rest of the unshaded panels in the row (Sargosis Solar & Electric, 2014).

Since the diodes have a negligible voltage drop, the power loss induced by their presence is small. The only real loss from a shaded group of cells is whatever voltage they were providing (Sargosis Solar & Electric, 2014).

## 2.4 Methods for Calculating the Shade Factor for a Photovoltaic System

The analysis of the various effects due to the presence of partial shading on PV systems is essential to avoid excessive power losses and to determine, for this cases, which is the best configuration to minimise adverse effects (Alonso-García, Ruiz, and Herrmann, 2006).

Considering the losses in performance provoked by the previously mentioned types of shading, the importance of taking shade effects into account and estimate them ahead is crucial as it can avoid unexpected results when setting up a photovoltaic system (Quaschning and Hanitsch, 1995).

In a PV system formed by several rows of panels, shading effects reduce the output energy essentially in three cases:

- Temporary shading;
- Shading due to the location;
- Shading cast by the building itself.

Temporary shading results from the presence of snow, fallen leaves in forested areas, bird droppings, and other types of dirt. For example, snow can be a significant factor for a system located at Serra da Estrela. The permanence of this dirt will be lesser as result of the self-cleaning of the system provided by the water of the rainfall (Greenpro, 2004; Karatepe, Boztepe, and Çolak, 2007).

Shading as a result of the location agglomerates all of the shading produced by surrounding high objects, including the neighbour buildings and trees which can possibly shade the photovoltaic system and/or at least darken of the horizon. The existence of cables above the building can also have a particularly negative effect, projecting shadows that are continuously moving (Greenpro, 2004).

Shading cast by the building itself comes from chimneys, antennas, lightning rods, satellite antennas, roof and façade prominences, rebounds of the structure of the building

structure, etc.. These shadows are constant therefore should be carefully considered when designing a photovoltaic installation, either trying to avoid them by moving the solar cells array or by moving the object that causes the shade. If none of these solutions are possible, the impact of the shading can be minimized in the system design phase, for example through the choice of how the cells and modules are interconnected (Greenpro, 2004).

Another degrading effect, apart from the three mentioned above, is concealing or masking the radiation from a panel row because of shade cast on it from the panel row in front. This is particularly serious if the distance between the rows is small, the position of the sun is low and the inclination is such that a large fraction of the total radiation is shaded possibly leading panel rows to become partly or even totally shaded by the previous rows (Passias and Källbäck, 1984).

These examples fortify the importance to have detailed knowledge of the system and its energy loss in order to determine its impact on the overall economy and performance of the installation.

The Shade Factor (SF) refers to the percentage of shade which the photovoltaic system is subjected to. The SF calculus assessment is intended to provide an indicative estimate of the potential shading on the solar array. This is done by indicating how much of the potential irradiance could be blocked by objects on the horizon at differing times of the day and of the year. This value can be calculated using numerical methods, either based only data obtained by observation or by computer means.

### 2.4.1 Calculations Based on Observation

One of the primordial stages in estimating irradiance on a shaded PV generator is conducting a survey of all objects/obstructions that can be found in its surroundings, such as: trees, buildings, etc. (Drif, Pérez, Aguilera, and Aguilar, 2008).

If there is an obvious clear horizon and no near or far shading, the assessment of SF can be considered non-existent and an SF value of 1 is assumed for all calculations. However, where there is a potential for shading, it should always be analysed and the reading should be taken from a location that represents the section of the array that is most potentially affected by shade. For systems with near shading in the northern hemisphere, this section will typically be just to the North of the near shading object ((MCS), 2012).

According to the *Guide to the Installation of Photovoltaic Systems* ((MCS), 2012), one way to calculate the amount of potential irradiance that could be blocked by objects on the horizon at different times of the day and of the year, is to draw a sun path diagram with different arcs, each one referring to the months of the year, and lines for the time of the day resulting in a total of 84 segments each with an attributed value of 1%, used to produce a shading analysis for whichever objects in the horizon.

There are other viable ways to draw this diagram resulting in more or less segments, according to the number of arcs and lines, each with a smaller or higher value associated

for the shading analyses respectively. It should be taken into account that the higher the number of segments, the best the accuracy estimating the Shade Factor.

To apply the method presented in *Guide to the Installation of Photovoltaic Systems* the observer has to stand as near as possible to the base and centre of the proposed array and face south, unless there is shading from objects within 10 m of distance ((MCS), 2012).

Once properly positioned, the observer should draw a line showing the uppermost edge of any objects that are visible on the horizon, either near or far, onto the sun path diagram. After the horizon line has been drawn, the number of segments that have been touched by the line, or that fall under the horizon line shall be counted. In figure 2.19 an example of this method is shown where is possible to see that there are 11 segments covered or touched by the horizon line ((MCS), 2012).

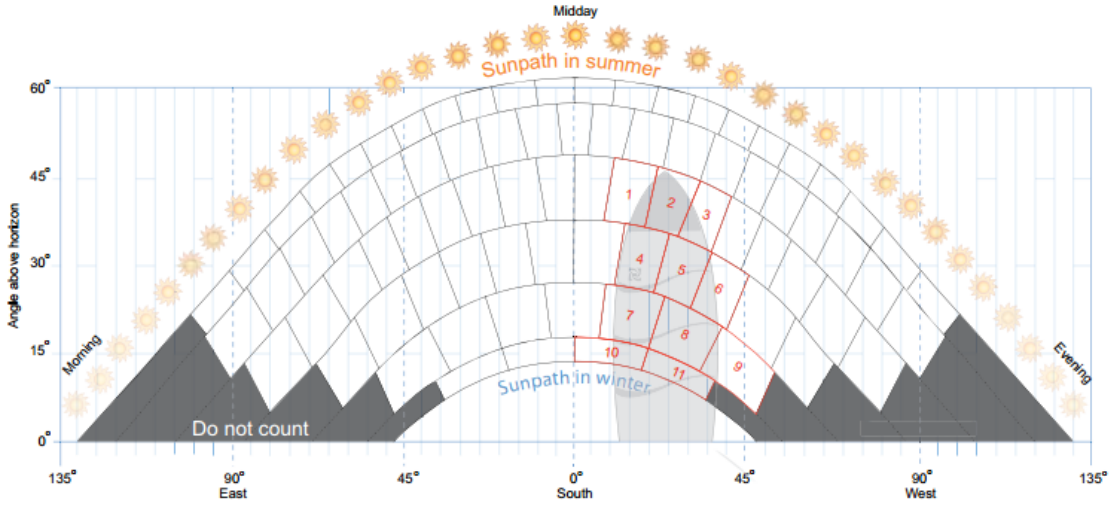


Figure 2.19: Sun path diagram of shading from objects over 10 m away. Source: (MCS), 2012.

The total number of segments is multiplied by their value $(0,01)$ and the total value shall be deducted from 1 to arrive at the shading factor. In the example in figure 2.19 the shading factor is calculated as follows.

SF determination for the example in figure 2.19:

$$1 - (11 \times 0,01) = 1 - 0,11 = 0,89$$

It is estimated that this shade assessment method will yield results within 10% of the actual annual energy yield for most systems. Unusual systems or environments may produce different results ((MCS), 2012).

The difference between considering the shade of objects further than 10 m away or within that distance is that the impact on system performance is higher at smaller distances from the array.

If there are objects adjacent to the array (for example: vent pipes, chimneys, satellite dishes, etc.) either the array should be repositioned out of the shade zone, or the object

casting the shade should be relocated. If case this is not viable, the assessment of shading must be taken from a position more representative of the centre and base of the potentially affected array position.

As described previously, a standard horizon line shall be drawn to represent the worst case. This means the observer should stand on the array location most affected by shade. In addition, any objects on the horizon diagram, that are at 10 m or closer to any part of the array, shall have a shade circle added to the diagram to reflect the severe impact that these items may have on the array performance. Where there are multiple objects within 10 m, then multiple circles shall be drawn, one for each object ((MCS), 2012).

The shade circle shall have a radius equal to the height of the object and should be located so that the apex of the circle sits on the highest point of the shade object. All segments touched by, or within, the shade circle should be counted as part of the overall shade analysis ((MCS), 2012).

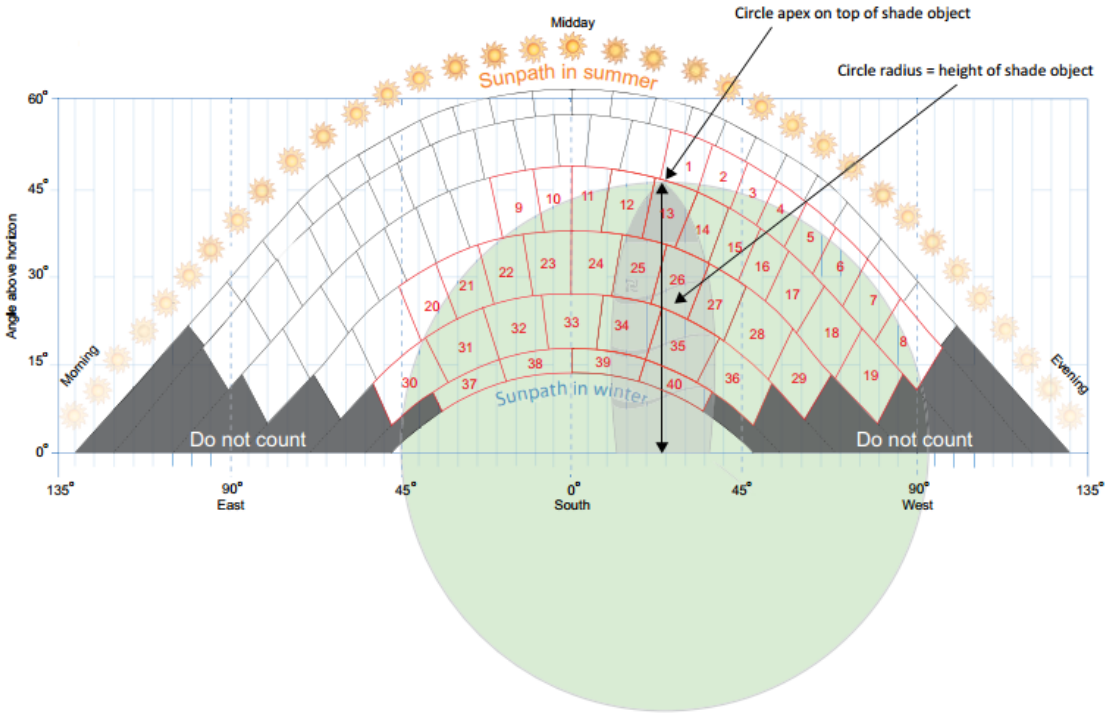


Figure 2.20: Sun path diagram of shading from objects within 10 m of distance from the away. Source: (MCS), 2012.

SF determination for the example in figure 2.20:

$$1 - (40 \times 0,01) = 1 - 0,4 = 0,6$$

The diagram in figure 2.20 uses the same shade object as the worked example in figure 2.19, assuming in this case that the object is closer to the array and considering the same

value per section, it results in a shade factor of 0.6, as the calculus shows, compared with 0.89 obtained in the previous calculation.

### 2.4.2 Computer Aided Calculations and Software

More than a decade ago, budgeting, designing and planning of photovoltaic systems, was based on experience from past installations (Alonso-García, Ruiz, and Herrmann, 2006). Today it is possible to save time and money with the appropriate use of computer programs. System dimensioning and accurate enegy forecasts can be easily estimated in order to find the best choice from the energetic, economic and ecological point of view (Greenpro, 2004). Computer simulation is, therefore, a valuable tool since it makes it possible to model a great variety of situations impacting the performance of a system.

There is a wide range of software and simulation programs that can be used when planning a photovoltaic installation. These tools' role is to assist with the design of photovoltaic systems by solving design problems and optimizing efficiency. A wide range of outputs can be generated by these programs, from the estimated produced energy, or the $CO_2$ emission reduction level to an economic viability analysis (Greenpro, 2004).

Sizing programs and simulators permit the estimation of threshold values and operating states,make possible the simulation of the operation in different conditions. In order to get accurate yield forecasts and yield reports, the use of simulators is mandatory. They have traditionally been employed in research and development, and component manufacturing.

In the process of improving, optimizing or developing new components and system concepts, simulation software is typically used. This helps reducing undesirable developments and can also lessen the scope of experiments. Furthermore these applications can also be put to good use for education and training purposes.

Usually, on simple programs, data parameters, meteorological data and its components, system surrounding details, and the intervention means, must be obtained from user descriptions and default tables (Greenpro, 2004).

As in most software applications, it must be noted that the greater the complexity and flexibility of a program, the higher the skills required from the user in order to take full advantage of its features (Deutsche Gesellschaft für Sonnenenergie, 2008; Greenpro, 2004).

Complex simulation programs, make possible to accelerate the planning process and avoid planning errors. However, they can create a lot of room for user mistakes, leading to unreliable results. The results of the simulation are only as good as the the quality of the inputs provided. Simulation results should be thought through critically and not blindly trusted (Deutsche Gesellschaft für Sonnenenergie, 2008).

Software and simulation programs for photovoltaic systems can be classified according to the methods of programming and the type of calculations performed. The programming method determines the accuracy, flexibility, scope of application, processing speed, and cost of the program.

PV software was divided into the following categories, according to their main purposes:

**Simulation Tools** - Energy simulation programs which provide functions that can be linked to concrete solutions such as simulating meteorological data, electrical and thermal energy components etc.

**Economic Evaluation Tools** - Performance and economic model software, designed to facilitate decision making for the photovoltaic energy investment community.

**Photovoltaic Industry Related Tools** - Software tools for every manufacturing step of PV installations. This kind of tool includes analysing experimental data, calculating optimum architecture based on specific materials, and even research assistant tools. Using PV industry related tools suppliers can simulate their new products and measure the impact of design decisions in a virtual process flow.

**Analysis, Design and Planning Tools** - PV software calculator of potential electricity production. These tools can compare PV output on the basis of different technology options such as module type, inverter efficiency, and mounting type. They may also contain an interactive horizon editor for the purpose of shading analysis.

**Monitoring and Control Tools** - Satellite based tool for local and/or remote monitoring of photovoltaic systems which use solar and meteo data. They feature new generation software to calculate the expected energy yield of PV systems,without the need to rely on data loggers or ground sensors. Hence, the calculated yield is not influenced by faulty or ill maintained sensors.

**Site Analysis Tools** - Range of analysis programs that allow designers to work in 3D with an advanced parametric CAD tool. These standardization tools also provide developers and designers access to a comprehensive. One additional feature typically present is the ability to calculate shadows on arbitrarily oriented surfaces.

**Solar Radiation Maps** - Tools that provide geographical assessment of solar resource and performance, based upon satellite earth observations. They were introduced in order to allow a worldwide study of how much energy is provided by the sun under different weather conditions.

Following the trend of the software industry, a number of Smart Phone Apps became available. Those typically allow users to make measurements, check solar irradiation and potential shading. They can be useful when projecting a new installation in situations where access to a more comprehensive software is not available.

The same happens with online tools. The evolution to "cloud based", software as a service tools also reached this industry. They provide users with the ability to rapidly size grid tied pho- tovoltaic systems and simulate accurate hour by hour energy production from anywhere on any device.

Concluding, it can be said that currently there is a widespread availability of mature, sophisticated tools that can be used in any phase of photovoltaic system deployment, from the business plan to the monitoring tasks.

The following table (table 2.1) lits existing software applications according to their category:

Table 2.1: Examples of photovoltaic software per category.

| Photovoltaic Software Categories | |
|---|---|
| Categories | Software Examples |
| Simulation | INSEL<br>TRaNsient SYstem Simulation Program (TRNSYS)<br>DASTPVPS<br>SOLinvest Pro<br>PVsim<br>SITOP<br>Solar Pro |
| Economic Evaluation | HOMER<br>Solar Advisor Model (SAM)<br>RETScreen<br>SOLinvest<br>EnergyPeriscope<br>PVWatts Calculator |
| PV Industry Related | APOS photovoltaic StatLab<br>Organic Photovoltaics Analysis Platform<br>PV Cost Simulation Tool |
| Analysis, Design and Planning | pvPlanner<br>Archelios PRO<br>String Design Tool<br>PVSYST<br>PV*Sol<br>Solarius-PV<br>PV F-CHART<br>PV DesingPro<br>Greenius<br>SUNDI<br>PVCad |
| Monitoring and Control | Meteocontrol<br>SPYCE<br>pvspot |

| Continuation of Table 2.1 | |
|---|---|
| Categories | Software Examples |
| Site Analysis | Autodesk ECOTECT Analysis<br>Shadow Analyzer<br>Shadows<br>MeteoNorm<br>Amethyst ShadowFX<br>Horizon<br>Skelion |
| Solar Radiation Maps | Photovoltaic Geographical Information System (PVGIS)<br>Focus Solar<br>SolarGIS<br>White Box Technologies |

Available Mobile apps (smartphone/PDA) include EasySolar, Scan The Sun and Pyrometer. Examples of Cloud Based tools include SolarDesignTool, PVAnalytics and modsolar.

### 2.4.3 Shading Simulation Software Review

In this subsection, a review of the software used for dealing with or avoiding the various shading effects is made.

As previously discussed, shading situations present a particular challenge in the planning process. The following aspects have to be considered: shading occurrence at many sites for PV systems, module rows shading each other, edge shading or elevated horizons, the environment, among others. Shading has an effect on the system yield and should be considered on optimised system design (where bypass and blocking diodes, module wiring and inverter behaviour are considered). Simulation programs are therefore essential for calculating shading losses and optimising the electrical and geometric system design (Deutsche Gesellschaft für Sonnenenergie, 2008).

On basic applications, the losses due to shading are estimated by the user and may, therefore, be detached from reality. Since shading calculations based mainly on observation and set by a common user have a relatively high rate of error, vendors of sophisticated applications invested in the modelling of shading behaviour and developed algorithms to estimate its effects on the system performance.

In table 2.1, under the categories **Analysis, Design and Planning** and **Site Analysis** we listed several software applications that allow a detailed shading analysis and are able to determinate the SF of a photovoltaic installation.

Below, in table 2.2 are identified the most popular products and their features:

| | pvPlanner | Shadow Analyzer | Shadows | ShadowFX | PVCad | PVSYST | PV*Sol | Archelios PRO |
|---|---|---|---|---|---|---|---|---|
| Project Location with Google Maps | ✔ | ✖ | ✖ | ✔ | ✖ | ✖ | ✖ | ✔ |
| World wide Meteo Database | ✔ | ✖ | ✔ | ✔ | ✔ | ✔ | ✔ | ✔ |
| PV Devices Database | ✔ | ✖ | ✖ | ✖ | ✔ | ✔ | ✔ | ✔ |
| Sunpath Diagrams | ✔ | ✔ | ✔ | ✔ | ✔ | ✖ | ✖ | ✔ |
| 3D Solar Models | ✖ | ✔ | ✖ | ✔ | ✔ | ✔ | ✔ | ✔ |
| Solar Reports | ✔ | ✔ | ✔ | ✔ | ✔ | ✔ | ✔ | ✔ |
| Economics Results | ✔ | ✖ | ✖ | ✖ | ✔ | ✔ | ✔ | ✔ |

Table 2.2: Shading software chart.

Most of the software mentioned in table 2.2 has a whole range of other less meaningful features, besides its 3D shading calculations tool, such as the ability to import system measurement data for directly comparing measured and simulated values, and the availability toolboxes for solar geometry, meteorology and photovoltaic operational behaviour.

Programs, like **PVSYS**, **Archelios PRO** and **PVCad** also allow special analysis, such as the calculation of module characteristic curves in partial shading situations, enabling, for example, the determination of the thermal loading on solar modules. Moreover, it is possible to produce outputs containing all sorts of parameters, such as meteorological data, electrical voltages, currents, energies and performances (Deutsche Gesellschaft für Sonnenenergie, 2008; Greenpro, 2004).

Snaps of PVSYST and PVCad are shown in figures 2.21 and 2.22.

Google SketchUp plug-in **Archelios PRO** is one of the most recent and complete programs in the market nowadays. It offers numerous features and can be used as photovoltaic design software, layout software and sizing software, for the design and analysis

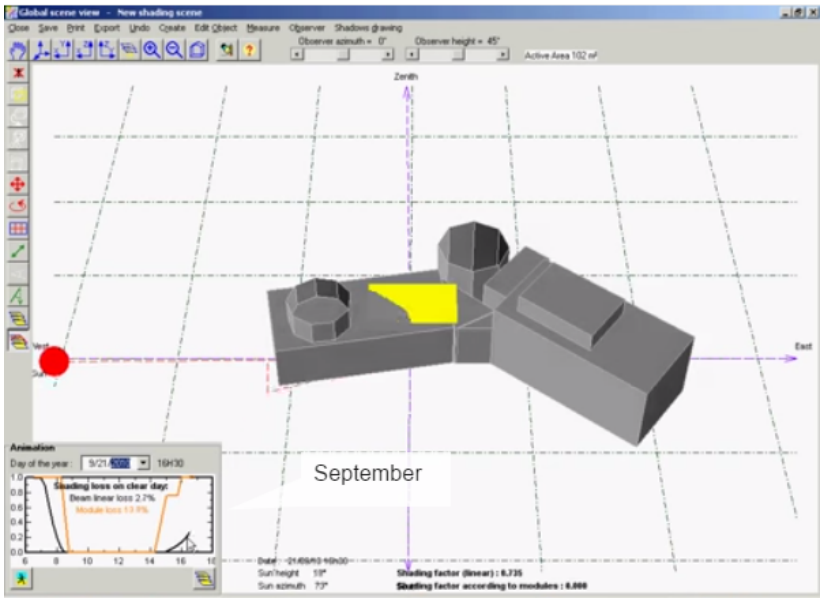


Figure 2.21: 3D editing tool on PVSYST. Source: *Solar PV System Shading Calculation with PVSYST - YouTube* 2009.

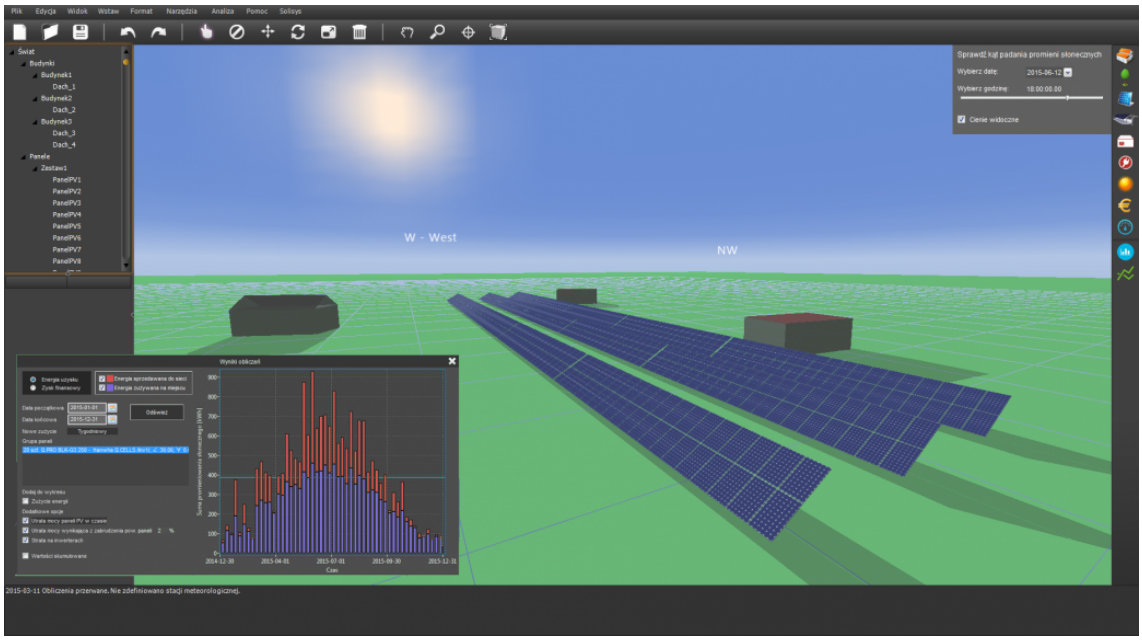


Figure 2.22: Module positioning analysis on PVCad. Source: *Controlling software for photovoltaics - PVCAD* 2015.

of photovoltaic systems. Its shading analysis undergoes automatic calculation of distant shadows and the shading factor. It has the capability of importing data from different sources such as [7]PVGIS shading data, 3D Google SketchUp files for near shading factor calculation and Solmetric SunEye shade measurements. Archelios also integrates with

[7]PVGIS, short for Photovoltaic Geographical Information System, is a solar radiation database, built for the European Commission and developed from climatological data homogenized for Europe and most recently, Africa and Asia. It combines measured and modelled elements (PVGIS - JRC's Institute for Energy and Transport, 2012b).

weather information from [8]MeteoNorm, and includes a comprehensive database with characteristics of several components typical of photovoltaic installations (PV modules, inverters, batteries, regulators, etc.). Finally it includes a reporting tool that generates different diagrams such as detailed photovoltaic losses diagram, graphic of direct/diffuse radiation, photovoltaic production and income as can be seen in figure 2.23 (*Archelios PRO*).

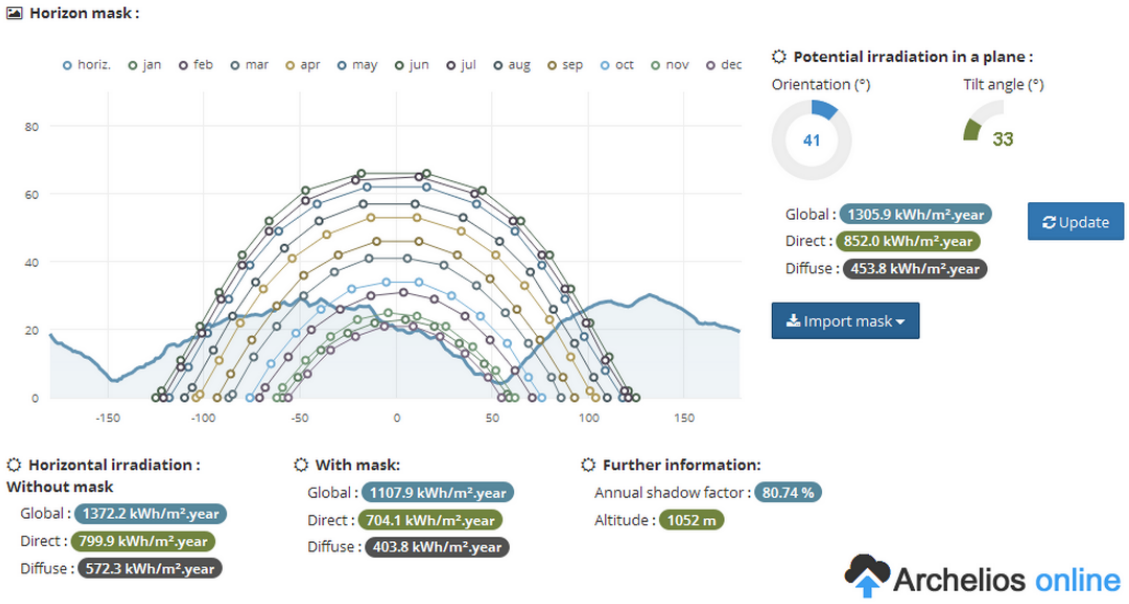


Figure 2.23: Archelios report on shadow analysis. Source: *Archelios PRO*.

PV software **PV*Sol Premium** has a tool that allows the simulation of the influence of the power optimizer chosen. Thanks to the detailed shading analysis down to the level of the module itself, this software can determine exactly, for each application, whether the use of a power optimizer is advisable and economical (Valentin Software GmbH, 2015). System designers, installers and financial analysts will now be able to accurately model and predict the energy harvest benefits that smart Modules provide for any site or condition (Zipp, 2014). This can be seen in figure 2.24.

There are other types of shading analysing PV software like **PV Designer Solmetric** that uses external devices, (such as **SunEye**) to obtain exact readings in order to evaluate the site desired for the installation. This program enables the user to easily draw a roof outline, specify set-backs and keep-out regions, and incorporate SunEye shade measurements at specific locations on the roof. The sizing of strings, checking inverter limits, and calculation of the AC energy production for the system. An extensive world-wide

[8]MeteoNorm, climatological data reference world wide. It possesses a catalogue of meteorological data for solar applications and system design at any desired location in the world. It is based on years of experience in the development of meteorological databases for energy applications. Software like PVSyst, PV*Sol and Archelios Pro use this reference (*Meteonorm*).

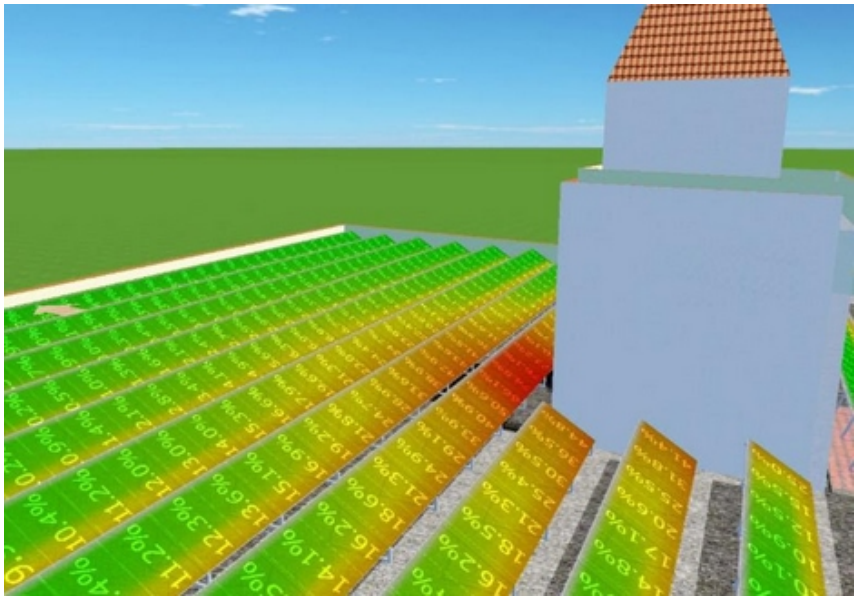

Figure 2.24: Simulation with power optimizers in 3D mode. Source: Zipp, 2014.

database of modules, inverters, and historical weather is also provided (Solmetric, Inc., 2015). Solarmetric Suneye device is shown below in figure 2.25.


Figure 2.25: Solmetric Suneye solar reading. Source: Home Power Inc., 2015.

Another growing market is the PV app market. For example, **EasySolar** makes it possible to prepare designs and customized commercial offers within minutes, as is seen in figure 2.26.

Thanks to cloud technology, solar professionals can work on the go just using smart phones or other mobile devices or computers. Flexible designs can be made on images, Google maps or sketches. Built-in measurement tools let designers verify azimuth and

inclination of the roof for specific locations. Cloud technology now gives mobile access to the most important algorithms present up to now only in PC software (Solar Server, 2015).


Figure 2.26: Easy solar app - PV designing tool. Source: Zipp, 2014.

CHAPTER 3

# IMPLEMENTATION SIMULATIONS IN SIMULINK

This chapter introduces and details the theoretical implementations performed in the thesis, starting with the explanation of the simulation model using Simulink[1] proceeding to the various simulations performed on this phase and finalizing with the analyses the obtained results.

A few stages of the practical implementation were set using different adaptations of the model, these are fully described on section 3.2, Simulations, and have been organized in a sub-section fashion.

Results and conclusions are discussed along the chapter at the end of the explanation of each phase.

## 3.1 Introduction to the ECEN2026 Model

ECEN2026 Model is basically the simulation using Simulink of PV modules, developed by the Electrical & Computer Energy Engineering department of the University of Colorado (*ECEN2060 Renewable Sources and Efficient Electrical Energy Systems*).

Following on sub-subsection 3.1.1, the specifications of this model are explained in detail as well as its importance for the work developed here.

This model uses the equivalent circuit of a PV cell depicted in figure 3.1.

[1]Simulink is a block diagram environment for multi-domain simulation and Model-Based Design which supports simulation, automatic code generation, and continuous test and verification of embedded systems. It is integrated with MATLAB, enabling the user to export simulation results to MATLAB for further analysis (The MathWorks, Inc., 2015).

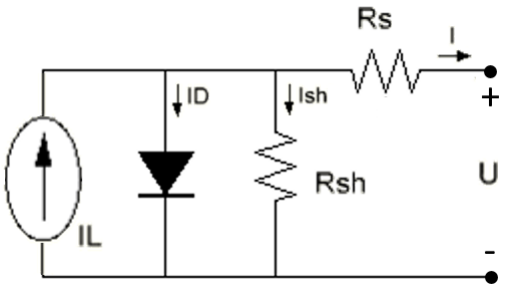


Figure 3.1: Equivalent circuit of a PV cell used on the ECEN2026 model. Source: Marnoto, Sopian, Daud, Algoul, and Zaharim, 2007.

The same circuit was previously shown in chapter 2, *State of The Art*, in sub-subsection 2.2.2 where the expressions expressed by it were established and are now put to use.

### 3.1.1 Specifications of the Model

The model has two input possibilities for PV module connections:

**Current-input module** - applied in the case when modules are connected in series and therefore share the same current (figure 3.2a);

**Voltage-input module** - suited for the case when modules are connected in parallel and therefore share the same voltage (figure 3.2b).

Both PV module models are implemented as masked subsystems in Simulink as can be seen in figure 3.2.

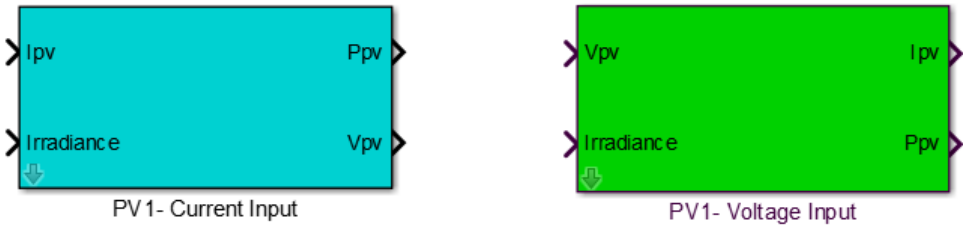


(a) Current-input module

(b) Voltage-input module

Figure 3.2: Current and voltage module inputs designed using Simulink

The ECEN2026 model assumes standard test conditions (1000 W/m$^2$, 1.5 Air Mass and 25 °C). The effects of temperature changes are not considered in this model.

A bypass diode (a single diode across the entire module) can be included.

### 3.1.2 Simulink Implementation

Model parameters, for both current-input and voltage-input cases, are the standard parameters displayed on the data-sheet of the chosen solar module:

- Short-circuit current $I_{SC}$;
- Open-circuit voltage $V_{OC}$;
- Rated current $I_R$ at MPP;
- Rated voltage $V_R$ at MPP.

For illustrative purposes the parameter input dialogue box is depicted in figure 3.3.

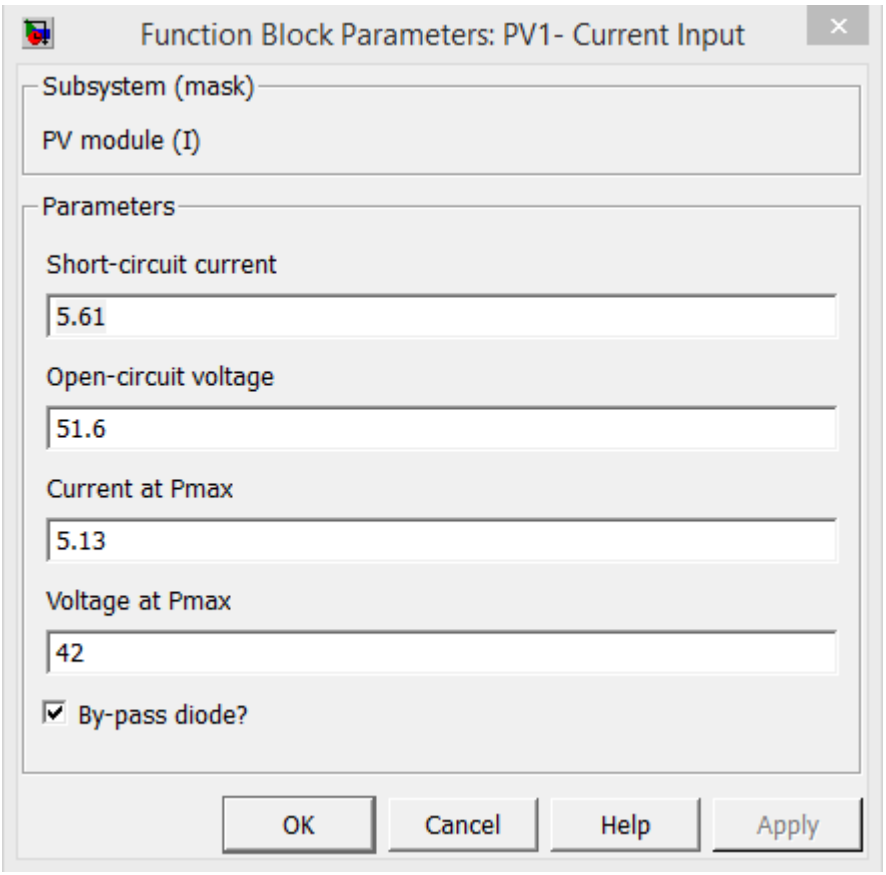


Figure 3.3: Parameters of the PV current and voltage input modules designed.

The initialization of the block is defined on the same menu. It computes model parameters $I_O$, $R_S$, $R_{SH}$ based on the parameters listed above and can be consulted in the *Appendix* section (chapter A) under listing A.1.

In figures 3.4 and 3.5 it is possible to see the undermask subsystems of the current-input and voltage-input model respectively.

On the current-input module model undermask subsystem, two *Inport*[2] blocks were used referring to, $Ipv$ and *Irradiance*, and two *Outport*[3] blocks were used referred to as, $Ppv$ and $Vpv$. This set-up allows the input and output to be set straight from the mask as illustrated in figure 3.2a.

Current-input module undermask subsystem can be seen, below, in figure 3.4.

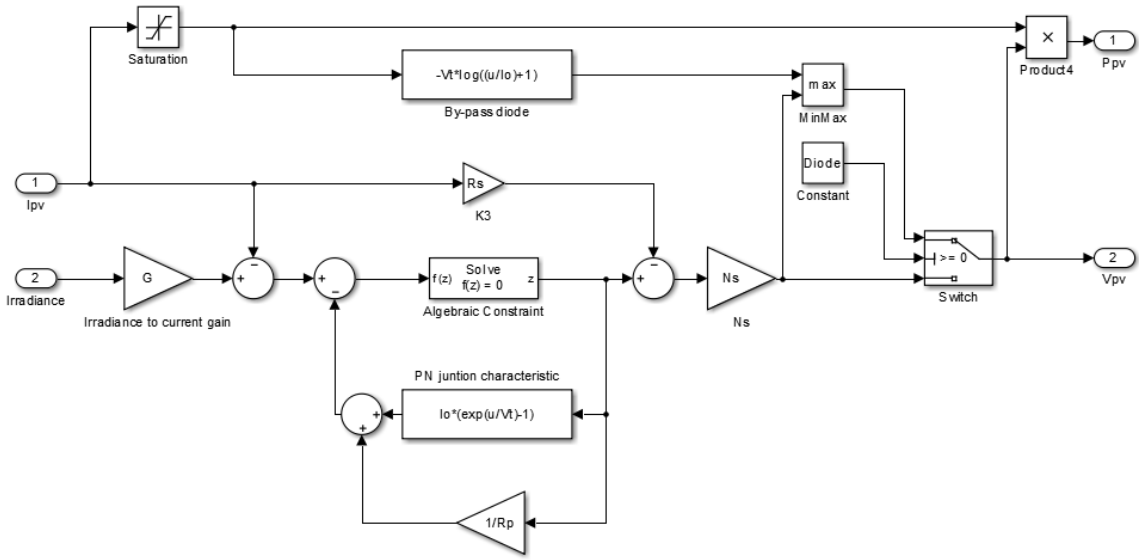


Figure 3.4: Parameters of the PV current-input module mask designed.

On the voltage-input module undermask subsystem, the already defined current-input mask is used. As happens in the current-input model, previously described, two *Inport* blocks and two *Outport* blocks are used, named respectively $Vpv$ and *Irradiance*, and $Ppv$ and $Ipv$. This set-up allows the input and output to be set straight from the voltage-input module mask, as illustrated in figure 3.2b.

Voltage-input module undermask subsystem can be seen in figure 3.5.

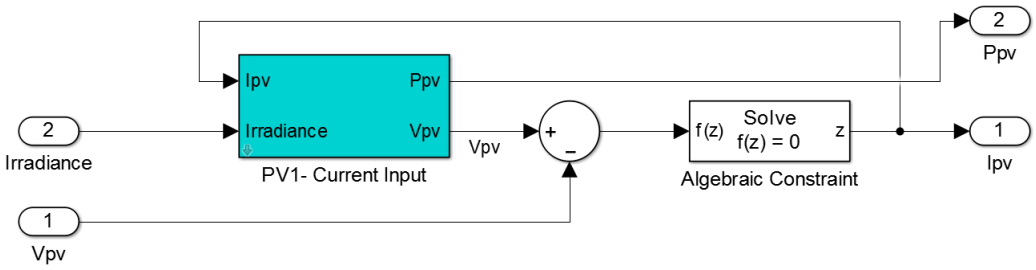


Figure 3.5: Voltage-input module undermask subsystem design.

Once these two mask models are set, any installation conceived by the user can be simulated.

[2] *Inport* blocks are the links from outside a system into the system. These work as input ports for subsystems or external inputs (*Inport*).

[3] *Outport* blocks are the links from a system to a destination outside the system. These work as output ports for subsystems or external outputs (*Outport*).

## 3.2 Simulations

The use of the ECEN2026 model was instrumental on the elaboration of this thesis. The existence of theoretic PV models, whose behaviour closely follows the modules, allows meaningful simulations for a wide variety of test cases. Using such model as a basis, permitted the following stages of work:

1. Designing and testing theoretic photovoltaic installations;
2. Obtaining IV and PV characteristic curves for different cases of shading using installation design in Simulink;
3. Development of the power output expression of a specific PV installation according to shade variation;
4. Determination of the annual output power production of one single PV module assuming a previously defined shade;
5. Comparison of the impact of the calculated Shade Factor on the production of an instalaltion with the one simulated;
6. Comparison of the obtained theoretic IV and PV characteristic curves with the ones obtained from the tests made with real modules.

The implementation of stages 1 to 5 is explained in full detail along the present chapter. Stage 6 is only presented in chapter 4, *Experimental Results - Testing PV Modules*, as it includes a comparison with tests made in the next phase of this work.

**Note:**
All simulations detailed in this chapter use the specifications of *SANYO PV Module HIP-215NHE5*, as follows:

- Short-circuit current $I_{SC} = 5.61$ A;
- Open-circuit voltage $V_{OC} = 51.6$ V;
- Rated current at MPP $I_R = 5.13$ A;
- Rated voltage at MPP $V_R = 42$ V.

### 3.2.1 Designing and Testing Theoretic Photovoltaic Installations

Three main installations were used applying this model to test theoretic photovoltaic installations.

The first one, shown in figure 3.6, uses seven modules linked in series. The goal of this model was to analyse and conclude on the effect of shade in more than one module at a time.

On this design, seven PV modules are connected in series linked to two *XY Graph*[4] blocks, plotting the IV and PV curves. The output of the seven module model is also fed to a *To Workspace*[5] block, so that their global power production is saved to workspace becoming available to be used directly from MATBLAB.

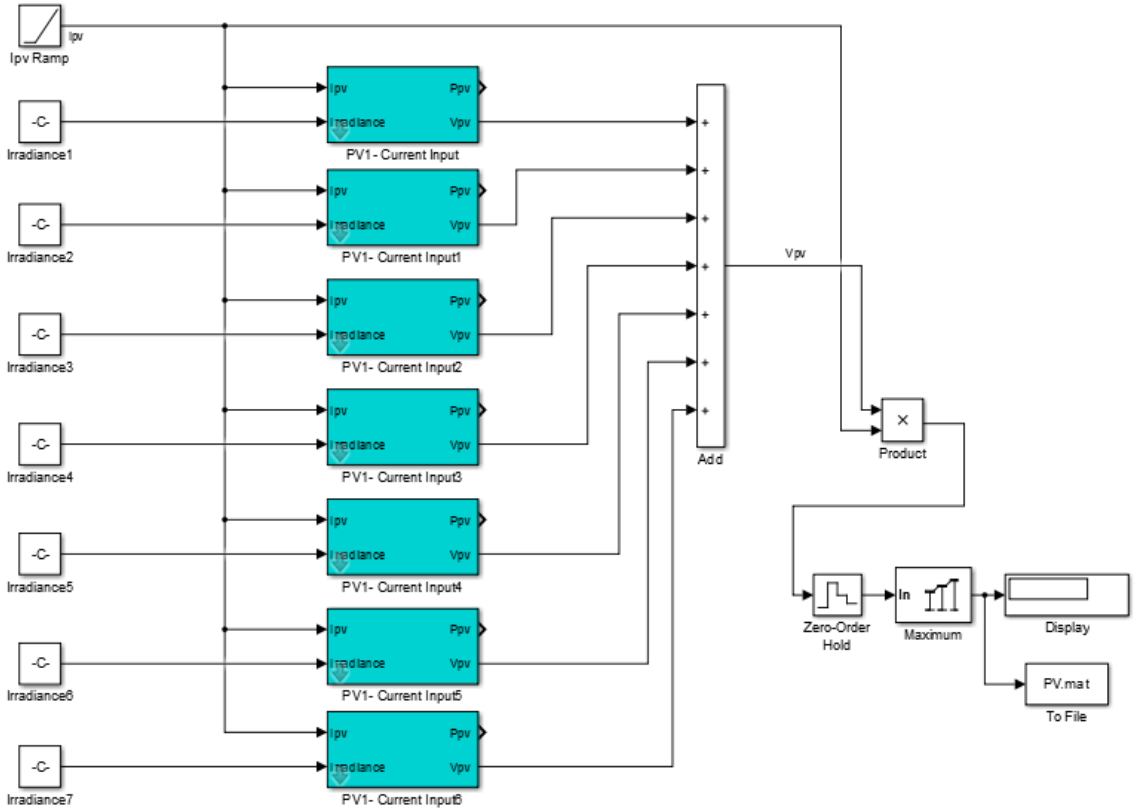


Figure 3.6: PV installation with seven modules designed using Simulink.

The second model consists in one single PV module, also linked to a *To Workspace* block for the same reason as the previous model. This model can be seen in figure 3.7, and it was designed to study the power output on a single module when shade is present on specific times of the day which changes from month to month.

[4] *XY Graph* block displays X-Y plots of signals using MATLAB figure window. The block has two scalar inputs. It plots data in the first input on the x direction, against data in the second input, on the y direction (*XY Graph*).

[5] *To Workspace* block inputs a signal and writes the signal data to the MATLAB workspace. During the simulation, the block writes data to an internal buffer. When the simulation is completed or paused, that data is written to the workspace (*To Workspace*).

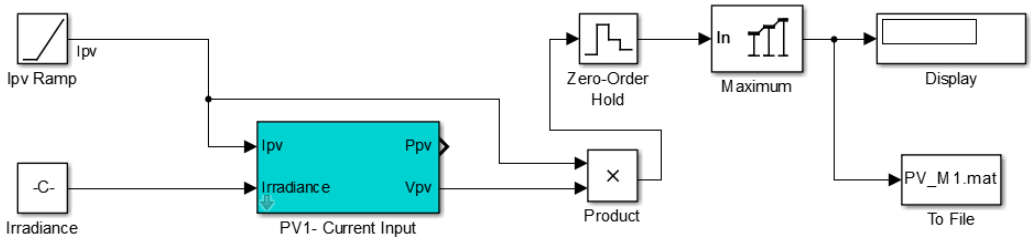


Figure 3.7: PV installation with a single module designed using Simulink.

The third model is very similar the previous one, the main difference being that it uses two PV modules instead of only one. This model was designed mostly to study the IV and PV characteristic curves when shade affects part of an installation, on this case, one of the modules.

Both modules of this model are connected in series, also linked to *XY Graph* and *To Workspace* blocks, for the same reason as in the first model, as can be seen in figure 3.8.

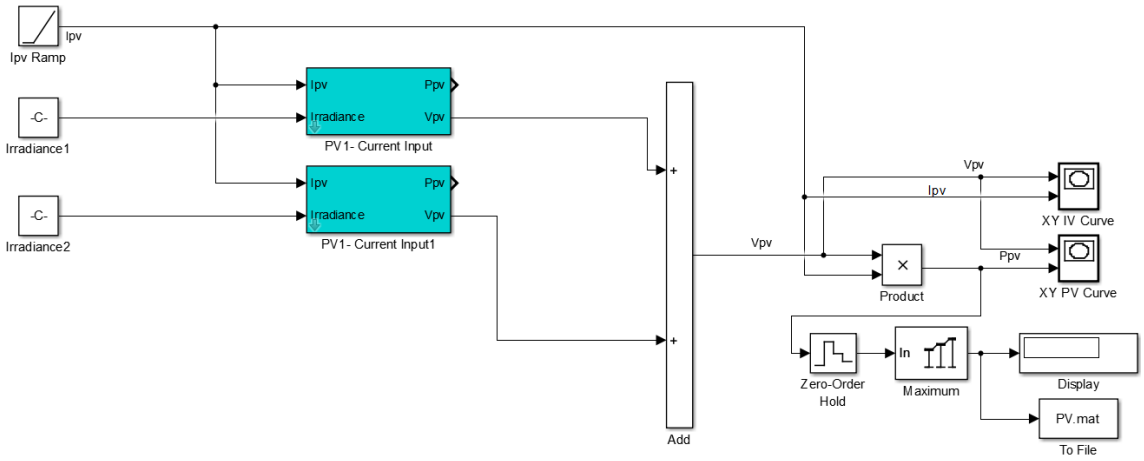


Figure 3.8: PV installation with two PV modules designed using Simulink.

It is important to mention that using model ECEN2026, the four specification values of the PV modules can be changed, though typically, once the module is chosen, these remain constant.

Another parameter that can be adjusted is the *Irradiance* input on each module. This value is the most important for this study, since it is directly associated with the presence of shadows on an installation.

### 3.2.2 Simulation and Study of IV and PV Characteristic Curves for Different Cases of Shading

It is possible, for each of the installations designed, to simulate the expected PV and IV characteristic curves. For this part of the study, both installations designed with more than one module (represented by figures 3.8 and 3.6), were used.

XY Simulink Plots were traced for two "shading cases":

- Shading case 1 assumptions: The installation design that uses two PV modules was used. It was assumed that no shade would be cast on module 1 and a soft shade would be be cast on module 2;
- Shading case 2 assumptions: For the second case, using the designed installation with seven PV modules, the process was basically the same. The values of irradiation (or irradiance) were chosen based on theoretical considerations, taking into account what could be realistic values in a practical installation.

Both cases resulting plots are depicted next, on figures 3.9 and 3.10, for cases 1 and 2, respectively.

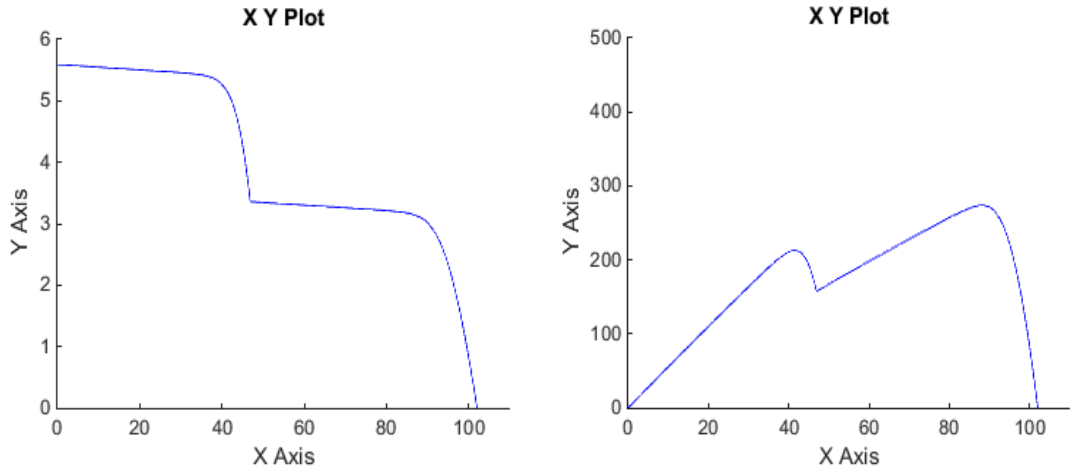


(a) Current-voltage characteristic curve.

(b) Power-voltage characteristic curve.

Figure 3.9: Case 1: Simulink XY plot of the IV and PV curves for a PV installation with two modules.

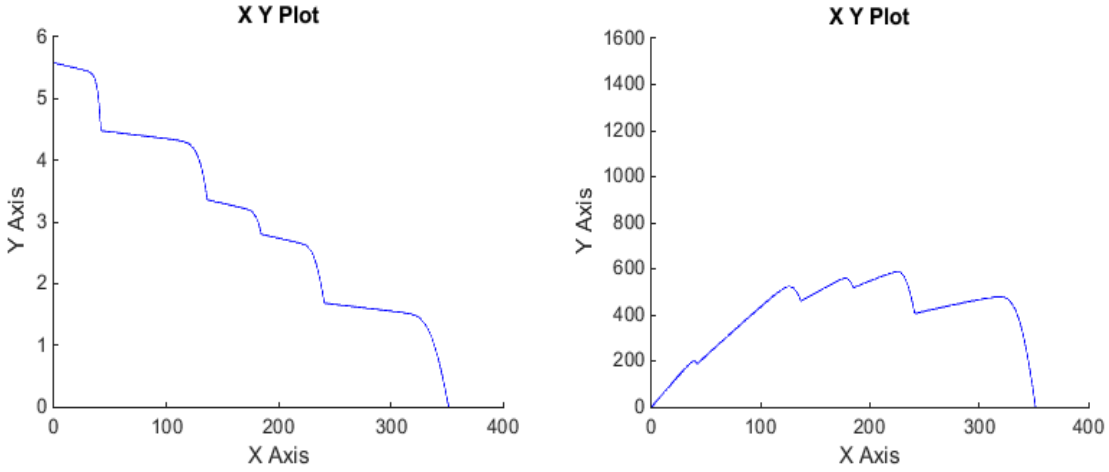


(a) Current-voltage characteristic curve.

(b) Power-voltage characteristic curve.

Figure 3.10: Case 2: Simulink XY plot of the IV and PV curves for a PV installation with seven modules.

To simulate case 1, an *Irrandiance* value of 1000 W/m$^2$ was defined on the input irradiance of module 1 (*Irradiance1*) and a lower value of 600 W/m$^2$ was defined on module 1 (*Irradiance2*). The XY plots produced representing the IV and PV characteristic curves of this installation are shown in figures 3.9a and 3.9b.

For case 2, the values used for the irradiance parameters input to each of the seven modules (*Irradiancel* to *Irradiance7*) oscillate between 1000 and 300 W/m$^2$. The resulting XY plots, representing the IV and PV characteristic curves of this installation can be seen in figures 3.10a and 3.10b, below.

**Comments:**

The four-figure group of plots obtained have the expected shape for the shaded cases considered, in line with the theoretical study presented in chapter 2, *State of The Art*.

### 3.2.3 Development of the Power Output Expression of a Specific PV Installation According to Shade Variation

For this particular goal, the seven module installation shown in 3.6 was used. The main purpose was to study the produced power of this specific PV installation according to shade variation, and to develop an expression suited to behaviour of the model.

A script was develop using MATLAB to help manage the required steps to control the variation on the installation inputs and save the produced power value for each situation. The code on the script can be consulted in the *Appendix* section (chapter A) under listing A.2.

To generate the mentioned expression, the input irradiation on each of the seven modules was shifted between 0 and 750 W/m$^2$ in four steps (750, 500, 250 and 0. These values were defined on the script on the vector *Irradiance = [750 500 250 0]*.

The purpose was that each of the seven modules passes through the four combinations of input irradiance, generating 28 simulations and readings, one for each of the four irradiance values changing for each of the 7 modules on the installation, individually. This process is detailed further and resumed in figure 3.11 for a better understanding.

The sequence of irradiance values used in the simulations is as follows:

1. The installation initializes with all modules *Irradiance* input equal to 1000 W/m$^2$.
2. On the first simulation, the module 1 irradiance value (*Irradiance1*) is set to the first value of vector *Irradiance* (750), while the remaining modules keep the initial irradiance value (1000).
3. For the second simulation, the module 2 irradiance value (*Irradiance2*) is also changed to the first value of vector *Irradiance* (750), while keeping the remaining irradiance values unchanged.
4. The process is repeated until the $8^{th}$ reading, where the module 1 irradiance value changes, to the second value of vector *Irradiance* (500), keeping the irradiance value

of the remaining modules at their last imposed input value, (750). This process continues until all modules irradiance input is equal to the fourth and last position of vector *Irradiance* (0).

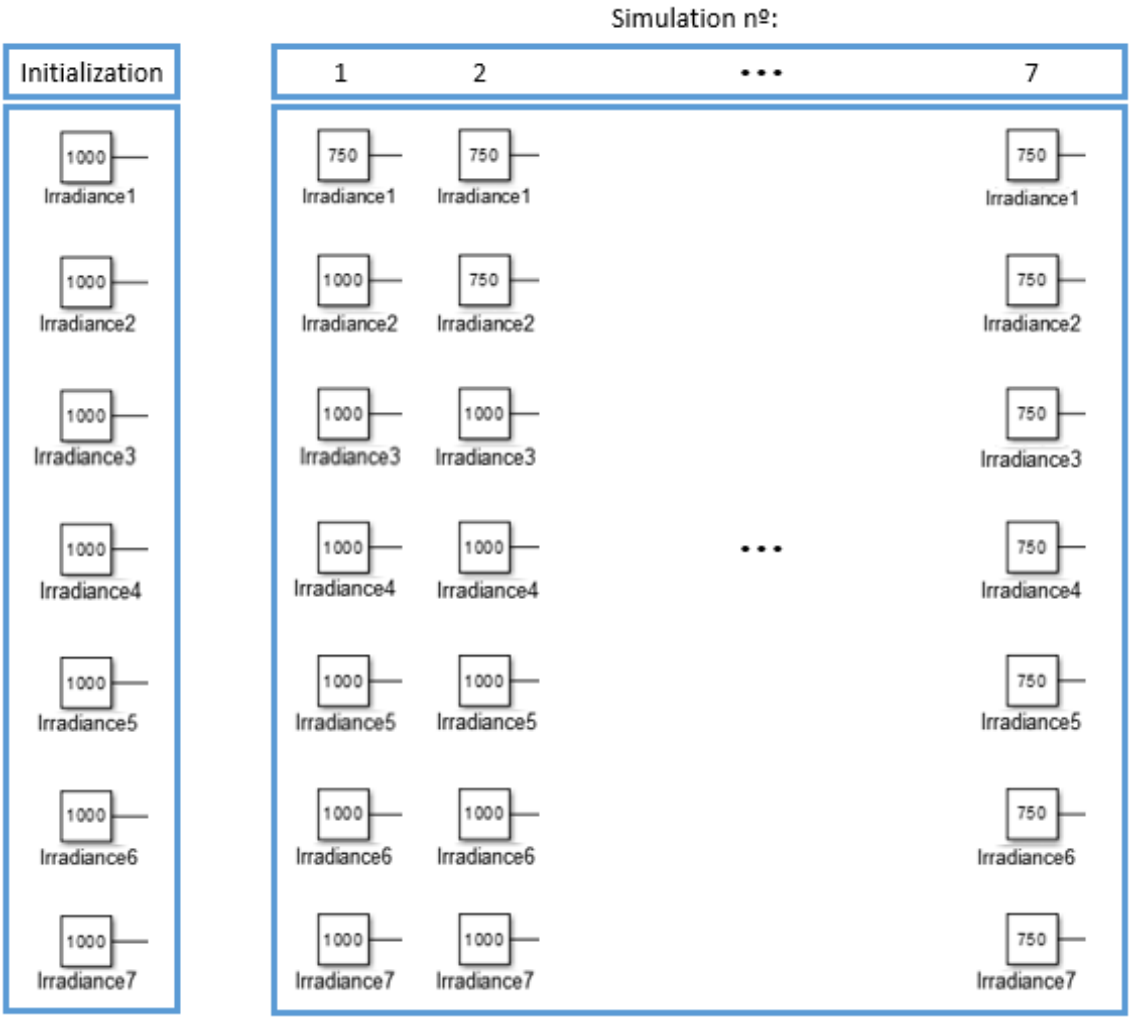


Figure 3.11: Explanatory diagram of the process used on scrip A.2 (steps 1 to 4).

The previously mentioned script saves the value of the maximum produced power for each simulation, the number of modules that are being shaded and the percentage of shading severity on the global installation. Using this values it was possible to plot figure 3.12.

Once this relation was determined, using MATLAB curve fitting tool - cftool[6], it was possible to come up with an expression the correlates the maximum power production

[6]Cftool is a Curve Fitting app whixh provides a flexible interface where users can interactively fit curves and surfaces to data and view plots.

It allows the comparison between multiple fits, linear or non-linear regression, interpolation, local smoothing regression, or custom equations. This tool also shows the goodness-of-fit statistics, displays confidence intervals and residuals, removes outliers and assess fits with validation data and automatically generates code for fitting and plotting surfaces, or export fits to workspace for further analysis.

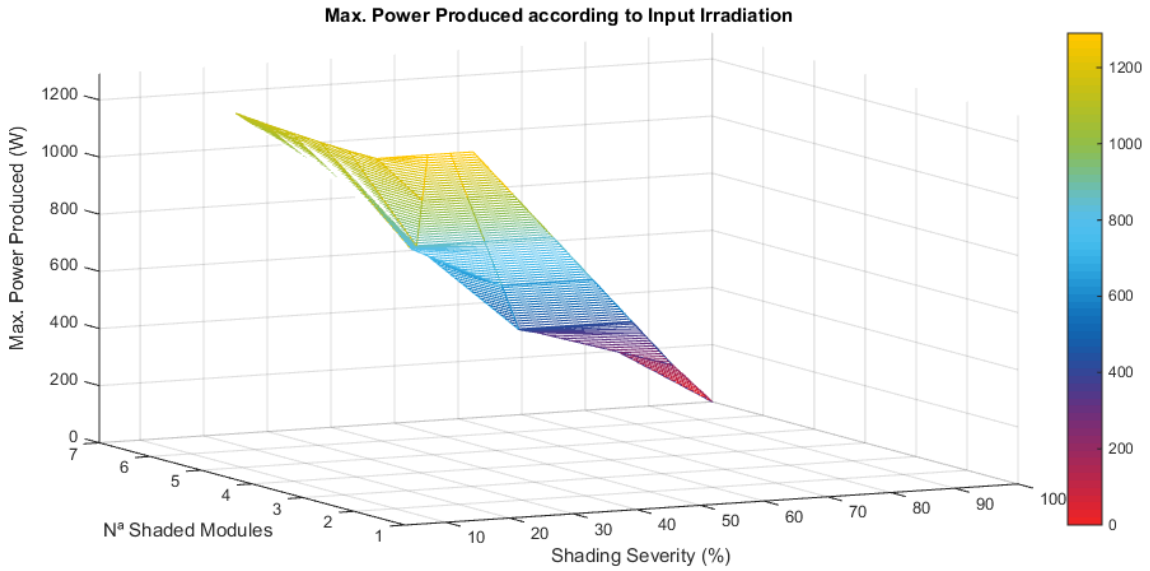


Figure 3.12: Correlation between maximum power produced, number of shaded modules and shade severity plotted using MATLAB.

with the number of shaded modules and the shade severity.

This tool permits to estimate the accuracy of a particular fit, based upon the standard goodness-of-fit statistics such as R-Square, Adjusted R-Square, Sum of Squares Due to Error and Root Mean Squared Error.

For this determination, only the R-Square value was take into account:

**R-square** , is a statistical measure of how close the data is to the fitted regression line. It is the square of the correlation between the response values and the predicted response values. R-square can take on any value between 0 and 1, with a value closer to 1 indicating that a greater proportion of variance is accounted for by the model and 0 indicating that the model explains none of the variability of the response data around its mean. R-square value represents the percentage the fit explains of the total variation in the data about the average (Frost, 2013);

**Analysis and Results:**

Using a trial and error process on the cftool app, it was possible to find an equation that fits the previous plotted data set, correlating the maximum power production with the number of shaded modules and the shade severity, to an equation.

The fit obtained is can be visualized below in figure 3.13.

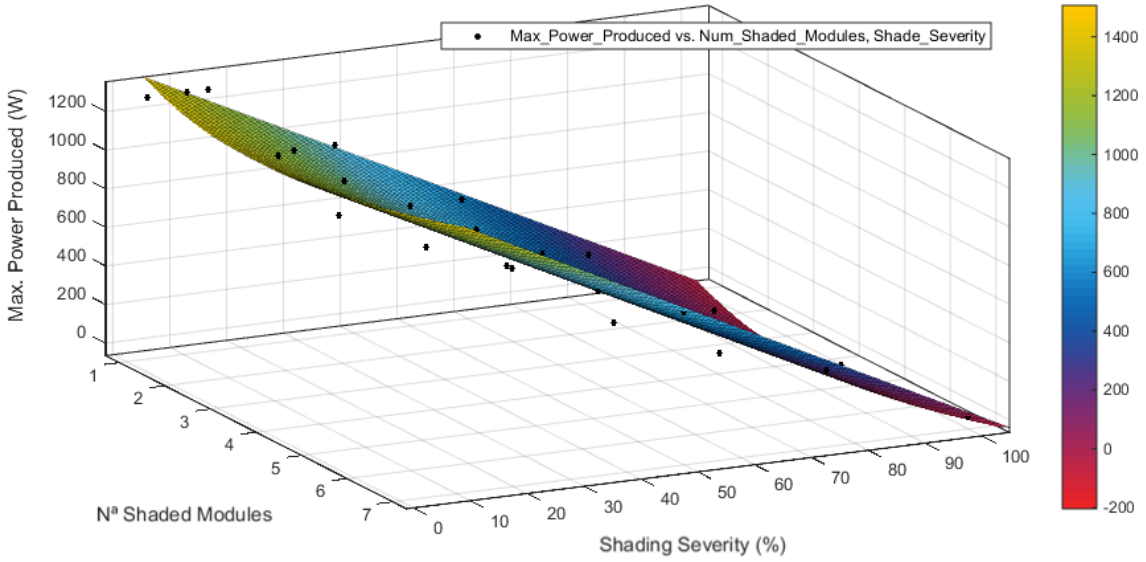


Figure 3.13: Fit of the correlation between maximum power produced, number of shaded modules and shade severity plotted using MATLAB'c fitting tool - Cftoll.

The equation obtained on custom equation mode is shown below on equation 3.2:

$$f(x,y) = ax^3 + (b+x)^2 + cx + dy + e \tag{3.1}$$

$$f(x,y) = 0.97x^3 + (-57.21+x)^2 + 57.66x + -14.56y - 1801 \tag{3.2}$$

Where the coefficients and respective 95% confidence bounds are:

- $a = 0.9698,\ (0.0744\,;\ 1.865)$
- $b = -57.21,\ (-8.845 \times 10^7\,;\ 8.845 \times 10^7)$
- $c = 57.66,\ (-1.769 \times 10^8\,;\ 1.769 \times 10^8)$
- $d = -14.56,\ (-16.59\,;\ -12.54)$
- $e = -1801,\ (-1.012 \times 10^{10}\,;\ 1.012 \times 10^{10})$

And the Goodness-of-fit:
R-square: 0.9473

**Comments:**

According to the specifications of the goodness-of-fit it is possible to conclude that this is a good approximation according to the value of R-Square, approximately 95%, as it is extremely close to 1.

### 3.2.4 Determination of the Annual Energy Production of a Single PV Module Assuming a Previously Defined Shade

For this task, the single module installation shown previously on figure 3.7 was used. The goal was to determinate the power production of this particular installation during one year assuming a predefined shade cast on the single PV module.

In order to run the model, initially it was necessary to collect data for several parameters, as follows:

$t$, Local Solar Time[7] (hh:mm);

$G$, Global Irradiance[8] ($W/m^2$);

$Gd$, Diffuse Irradiance[9] ($W/m^2$);

$Td$, Average Daytime Temperature ($^\circ$ C).

A table similar to 3.1 was created for each month of the year using data from PVGIS, using the solar radiation database PVGIS-CMSAF (JRC's Institute for Energy and Transport, 2012a). Solar times between 4:37 and 18:22, with 15 minute gaps were used. The location considered was Lisbon (Lat: 38.722; Long: -9.139) and it was assumed an inclination of plane of 35°and orientation of plane (azimuth) of 180°(or 0°).

All 48 column vectors (12 months $\times$ 4 columns) were exported to variable vectors in MATLAB, for convenience of use.

The first part of the experiment consisted on calculating the maximum power production of the installation , using the irradiance values for each month.

To facilitate the input of the necessary values on each simulation and the usage of the collected data from PVGIS, a MATLAB script was developed. The role of the script is to load the exported data and use it accordingly to the shading caused by an object defined as *object 1*. The shade from this object form factor and the hour interval when it affects the power production can be visualized further.

For example, for solar hours when shade is cast upon the PV module, the script chooses to input to Simulink *Irradiance* value, the diffuse irradiance (Gd) or no irradiance at all (0 $W/m^2$), to simulate the effect of a soft or a hard shade respectively, instead of

[7] Local Solar Time, is the time based on the rotation of the earth and position of the sun in the sky with respect to the local meridian.

[8] Global Irradiance, is the total amount of solar irradiance entering the surface of the Earth.

[9] Diffuse Irradiance, represents a short wavelength radiation coming from all parts of the sky, describes the sunlight that has been scattered by molecules and particles in the atmosphere but that has still makes it down to the surface of the earth.

Table 3.1: Data gathered using PGVIS-CMSAF database report for a daily profile of the month June for the location Lisbon.

| Solar Time | G | Gd | Td |
|---|---|---|---|
| 04:37 | 0 | 0 | 15.9 |
| 04:52 | 0 | 0 | 15.9 |
| 05:07 | 22 | 22 | 16.0 |
| 05:22 | 34 | 34 | 16.0 |
| 05:37 | 47 | 46 | 16.2 |
| 05:52 | 59 | 58 | 16.3 |
| 06:07 | 70 | 69 | 16.6 |
| 06:22 | 92 | 69 | 16.9 |
| 06:37 | 132 | 81 | 17.2 |
| 06:52 | 174 | 92 | 17.6 |
| 07:07 | 219 | 103 | 18.1 |
| 07:22 | 266 | 113 | 18.6 |
| 07:37 | 314 | 122 | 19.0 |
| 07:52 | 361 | 131 | 19.5 |
| 08:07 | 409 | 138 | 20.0 |
| 08:22 | 455 | 145 | 20.5 |
| 08:37 | 500 | 151 | 21.0 |
| 08:52 | 543 | 156 | 21.5 |
| 09:07 | 585 | 161 | 21.9 |
| 09:22 | 624 | 164 | 22.2 |
| 09:37 | 660 | 168 | 22.6 |
| 09:52 | 694 | 170 | 22.9 |
| 10:07 | 725 | 172 | 23.2 |
| 10:22 | 753 | 174 | 23.4 |
| 10:37 | 777 | 175 | 23.7 |
| 10:52 | 798 | 176 | 23.9 |
| 11:07 | 816 | 177 | 24.1 |
| 11:22 | 831 | 177 | 24.3 |

| Solar Time | G | Gd | Td |
|---|---|---|---|
| 11:37 | 841 | 177 | 24.5 |
| 11:52 | 849 | 178 | 24.6 |
| 12:07 | 852 | 178 | 24.8 |
| 12:22 | 852 | 178 | 25.0 |
| 12:37 | 849 | 178 | 25.1 |
| 12:52 | 841 | 177 | 25.3 |
| 13:07 | 831 | 177 | 25.4 |
| 13:22 | 816 | 177 | 25.5 |
| 13:37 | 798 | 176 | 25.6 |
| 13:52 | 777 | 175 | 25.7 |
| 14:07 | 753 | 174 | 25.8 |
| 14:22 | 725 | 172 | 25.8 |
| 14:37 | 694 | 170 | 25.9 |
| 14:52 | 660 | 168 | 25.9 |
| 15:07 | 624 | 164 | 25.8 |
| 15:22 | 585 | 161 | 25.7 |
| 15:37 | 543 | 156 | 25.6 |
| 15:52 | 500 | 151 | 25.5 |
| 16:07 | 455 | 145 | 25.4 |
| 16:22 | 409 | 138 | 25.2 |
| 16:37 | 361 | 131 | 25.0 |
| 16:52 | 314 | 122 | 24.7 |
| 17:07 | 266 | 113 | 24.5 |
| 17:22 | 219 | 103 | 24.2 |
| 17:37 | 174 | 92 | 23.9 |
| 17:52 | 132 | 81 | 23.6 |
| 18:07 | 92 | 69 | 23.2 |
| 18:22 | 70 | 69 | 22.9 |

inputting total irradiance (G) representing a situation with no shade. This will produce a substantially lower power production for that time.

The script runs the Simulink model 672 times (56 lines of PVGIS collected data $\times$ 12 months) and saves the estimated max power production for each reading on a vector (*Pmax*). This code can be consulted in the *Appendix* section (chapter A) under listing A.3.

**Procedure:**

To determine the solar hours intervals affected by the shade for each month, a solar path chart was drawn, using the same latitude and longitude as in PVGIS and UTC timezone for the year 2015. This work was conducted recurring to the *University of Oregon Sun Path Chart Program* (available online at `http://ecee.colorado.edu/~ecen2060/matlab.html`).

This chart plots dates 30 or 31 days apart, between solstices from June through December, which would be exactly the same as if it were from December through June in terms of solar elevation per solar azimuth as this values are considered the same along the year. Per example, January has the same solar elevation per solar azimuth as November, so do February and October, and so on. The resulting chart is represented figure 3.14.

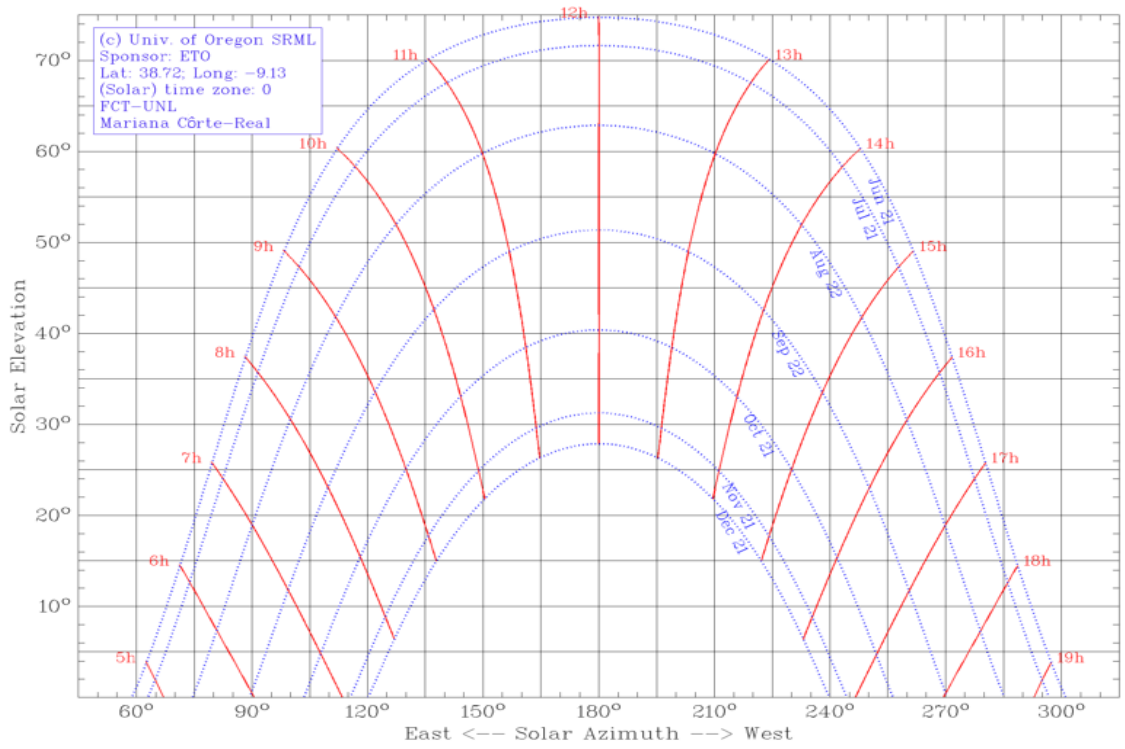


Figure 3.14: Sun path chart of Lisbon 2015 designed using *University of Oregon Sun Path Chart Program* available online. Source: University of Oregon, Solar Radiation Monitoring Laboratory, 2007.

Once the sun-path chart was obtained, the shade caused by *object 1* was added to the chart so that the solar hours and months affected by shade could be easily identified, as can be seen in figure 3.15.

The affected solar times were defined by observation of the chart. This process consists of identifying the crossing points where each month parable meets the boundaries of the gray rectangle which represents the shade from *object 1*. For this purpose a dashed green line was traced between such crossing points and the top of the graph to facilitate the reading.

This process can be visualized on figure 3.16 and the obtained affected solar hour intervals are displayed below, in table 3.2.

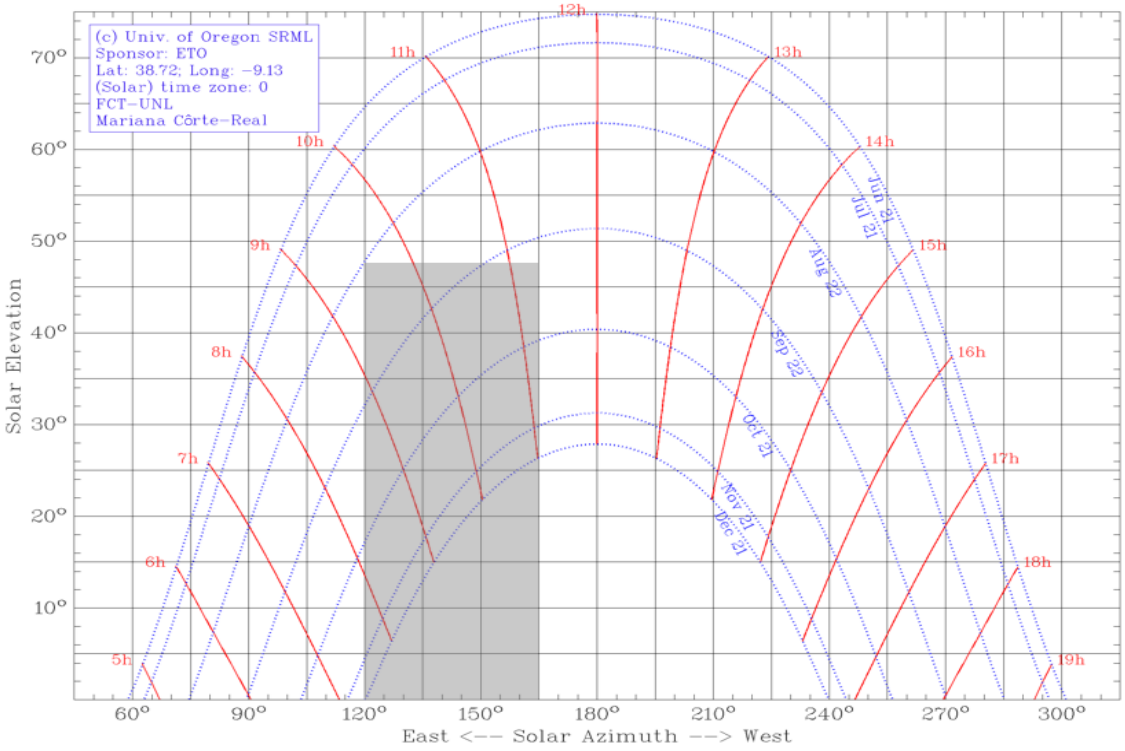


Figure 3.15: Sun path chart of Lisbon 2015 with shade cast by *object 1*.

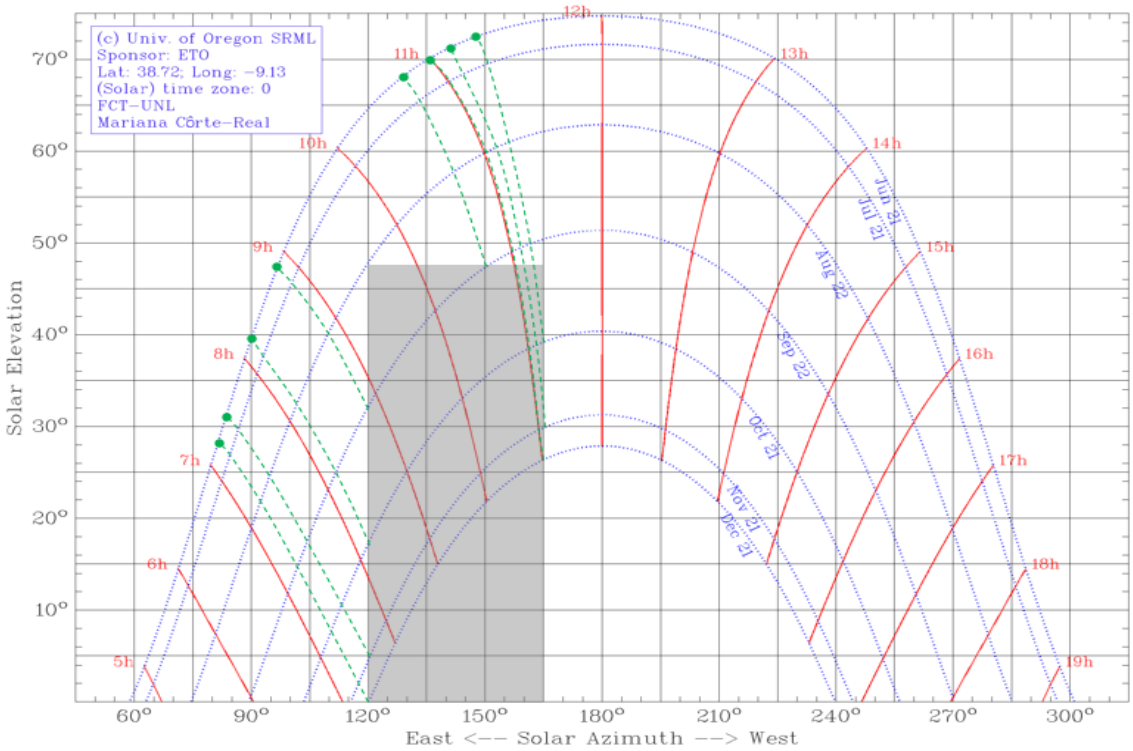


Figure 3.16: Parameters of the PV voltage-input module mask designed. Source: University of Oregon, Solar Radiation Monitoring Laboratory, 2007.

Table 3.2: Interval of solar time where the installation is suffering from the presence of shade from object 2.

| Months | Solar Time Interval |
|---|---|
| December | 07:20 - 11:00 |
| January & November | 07:35 - 11:05 |
| February & October | 08:05 - 11:10 |
| March & September | 08:55 - 10:45 |

**Following steps:**

Considering the case of January, the power production pattern behaves as shown in figure 3.17 below. If considered that while shaded (between 8:00 h and 9:30 h), the module is receiving diffuse irradiation, the power production plot corresponds to figure 3.17a. Conversely if it is assumed that, there is no irradiation on the module while shaded, the power production plot corresponds to the one in figure 3.17b.

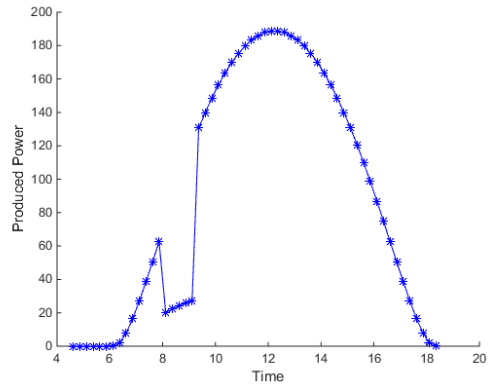


(a) Power production from January if diffuse irradiance is cast upon the module when shaded.

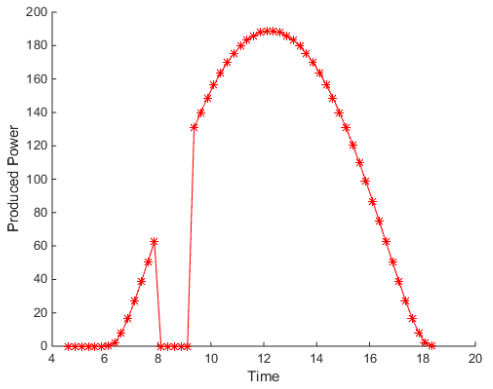


(b) Power production from January if zero irradiance is cast upon the module when shaded.

Figure 3.17: Power production from January for diffuse or zero irradiance cast upon the module when shaded by *object 1*.

In order to analyse the behaviour throughout one entire year, let us first consider a situation where no shade is cast upon the PV module, i.e., total irradiation values are always considered as input on the PV module. This global monthly power production is represented by the plot on figure 3.18.

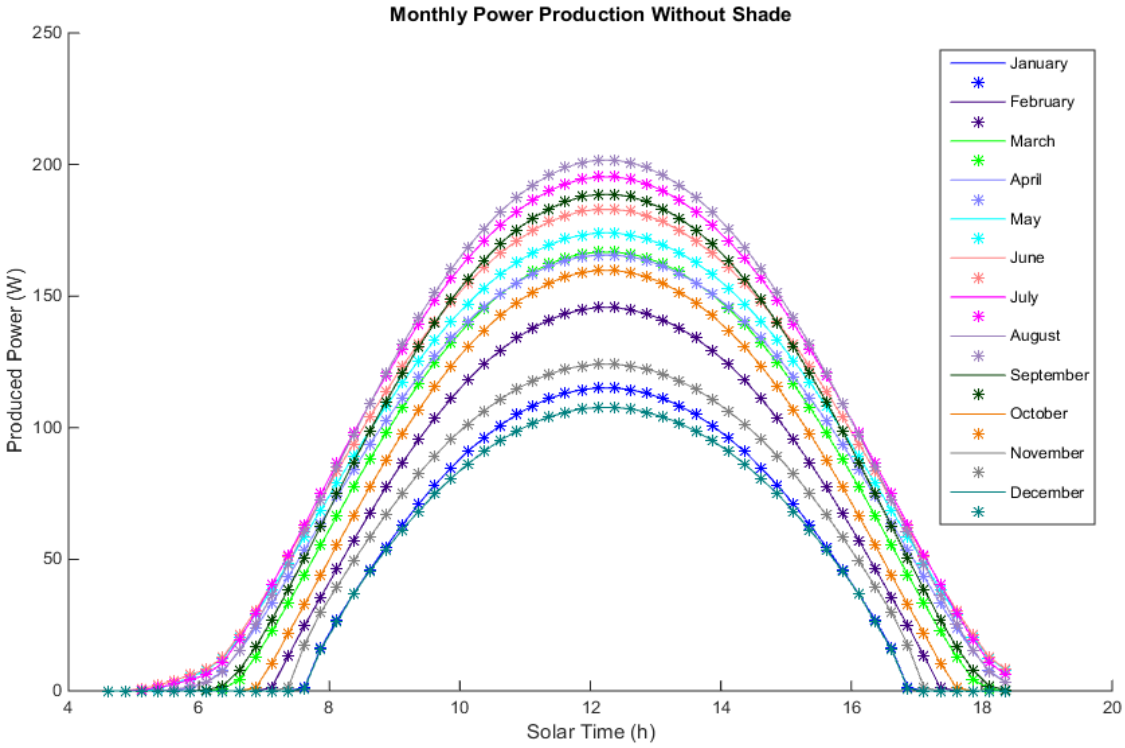


Figure 3.18: Monthly power production estimation without shade - simulated using Simulink and plotted using MATLAB.

The impact in each month's power production taking into account the power losses due to the *object 1* presence, can be seen in figure 3.19. In figure 3.19a the power production calculus is made considering diffuse irradiation when shaded, and in figure 3.19b, zero irradiation is considered for the same condition.

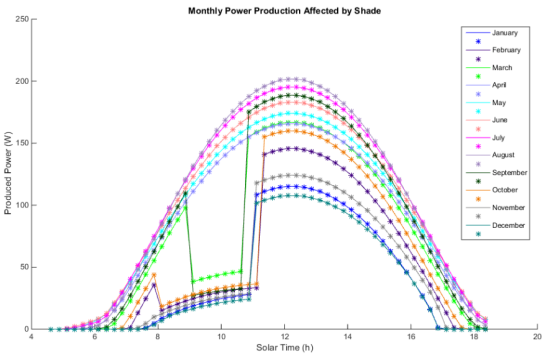


(a) Monthly power production estimation considering diffuse irradiation is cast on the module when shaded.

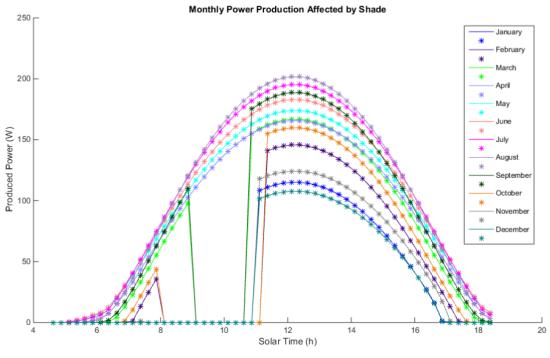


(b) Monthly power production estimation considering no irradiation is cast on the module when shaded.

Figure 3.19: Monthly power production estimation considering diffuse or zero irradiation is input on the installation when shaded by *object 1*.

**Analysis and Results:**

All three power production scenarios (total irradiation, diffuse irradition while shaded and zero irradiation while shaded) were used to calculate the energy production and the loss of energy due to this particular shade.

From the power yearly power production, represented on figure 3.18, it is possible to obtain the maximum estimated power produced, which is then used to calculate the maximum energy production estimated for this installation.

In equation 3.3 the energy general expression is displayed.

$$E = \sum P \times t \tag{3.3}$$

where:

$E$ is the Produced Energy (kWh);

$P$ is the Produced Power (kW);

$t$ is the Number of Hours producing energy (hour).

By Simulink simulation, it was possible to gather daily power production estimations, 15 minutes apart, for each month. Based on equation 3.3, those values were used to calculate the yearly energy production.

Firstly, the power production for each month was multiplied by the number of days in the month to obtain the monthly average production. All twelve values were added and the result was divided by four. This division is necessary because four power values are calculated per hour.

The mentioned calculation can be resumed in equation 3.4, where the the annual energy production is determined in kWh.

$$\begin{aligned} E &= \left( \sum_{Jan} P \times 31 + \sum_{Feb} P \times 28 + \cdots + \sum_{Nov} P \times 30 + \sum_{Dec} P \times 31 \right) \times 0.25 \Leftrightarrow \\ &\Leftrightarrow E = 433.15 \text{ kWh} \end{aligned} \tag{3.4}$$

A MATLAB script was developed to run the simulation and to manage the required steps to control the variation on the inputs of the installation and to save the produced power value for each situation. The code on the script can be consulted in the *Appendix* section (chapter A) under listing A.3.

Once obtained the maximum energy value for the installation, it was possible to compare it with the energy production values for the simulated shaded cases.

For **simulation 1**, where no shade is cast upon the used PV module, **simulation 2**, where diffuse irradiation is used for the shaded interval of solar time, and for **simulation**

**3**, where zero irradiation is input to the module while shaded, a table of simulated power and energy produced was created, table 3.3.

Table 3.3: Power and energy production for simulations 1, 2 and 3

| | Simulation 1 | Simulation 2 | Simulation 3 |
|---|---|---|---|
| Energy Generated (kWh) | 433.15 | 391.75 | 377.21 |

**Comments:**

The maximum energy produced value is within the typical range for a single 215 W module.

Power and energy productions in simulations 2 and 3 are consistent with the values obtained for simulation 1.

### 3.2.5 Comparison between the impact of a calculated Shade Factor on the production of an installation with the one simulated

The goal of this task was to compare two theoretical values:

- Severity or impact of shading given by the Shade Factor (SF), calculated based on the method expressed in *Guide to the Installation of Photovoltaic Systems*;
- Severity or impact of shading simulated using Simulink design on figure 3.7 using the method detailed in sub-subsection 3.2.4.

These are detailed further in this sub-subsection.

**Shade Factor Calculation Based on the *Guide to the Installation of Photovoltaic Systems* Method:**

As seen in subsection 2.4.1 of the State of The Art, it is possible do determine an proximate percentage of energy lost due to shading using an sun path chart by drawing segments such as in shown in figure 2.19.

By comparison of the solar path chart drawn with the help of University of Oregon Sun Path Chart Program (figure 3.14) with the method presented in *Guide to the Installation of Photovoltaic Systems* for the SF calculus (figure 2.19 shown in subsection 2.4.1 of the State of The Art), it was possible to draw a new sun path diagram for Lisbon, with the 84 segments essential to the calculus of the SF. These images are shown once more below in figure 3.20 for better understanding.

To determine the size and position of each of the 84 segments mentioned in subsection 2.4.1, a strict analysis of the chart made using the method explained on *Guide to the Installation of Photovoltaic Systems* (figure 3.20b). From this analysis, it was possible to verify that the segments closer to the solar noon are typically smaller, i.e., represent less solar

time than the ones closer to sun rise and down solar time. It was also accessed the times from which de solar produces should not be counted, shown in dark gray on the edges of the chart.

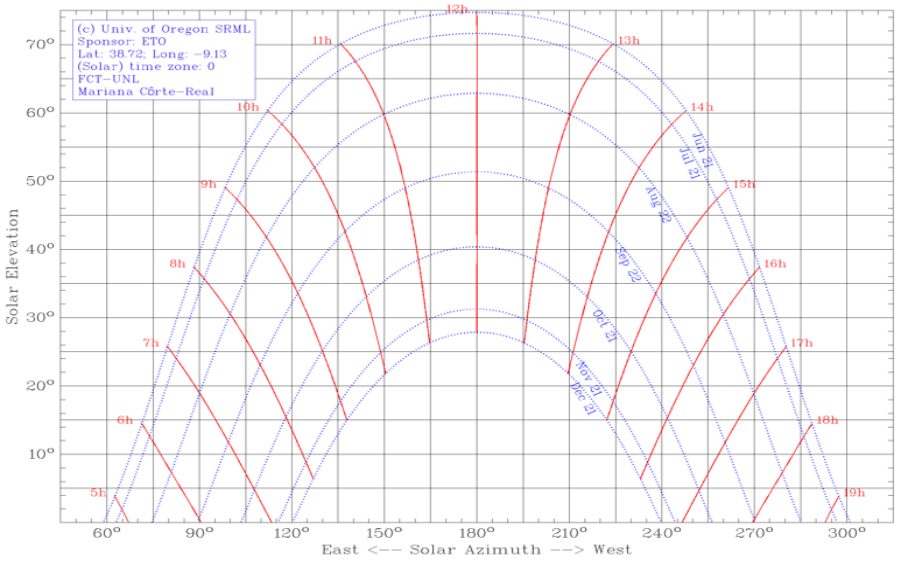


(a) Sun path chart of Lisbon 2015. Source: University of Oregon, Solar Radiation Monitoring Laboratory, 2007

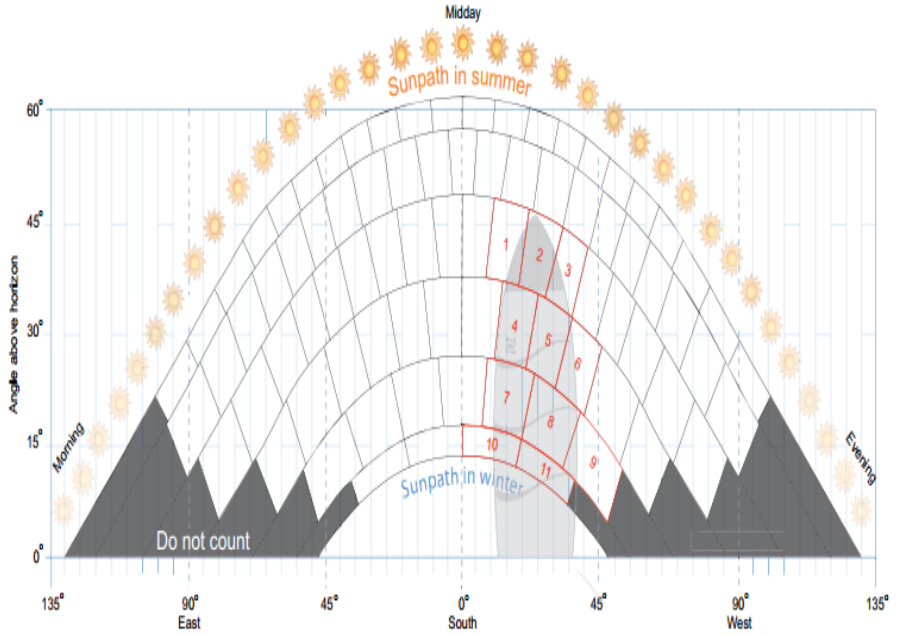


(b) Sun path Diagram used to calculate de SF from an object on a specific installation. Source: (MCS), 2012

Figure 3.20: Comparison between Images (a) and (b) to design a new sun path diagram with 84 segments, essential to the calculus of the SF.

The outcome was made using *SketchUp Make* and can be seen below on figure 3.21.

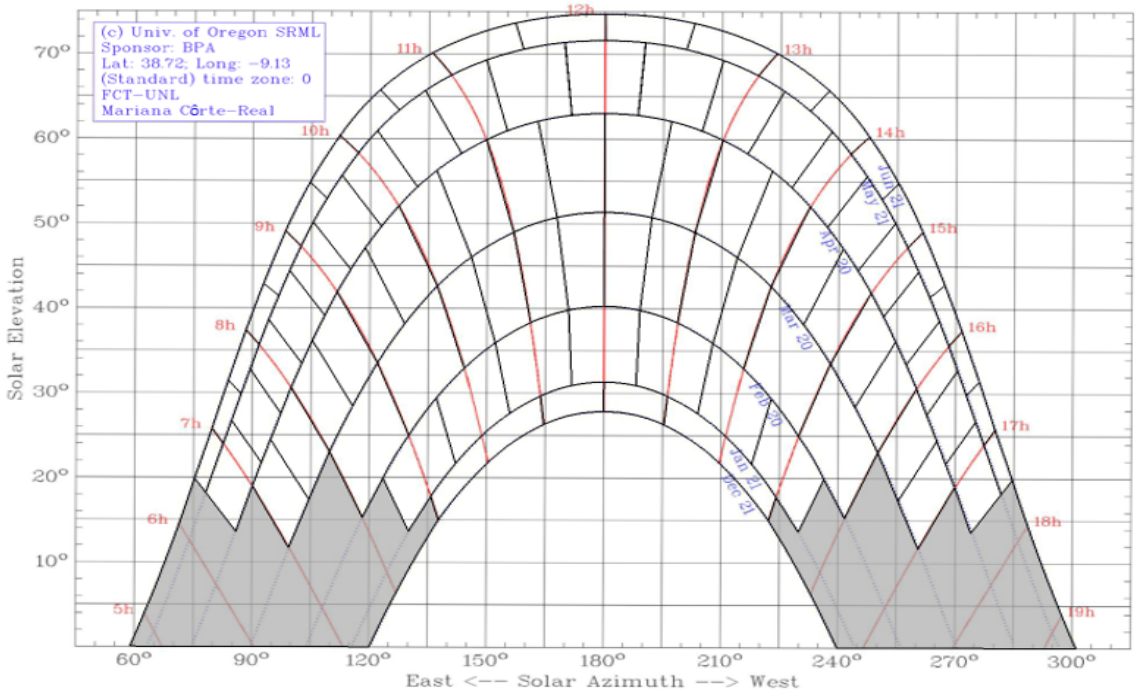


Figure 3.21: New solar path chart created by comparison of figures 3.20a and 3.20b.

The next step was to add the shadow cast by *object 1*. It was decided to use the same object as in the energy loss calculus presented in section sub-subsection 3.2.4 to increase the information gathered for this specific shaiding situation.

As can be seen in figure 3.22, the area of the shade cast by the object covers 15 segments of the sun path chart, which means that, according to the *Guide to the Installation of Photovoltaic Systems* explained previously shown in subsection 2.4.1 of the State of The Art, the SF in this case is equal to 85%.

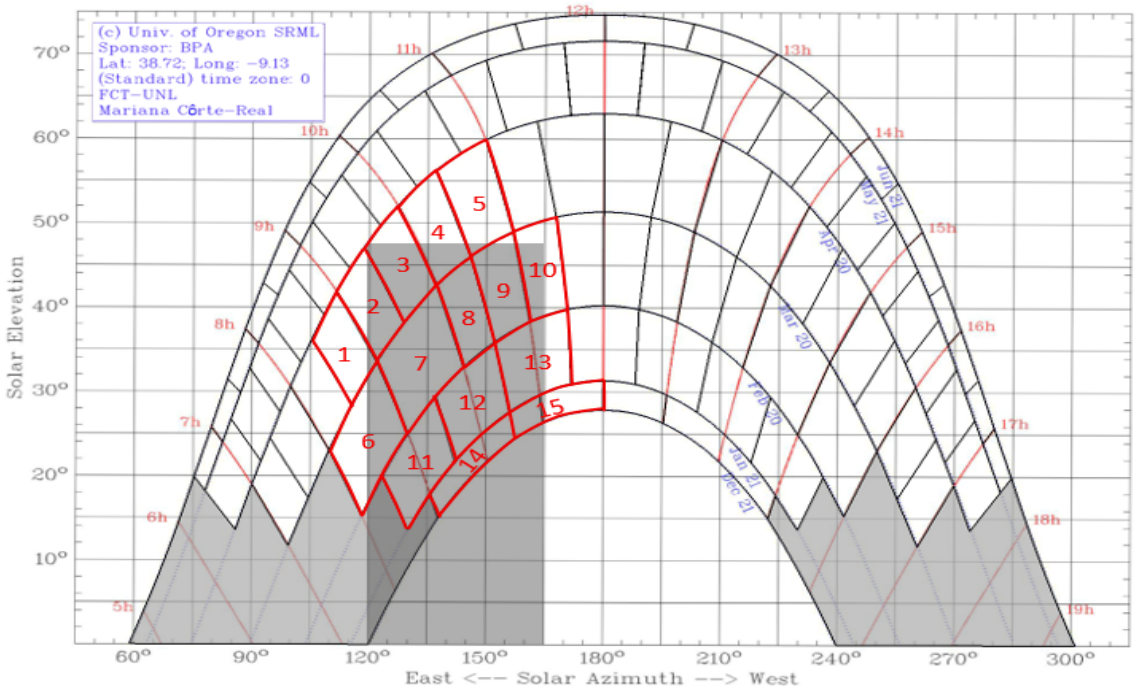


Figure 3.22: SF calculus of *Object 1* using the solar path chart developed for this propose.

**Severity of Shading Simulated using Simulink:**

For the percentage of energy loss simulated, the single module installation shown in figure 3.7 was used.

The goal was to obtain the percentage of loss due to the shade cast by *object 1*. To do this a comparison between the obtained energy values for the shaded situations simulated, with the simulation values where no shade is cast in the installation. This values were calculated in subsection 3.2.4 and are expressed in table 3.3.

Taking into account the acquired values, the percentage of loss due to shading for both of the shaded cases was calculated using the equation 3.5, represented below.

$$\text{Percentage of Loss} \;=\; 100 - \frac{\text{Energy Produced} \times 100}{\text{Maximum Energy}} \tag{3.5}$$

The calculated values for simulation 2 and 3, where diffuse irradiation is used for the shaded interval of solar time, and zero irradiation is input to the module while shaded, respectively. A table with the obtained percentage values is expressed below (table 3.4).

Table 3.4: Percentage of energy loss due to shading for simulations 2 and 3.

| | Simulation 2 | Simulation 3 |
|---|---|---|
| Percentage of Loss due to shading (%) | 9.56 | 12.91 |

**Further Development using Different Objects:**

To obtain a better reasoned conclusion on this matter, both this methods were re-made using two other different objects, *object 2* and *object 3* for the same installation and location.

For the Simulink simulations, the process expressed in sub-subsection 3.2.4 was repeated to calculate the power and energy productions for the same shaded situations detailed previously. Next, the method explained in this sub-subsection was used once more to calculate the percentages of energy loss as was made for *object 1*.

*Object 2* affects the evening energy production of this installation as can be seen in figure 3.23.

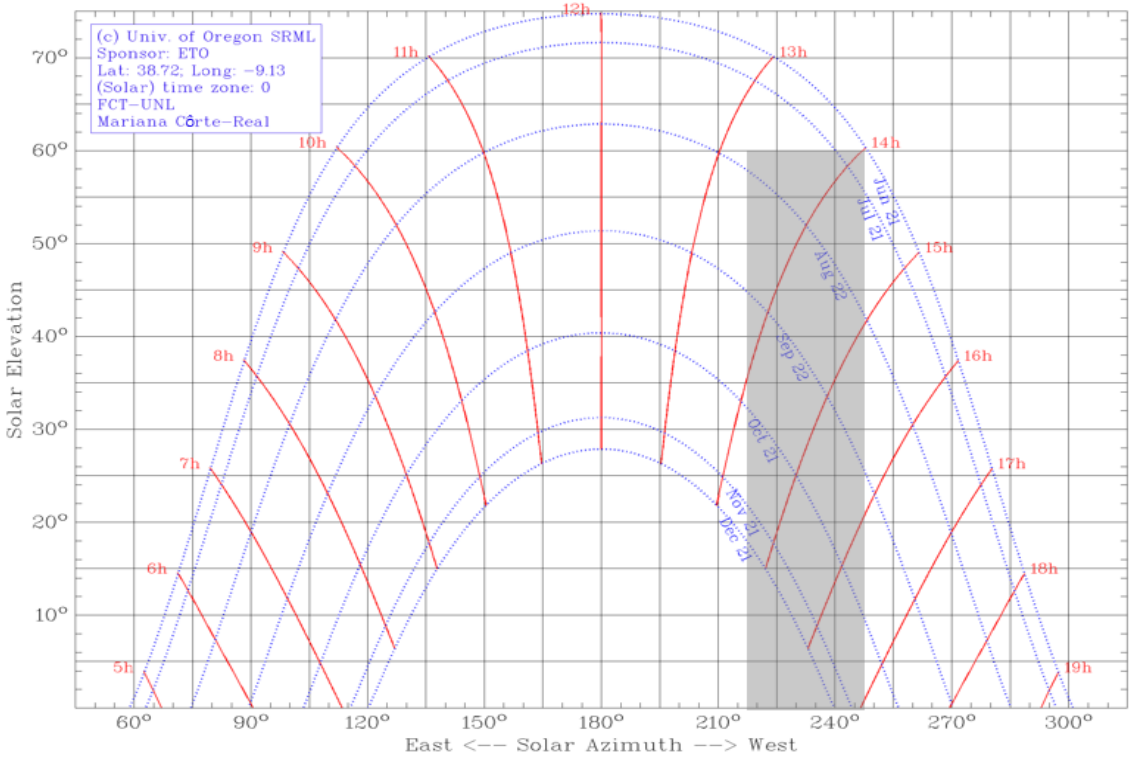


Figure 3.23: Display of *Object 2* on the sun path chart.

As happens in sub-subsection 3.2.4 a table of the intervals where shaded is cast upon the PV module was created to facilitate the simulation. The mentioned table is expressed below (table 3.5).

Once known the starting in ending solar hours when *object 2* affects the installation, a modification was made in the MATLAB script referring to the single module installation, expressed in listing A.3 in chapter A, where the variables for the shaded solar time interval were replaced by the ones in table 3.5.

For *object 3*, the exact same steps were followed. The object affects the hours where the sun is higher for the coldest months, as seen in figure 3.24, and the resultant solar time table is expressed in table 3.6.

Table 3.5: Interval of solar time where the installation is suffering for the presence of shade from object 3.

| Months | Solar Time Interval |
|---|---|
| December | 14:50 - 18:00 |
| January & November | 14:40 - 17:30 |
| February & October | 14:10 - 16:55 |
| March & September | 13:45 - 16:00 |
| April & August | 13:20 - 15:00 |
| May & July | 13:50 - 14:15 |

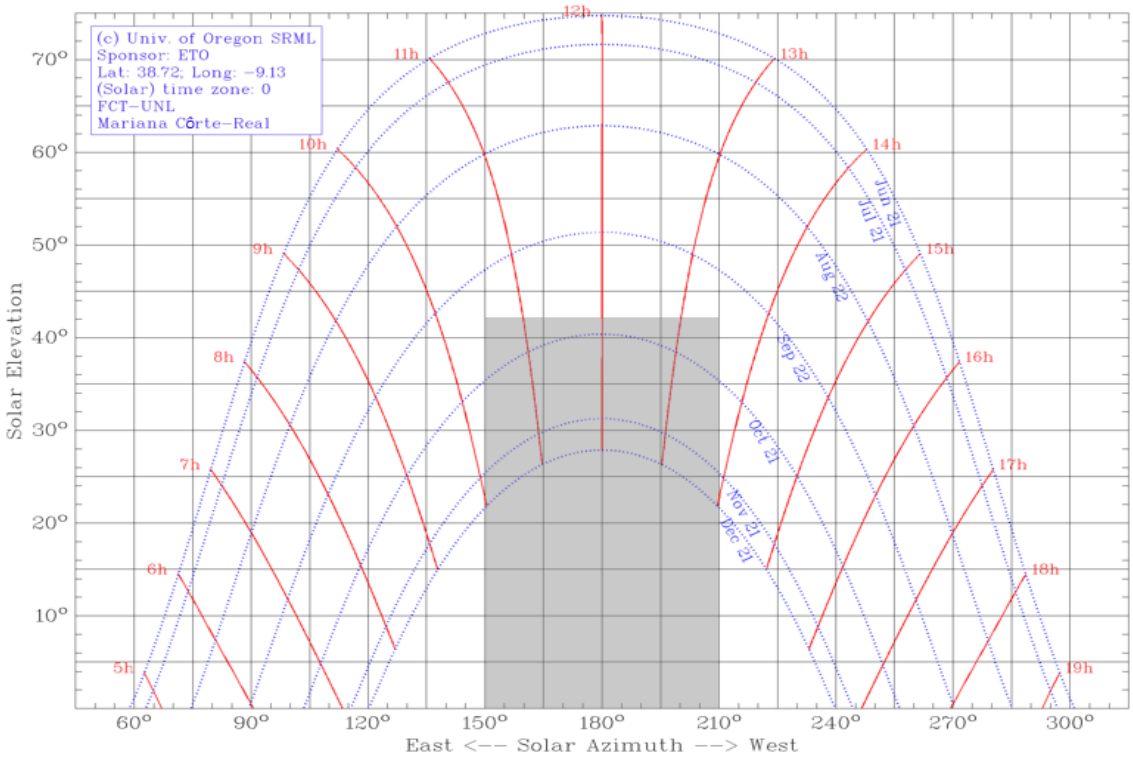


Figure 3.24: Display of *Object 3* on the sun path chart.

Table 3.6: Interval of solar time where the installation is suffering for the presence of shade.

| Months | Solar Time Interval |
|---|---|
| December | 10:00 - 14:00 |
| January & November | 10:10 - 13:50 |
| February & October | 10:20 - 13:40 |

Simulation results coming from the Simulink simulations performed were summarized in table 3.7.

Table 3.7: Simulation results.

| | | Simulation 2 | Simulation 3 |
|---|---|---|---|
| *Obj. 1* | Energy Generated (kWh) | 391.75 | 377.21 |
| | Loss Percentage due to shading (%) | 9.56 | 12.91 |
| *Obj. 2* | Energy Generated (kWh) | 376.55 | 357.84 |
| | Loss Percentage due to shading (%) | 13.07 | 17.39 |
| *Obj. 3* | Energy Generated (kWh) | 391.92 | 378.50 |
| | Loss Percentage due to shading (%) | 9.52 | 12.62 |

Following, both Shade Factor values from objects *2* and *3* were calculated using the same method used for object 1, expressed above in this sub-subsection.

As can be seen by figures 3.25 and 3.26, applying the process demonstrated previously in figure 3.22, it was possible to determine that for *object 2*, 18 segments are covered by shade on the sun path chart, and 17 segments are covered for *object 3*, which means the SF in this situations is 82% and 83% respectively.

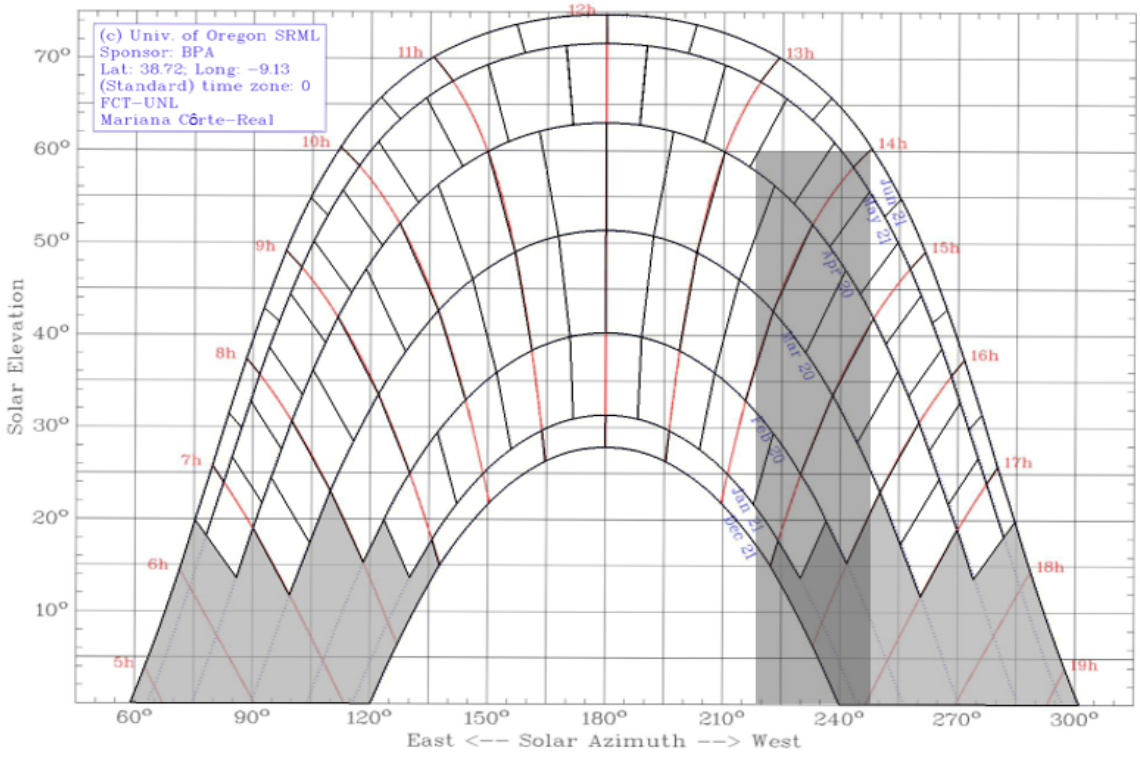


Figure 3.25: SF calculus of *Object 2* using the solar path chart developed for this propose.

**Comparison and comments on the Results:**

A comparative table containing the obtained energy loss percentages obtained for both methods is shown below (table 3.8).

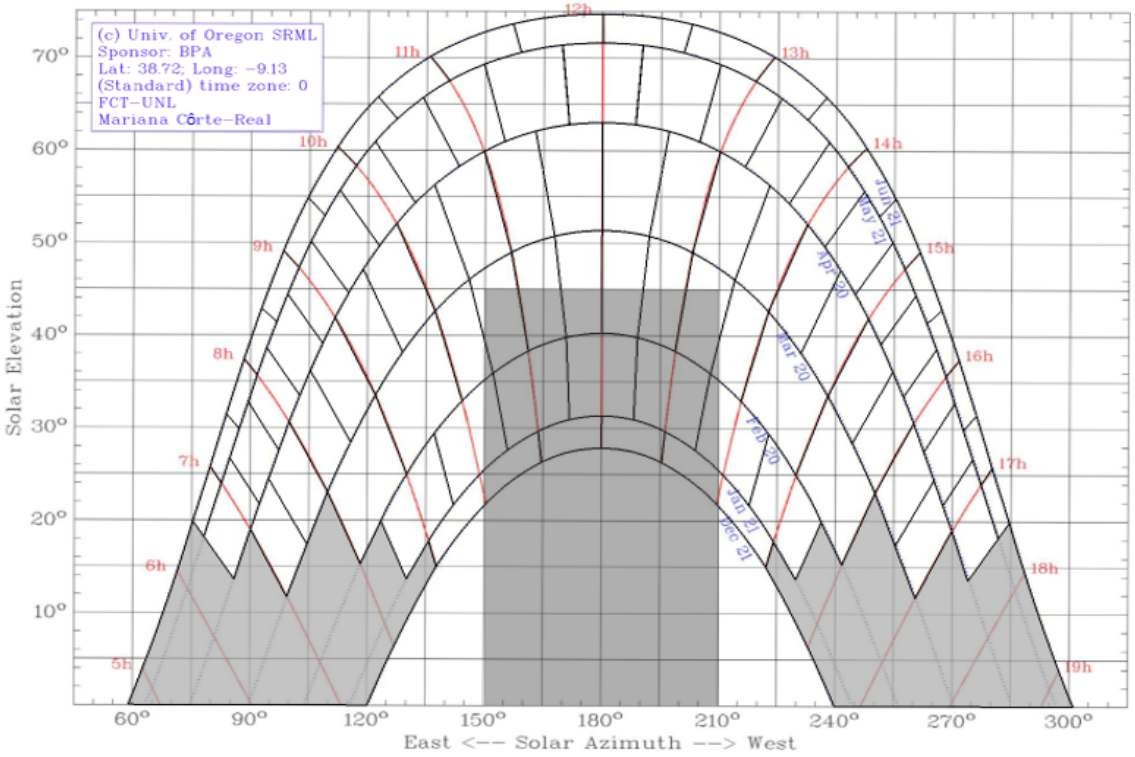


Figure 3.26: SF calculus of *Object 3* using the solar path chart developed for this propose.

Table 3.8: Power and energy production for simulations 1, 2 and 3

| | Simulation 2 | Simulation 3 | Shade Factor |
|---|---|---|---|
| *Object 1* | 9.56 | 12.91 | 15 |
| *Object 2* | 13.07 | 17.39 | 18 |
| *Object 3* | 9.52 | 12.62 | 17 |

As can be seen table 3.8, the percentage calculated by the Shade Factor value (method expresses in the *Guide to the Installation of Photovoltaic Systems*) is closer to the one obtain in simulations 3 using the Simulink simulation method where no irradiation is cast on the installation while shaded.

Although the percentages obtained are very similar for this two cases, the method expressed in *Guide to the Installation of Photovoltaic Systems* should have closer percentage values when compared with simulations 2 due to the way the shade draw is made, where, as seen in subsection 2.4.1 of the State of The Art, a shadow from an object wouldn't be obscuring the total area drawn in the sun-path diagram, meaning it would be more accurate to use and average percentage of the values obtained for simulations 2 and 3, so that both diffuse irradiation and zero radiation were considered for this cases, specially for objects over 10 m far from the installation.

The method expressed in *Guide to the Installation of Photovoltaic Systems* is said to have 10% range of error when compared to a real installation. It was concluded that this is a good approximation method even though it tends to approximate the shade factor by

excess.

It was also concluded that the segments sizing should be more strict on this method, segments closer to noon time should be even smaller and the ones closer to sun rise and down should be slightly bigger, the total number of segments could remain unaltered but each segments sizing should be reviewed.

CHAPTER 4

# EXPERIMENTAL RESULTS
# TESTING SHADINGS ON PHOTOVOLTAIC PANELS

This chapter introduces and details the practical implementations performed in the thesis.

The several stages of the practical implementation are fully described below, and have been organized in a section and sub-subsection fashion. Each section begins with an explanation of the experiment, followed by a brief discussion on the results obtained.

Results and conclusions are discussed along the chapter at the end of the explanation of each phase.

## 4.1 Test of Isolated Modules

### 4.1.1 Evaluation of IV and PV Curves on Photovoltaic Modules

By recording current and voltage outputs of a solar module while connected to a variable resistor, it is possible to determine the current-voltage and power-voltage relations, also called, the IV and PV characteristic curves of a solar module.

To obtain photovoltaic IV and PV characteristic curves, experiments 1 and 2 were performed, using one solar module under with different conditions. Their main goal is to observe the relationship of current, voltage and power in each solar panel and compare it with their characteristic values under similar conditions (irradiance and temperature).

This relation was made using a Microsoft Excel spreadsheet. The current and voltage of each data set is multiplied together to yield the corresponding power at that operating point. The power is then plotted as a function of voltage. The maximum value of the power curve corresponds to the maximum power point of the solar module.

**Experiment Specifications**
**Material Used:**

- HIP-215NHE5 Sanyo HIT (Heterojunction with Intrinsic Thin layer) Photovoltaic Module;
- One Ammeter and one Voltmeter or two Multimeters for voltage and current measurement (AMPROBE 37XR-A and ISO-TECH IDM9191E Multimeters);
- One Solar Power Meter for solar irradiance measurement (Lafayette SMB-SOLAR Solar Power Meter with incorporated Multimeter);
- Variable Resistors of different maximum values of resistance and current, according to the irradiance value and consequent current production of the module;
- One TFA Infra-red Thermometer;
- Alligator Clips;
- Wire Probes;
- Sun light or Artificial Light Source.

**Steps of the Procedure:**

1. Setup the circuit shown in figure 4.1;
2. Mount the solar module facing the source of light;
3. Measure the short circuit current, by shorting the variable resistor terminals;
4. Measure the open circuit voltage, by disconnecting the variable resistor;
5. Change the resistance of the variable resistor within the desired current or voltage range and record the resulting current and voltage values;
6. When the rate of changes of voltage measurements starts to increase more rapidly, decrease the range change in order to to obtain more data points in the steepest region of the curve;
7. Continue the procedure until the measured voltage value equals 0 V, or, until the maximum resistance in the variable resistor is reached;
8. Input the data gathered to the Microsoft Excel spreadsheet and plot the IV curve, with current in the vertical axis, and voltage in the horizontal axis;
9. Calculate the power for each point of current and voltage by multiplying them and plot the PV graph, with power in the vertical axis, and the voltage in the horizontal axis;
10. Identify the maximum power point (MPP) in the power curve, and find the respective voltage and current.

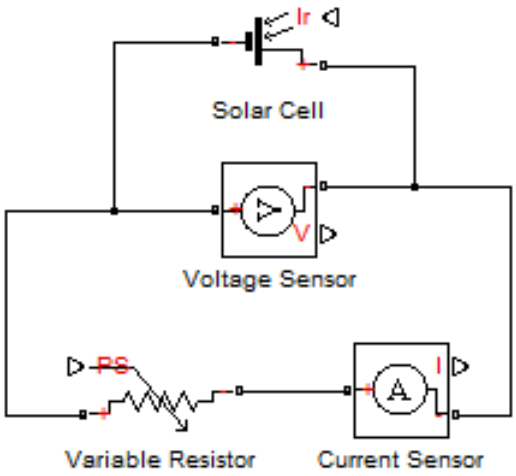


Figure 4.1: Diagram of the circuit composed of a photovoltaic module, designed using Simulink.

### 4.1.2 Experiment 1

At short circuit, the module produces electric current but no voltage while at open circuit, it produces voltage but no current.

The measurements to obtain photovoltaic IV and PV characteristic curves, which allow the study of the relationship between current and voltage, and power and voltage generated by the solar panel used, were made under the conditions summarized on the following table (table 4.1):

Table 4.1: External Conditions for Experiment 1.

| Experiment 1 - Existing Conditions | |
|---|---|
| Date | $4^{th}$ of June 2015 |
| Time | 14:35 |
| Solar Time | 13:58 |
| Irradiance | 892 $W/m^2$ |
| Cell Temperature | 51.2 °C |
| Weather Conditions | Clear / Slightly cloudy |

**Note:** The time shown is local solar time. To find GMT time, add 0.61 hours (PVGIS - JRC's Institute for Energy and Transport, 2012b)

**Obtained IV Characteristic Curve**

Accordingly to the procedure, 35 measurements of voltage and current were registered and plotted in the graphic showed in figure 4.2.

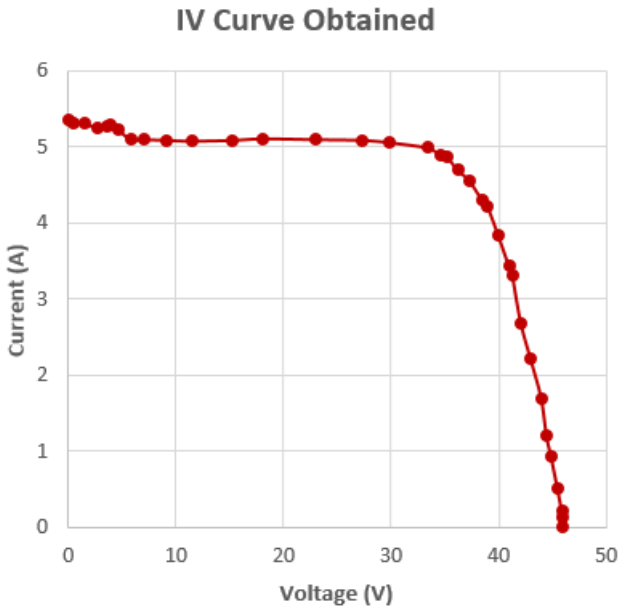


Figure 4.2: IV characteristic curve plotted using the values input to an Excel spreadsheet.

The result obtained was then compared with the graphics included in the Module data-sheet, presented in figures 4.3 and 4.4, which can be found in the *Appendix* section (chapter A).

Considering that the irradiance value at the time of the experiment was 892 $W/m^2$, and interpolating from the 800 and 1000 $W/m^2$ curves presented in figure 4.3 it was concluded that the current production should be close to 5 A. The IV curve obtained from the experiment shows current figures slightly above 5 A in the voltage interval from 5 to 35 V. A rise in current was experienced as the curve approaches the origin in the voltage axis (short circuit), reaching a peak of 5.36 A in that situation. The curves available from the module data-sheet do not exhibit a similar behaviour near the origin.

Although figure 4.3 curves are presented for the standard 25 $^oC$ temperature, and during the test a temperature of 51.2 $^oC$ was measured, this difference does not significantly impact in the current output as will be seen ahead.

In order to compare the open circuit output voltage provided by the module data sheet with the actual value obtained in the experiment, we resort to figure 4.4 that plots several IV curves for an irradiance of 1000 $W/m^2$ (the closest available to our measured value of 892 $W/m^2$). From the graph we find that for a 50 $^oC$ temperature the open circuit voltage is about 48 V, in line with the 46.2 V obtained in the experiment.

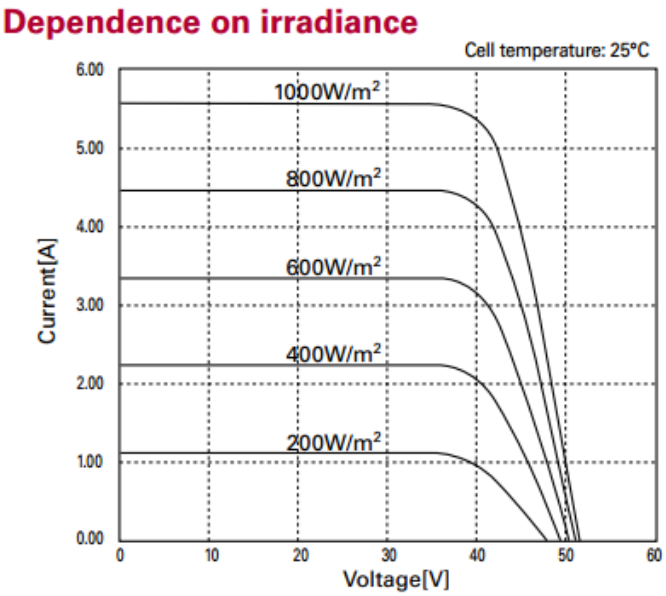


Figure 4.3: IV curve family for module, for a 25°C cell temperature, as a function of irradiace.

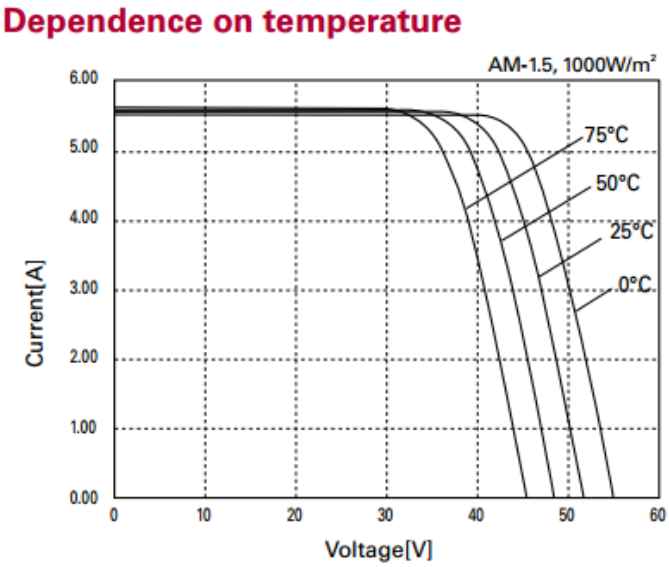


Figure 4.4: IV Curve family for Module HIP-215NHE5 for a 1000 W/m$^2$ irradiance as a function of temperature.

Although in this experiment measurements weren't made under different cell temperatures, in order to assess the impact of temperature variation, resort once more to figure 4.4, it was possible to conclude that:

1. The current output is very moderately dependent upon temperature.
2. The open circuit voltage varies inversely with the increase in temperature. From the graph we find that for a positive 75 °C variation in cell temperature we get an approximate negative variation in open circuit voltage of about 10 V.

**Obtained PV Characteristic Curve**

DC electric power is defined as the product of the current and the voltage. Hence, in both the short circuit and open circuit situations, the solar module produces no power. Somewhere in between these two operating points is situated the Maximum Power Point (MPP) which corresponds to the maximum power achieved by the module.

The PV curve of experiment 1 is shown below, in figure 4.5, where it is possible do identify the MPP pointed out in red.

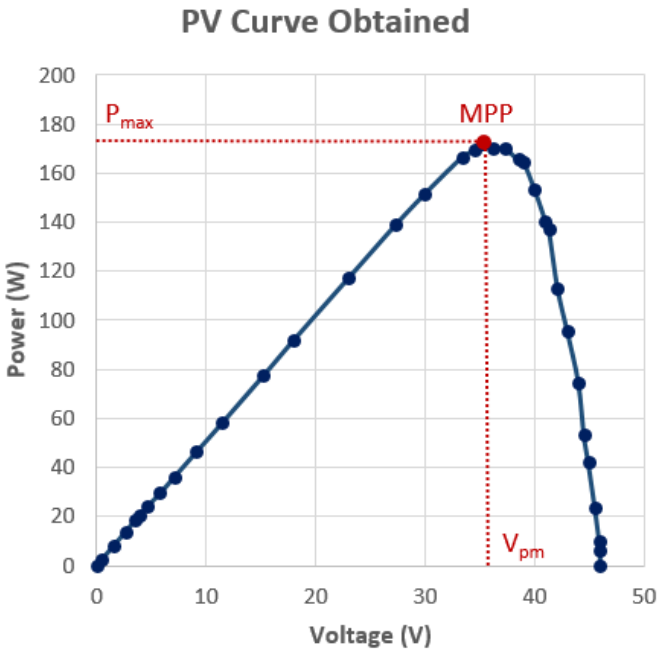


Figure 4.5: PV characteristic curve resulting from the values input to the Excel spreadsheet.

A resume of the obtained MPP values is presented below in table 4.2.

Table 4.2: Experiment 1 - Results obtained.

| Experiment 1 - MPP Values Obtained | |
|---|---|
| Maximum Power Point (Pmax) | 171.8 W |
| Maximum Power Voltage (Vpm) | 35.2 V |
| Maximum Power Current (Ipm) | 4.9 A |

As there are no PV curves available in the SANYO module HIP-215NHE5 data-sheet, it was only possible to compare the MPP experimental values with the specifications of the module (under standard conditions) shown in figure 4.6.

| | | Models HIP-xxxNHE5 | | |
|---|---|---|---|---|
| **Electrical data** | | **215** | **210** | **205** |
| Maximum power (Pmax) | [W] | 215 | 210 | 205 |
| Max. power voltage (Vpm) | [V] | 42.0 | 41.3 | 40.7 |
| Max. power current (Ipm) | [A] | 5.13 | 5.09 | 5.05 |
| Open circuit voltage (Voc) | [V] | 51.6 | 50.9 | 50.3 |
| Short circuit current (Isc) | [A] | 5.61 | 5.57 | 5.54 |
| Warranted minimum power (Pmin) | [W] | 204.3 | 199.5 | 194.8 |
| Output power tolerance | [%] | +10/-5 | | |
| Maximum system voltage | [Vdc] | 1000 | | |
| Temperature coefficient of Pmax | [%/°C] | -0.3 | | |
| Voc | [V/°C] | -0.129 | -0.127 | -0.126 |
| Isc | [mA/°C] | 1.68 | 1.67 | 1.66 |

Note 1: Standard test conditions: Air mass 1.5, Irradiance = 1000W/m$^2$, Cell temperature = 25°C
Note 2: The values in the above table are nominal.

Figure 4.6: Nominal electrical data for the SANYO HIP-xxxNHE5 module family (relevant data for the tested model contained in the "215" column).

**Analysis of the Results**

Comparing the nominal values for maximum power, maximum power current and maximum power voltage with those obtained in the experiment, it was concluded that inferior values were reached for all those values:

1. Maximum power current: the fact that the experiment was conducted with roughly 100 W/m$^2$ below the standard irradiance (1000 W/m$^2$) causes a decrease in produced current. Interpolating from the 800 W/m$^2$ and 1000 W/m$^2$ curves in figure 4.3 it is estimated that the current decrease vis a vis the standard would be 0.5 A in the "flat" part of the plot for a 900 W/m$^2$ curve.
2. Impact of temperature in maximum power voltage: assuming the temperature coefficient presented in the table 4.6 (Voc = -0.129 V/°C), and a delta T of 26° between the standard (25 °C) and the experiment, a -3.4 V difference in open circuit voltage was obtained.
3. Impact of temperature in maximum power current: assuming the temperature coefficient presented in the table 4.6(Isc = 1.68 mA/°C), it was concluded that the impact in the output current is not significant (< 1%) for a delta T of 26 °C.

4. The maximum power production occurs in the "knee" part of the IV curve, so any linear extrapolation contains a certain degree of error. Even so, if the aforementioned adjustments described in 1 and 2 are considered, the adjustment values are summarized in table 4.3:

Table 4.3: Realized adjustments for the obtained maximum power current and voltage values.

| | Nominal Value | Adjustment | Adjusted Value |
|---|---|---|---|
| Maximum Power Voltage | 42 V | -3.4 V | 38.6 V |
| Maximum Power Current | 5.1 A | -0.5 A | 4.6 A |

From the adjusted values assumed it was possible to obtain an adjusted maximum power value of 178.7 W:

$$\text{Adjusted Maximum Power} \ = \ 38.6 \times 4.63 \ = \ 178.7 \text{ W}$$

Based on simplistic assumptions, the calculated adjusted maximum power is very much in line with the experimental value (171.8 W).

### 4.1.3 Experiment 2

Experiment 2 was made under different external conditions as experiment 1, using the same photovoltaic module and experiment specifications, also to study the IV and PV characteristic curves generated.

Initial conditions for experiment 2 were summarized on the following table (table 4.4):

Table 4.4: External conditions for experiment 2.

| Experiment 2 - Existing Conditions | |
|---|---|
| Date | $23^{rd}$ of March 2015 |
| Time | 13:50 |
| Solar Time | 13:13 |
| Irradiance | 712 W/m$^2$ |
| Cell Temperature | 39.4 °C |
| Weather Conditions | Windy and Cloudy |

**IV and PV Characteristic Curves Obtained**

Accordingly to the procedure, 50 measurements of voltage and current were taken and resumed in the graphic showed below in figure 4.7.

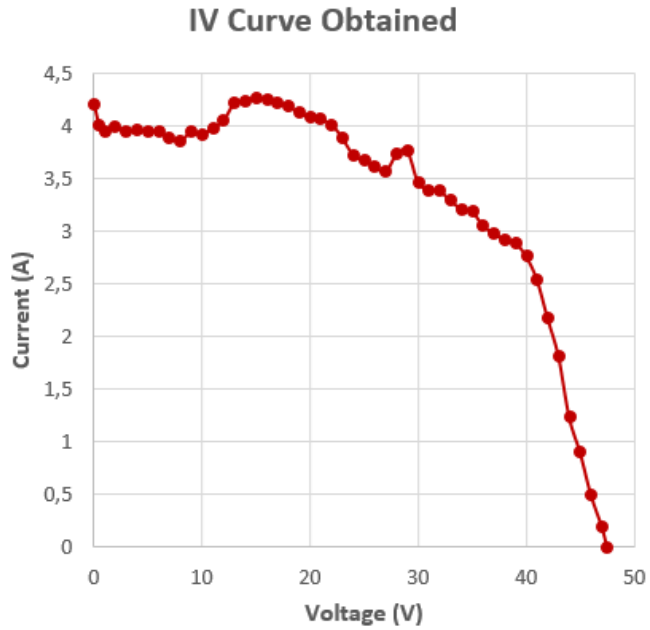


Figure 4.7: IV characteristic curve plotted using the values input to an Excel spreadsheet.

As for the PV characteristic curve the result is shown below in figure 4.8.

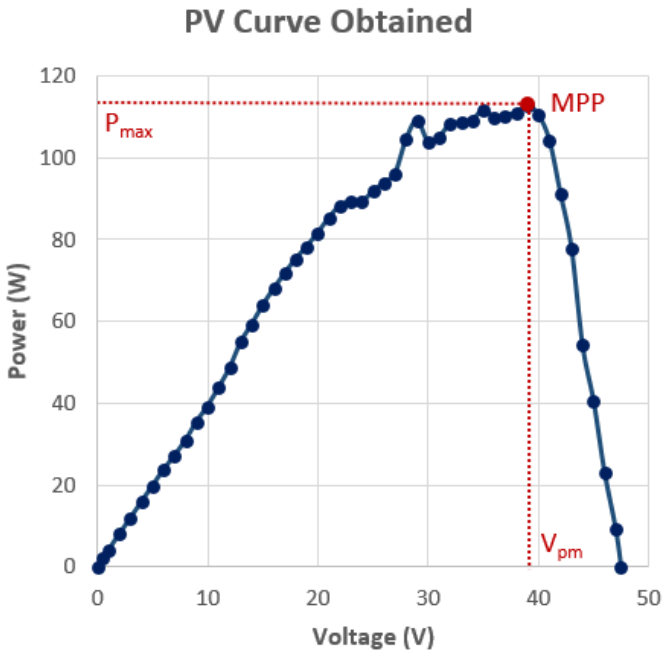


Figure 4.8: PV characteristic curve plotted using the values input to an Excel spreadsheet.

The MPP values are summarized in table 4.5, presented below.

Although it is possible to obtain one distinct MPP value from the spreadsheet, the existence of "bumps" in the curve could easily hamper an the choice of the inverter when deciding the MPP, as was mentioned before in the section 2.1.2 of chapter 2, State of the Art.

Table 4.5: Experiment 2 - Results obtained.

| Experiment 2 - MPP Values Obtained | |
|---|---|
| Maximum Power Point (Pmax) | 111,65 W |
| Maximum Power Voltage (Vpm) | 35,0 V |
| Maximum Power Current (Ipm) | 3,19 A |

**Analysis of the Results**

The main differences between experiments 1 and 2 are the weather conditions, which impact on the amount of irradiance projected on the solar cells and on their temperature. Figures 4.7 and 4.8 reflect, the impact of those changes in the characteristic curves of the module.

As happened with experiment 1, the curves obtained were compared with the graphics available in the SANYO HIP215NHE5 data-sheet, presented in figures 4.3 and 4.4. Contrary to what happens in the previous experiment, the presence of high clouds had an adverse impact in the shape of the curves, provoking an irregular ("bumpy") behaviour.

After looking at the obtained IV and PV curves, and MPP value, it is possible to verify that in the presence of soft shade, the current drops substantially while the voltage remains roughly the same, as was mentioned before in the State of the Art.

### 4.1.4 Remarks on the Outputs of Experiments 1 and 2

It was verified for both experiments, that the production of the module behaves according to expectations. Nevertheless, it is more difficult to compare real and nominal data for experiment 2 due to variations in irradiance throughout the measurements, caused by the presence of high clouds.

## 4.2 Test of Grid-connected Modules

### 4.2.1 Study of the Power Production on a two Module Installation

The main goal of the experiments detailed in the section is to compare the power production of a two PV module installation, such as the on represented on figure 4.9, on four different shading situations. The comparisons are made between each implemented situation, and on the cases that allow it, results are compared with the maximum power production estimated for same-condition simulations on Simulink.

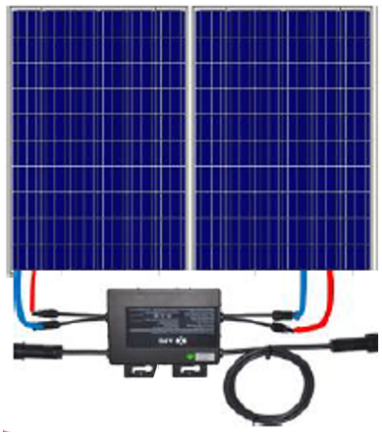

Figure 4.9: Shaded experiment 3 - Two module installation configuration with Micro-inverter.

To complete the experiments, an installation with two modules connected in parallel with each other and in series with a mirco-inverter was set and connected to a monitoring system to gather production data details.

Next, the previously dimensioned Simulink model which links two PV modules (illustrated in figure 3.8), was adapted for the panels characteristics and external conditions, simulating the real installation. This would allow the evaluation of the accuracy of IECEN2060 Simulink Model.

The following shaded experiments were chosen to validate, through test and simulation, a few statements made previously on the State of the Art (chapter 2) regarding the changes in power production due to different types of shading:

- Experiment 3: No shade cast on any of the Modules;
- Experiment 4: Partly soft shaded Module - Soft shade cast in half one of the panels;
- Experiment 5: Entirely soft shaded Module;
- Experiment 6: Partly hard Shaded Module - Hard shade cast in half one of the panels.

Experiments 3 to 6 are illustrated bellow in figure 4.10.

(a) Shaded experiment 4. (b) Shaded experiment 5. (c) Shaded experiment 6.

Figure 4.10: Illustrations of shaded cases B to D, where different shading situations are simulated.

**Experiment Specifications**
**Material Used:**

- 2 SM-255PC8 S-ENERGY 60-cell-series Polycrystalline Photovoltaic Modules;
- Mounting hardware suitable for module racking;
- Sockets and wrenches for mounting hardware;
- An APS YC500A-MIW Photovoltaic Grid-Connected Inverter;
- An AC connection junction box;
- An Alternergy Power System Energy Communication Unit (APS ECU);
- A Lafayette SMB-SOLAR Solar Power Meter with incorporated Multimeter;
- One TFA Infra-red Thermometer;
- An ECU Monitoring System;
- Opaque Fabric;
- Translucent Fabric.

**Steps of the Procedure:**

1. Set the circuit shown in figure 4.11;
2. Apply the desired shade upon the PV installation;
3. Link the Inverter output to a power sockect;
4. Set the PV Installation facing towards the source of light;
5. Plug the APS Energy Communication Unit power interface to a wall outlet connected to the same main electrical switchboard as inverter;

6. Connect the APS Energy Communication Unit to an IP router using an Ethernet cable;
7. Setup the APS Energy Monitor and Analysis (EMA)using the IP address shown in the ECU and monitor the two modules production;
8. Compare the obtained values with the simulated ones;

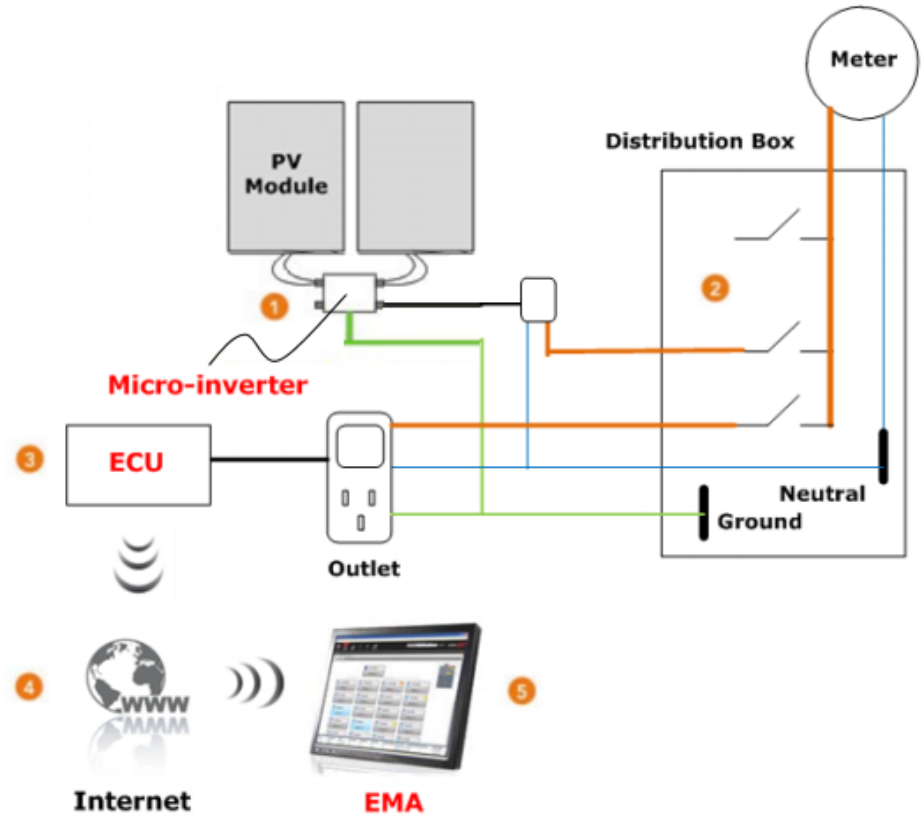


Figure 4.11: Diagram of the setup used to gather information from the installation to the APS EMA. Source: CivicSolar, 2015

where:

**1** is the APS Microinverter

**2** is an AC Power Line

**3** is the APS ECU

**4** is an Ethernet Router

**5** is the APS EMA

The APS ECU is installed by simply plugging it into any wall outlet and providing an Ethernet or Wi-Fi connection to a broadband router or modem. After installing the ECU, any APS Microinverter present and properly configured in the networks will automatically

reports to the APS Energy Monitor and Analysis (EMA) as long as a minimum power value is being produced (CivicSolar, 2015).

The micro-inverter communicates with the APS Energy Communication Unit (ECU) from opposite sides of FCT's Electrical Engineering building using [1]PLC technology.

The EMA interface allows the user to, visualize all the lifetime and real-time data pertaining the installation associated to the micro-inverter.

**Initial Conditions**

In order to normalize the results of all four experiments, the data gathered results from tests made in the same day, between 12:45 and 13:45 (GTM time).

The following table (table 4.6) resumes the initial conditions under which the experiments were made.

Table 4.6: External conditions for experiment 1.

| Experiment 1 - Existing Conditions | |
|---|---|
| Date | $29^{th}$ of November 2015 |
| Time | 12:45 to 13:45 |
| Solar Time | 13:22 to 14:22 |
| Irradiance | 876 $W/m^2$ |
| Cell Temperature | 35 to 37 °C |
| Weather Conditions | Clear sky |

To simulate soft and hard shade situations, two distinct fabrics (opaque and translucent) were placed top of one of the the modules, covering it partially and fully as depicted in figure 4.10 demonstrates. For each situation, the respective values of irradiance were measured and input to the Simulink model so that the power production could be simulated and compared to the real production value displayed on EMA platform.

[1]Power Line Communication (PLC), is a communication technology that enables sending data over existing power cables (UBM Communities, 2011). This technology came to minimize infrastructure and maintenance costs by avoiding the need to create new communication paths through obstacles such as buildings, hills, and basements that block wireless communications (Maxim Integrated, 2016).

### 4.2.2 Experiment 3 - No Shade Cast on the Installation:

On this experiment no shade is cast. This is important to set a base case comparison between the power output production value of the installation and the one obtained through Simulink simulation.

The experiment layout is shown in figure 4.12 below.

Figure 4.12: Layout of experiment 3 - Installation with two PV panels and a micro-inverter with no shade cast upon them.

To simulate this experiment, the irradiance on the real installation is measured using a solar power meter and is then input to Simulink model with two PV panels.

$$\text{Measured Irradiance} = 876\ \text{W/m}^2$$

The power production value displayed by the EMA platform on the *Real-time Data Screen* shown in figure 4.13.

| Inverter ID | Current Power | Grid Frequency | Grid Voltage | Temperature | Date |
|---|---|---|---|---|---|
| 404000120768-A | 223 W | 50.0 Hz | 232 V | 35 °C | 2015-11-29 13:01:13 |
| 404000120768-B | 228 W | 50.0 Hz | 232 V | 35 °C | 2015-11-29 13:01:13 |

Figure 4.13: EMA real-time data screen production for experiment 3.

From the EMA data screen it was possible to calculate the total of power being produced by the installation at the time of the experiment by adding the *Current Power* production of both modules.

$$\text{Currtent Power Production} = 451\ \text{W}$$

As it can be verified in the model presented in figure 4.14, both *Irradiation* values *1* and *2* (highlighted with red circles), were to the irradiation value measured in the experiment. The resulting output power value is highlighted by a dashed blue ellipse.

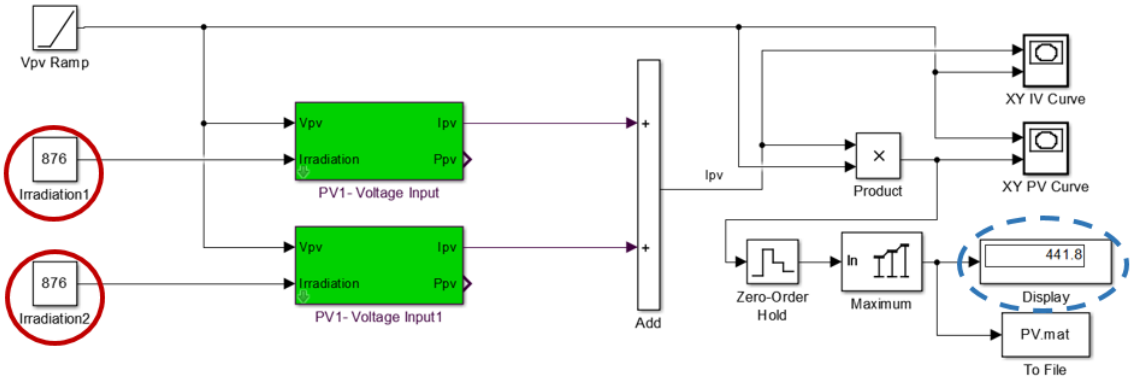


Figure 4.14: Simulink simulation of experience 3.

Where: circled in red is the irradiance values input and on a dash traced circle in blue is the estimated power production value output

The input irradiance and output maximum power estimated for this situation are summarized in table 4.7 below.

Table 4.7: Experiment 3 - Simulink simulation input and output values.

| Experiment 3 - Simulink Simulation Input and Output Values | |
|---|---|
| Input *Irradiation 1* | 876 W/m$^2$ |
| Input *Irradiation 2* | 876 W/m$^2$ |
| Maximum Power Estimated *Output* | 442 W |

### 4.2.3 Experiment 4 - A Single Module With Soft Shading cast upon it:

To implement experiment 4, a translucent fabric was laid on top of one of the modules, casting a soft shade upon all its surface, as can be seen in figure 4.15.

Figure 4.15: Layout of experiment 4 - Photovoltaic installation with a translucent fabric casting soft shade on totality of one module surface.

As it was done for experiment 3, the EMA interface was used to read the real-time power production. From figure 4.16 it is possible to computer the total generated power value of the installation for the established conditions.

| Inverter ID | Current Power | Grid Frequency | Grid Voltage | Temperature | Date |
|---|---|---|---|---|---|
| 404000120768-A | 31 W | 50.0 Hz | 231 V | 36 °C | 2015-11-29 13:11:13 |
| 404000120768-B | 197 W | 50.0 Hz | 231 V | 36 °C | 2015-11-29 13:11:13 |

Figure 4.16: EMA real-time data screen production for experiment 4.

$$\text{Current Power Production} = 228 \text{ W}$$

Next the irradiance value was measured for both modules to proceed to the next step of the experiment, the Simulink simulation. The same procedure detailed above, using the model shown in figure 4.14 was followed in this case using different values of irradition for *Irradiation1* and *Irradiation2*.

The input irradiance and output maximum power estimated for this situation are summarized in table 4.8 below.

Table 4.8: Experiment 4 - Simulink simulation input and output values.

| Experiment 4 - Simulink Simulation Input and Output Values | |
|---|---|
| Input *Irradiation 1* | 876 W/m$^2$ |
| Input *Irradiation 2* | 279 W/m$^2$ |
| Estimated Power Production *Output* | 217 W |

### 4.2.4 Experiment 5 - One Module Partly Soft Shaded:

Similarly to what was done in experiments 3 and 4, for experiment 5, a translucent fabric was laid of half on one of the panels of the installation as is shown in figure 4.17.

Figure 4.17: Layout of experiment 5 - Installation with a translucent fabric casting soft shade on half of the surface of one module.

For this experiment the EMA reading for the real-time power production is shown in figure 4.18. As was done for the previous experiments, the total generated power value of the installation for the established conditions was calculated.

| Inverter ID | Current Power | Grid Frequency | Grid Voltage | Temperature | Date |
|---|---|---|---|---|---|
| 404000120768-A | 20 W | 50.0 Hz | 232 V | 37 °C | 2015-11-29 13:21:13 |
| 404000120768-B | 212 W | 50.0 Hz | 232 V | 37 °C | 2015-11-29 13:21:13 |

Figure 4.18: EMA real-time data screen production for experiment 5.

$$\text{Current Power Production} = 232 \text{ W}$$

For this experiment it is not possible to use Simulink model as it does not have any mechanism that permits modelling partly shaded modules.

### 4.2.5 Experiment 6 - One Module Partly Hard Shaded:

For the last experiment, similarly to experience 5, an opaque fabric was laid on top of one of the PV modules, casting a hard shade upon half of its surface, as it is shown in figure 4.19.

Figure 4.19: Layout of experiment 6 - Installation with an opaque fabric casting soft shade on half of the surface of a module.

Real-time power production output is shown in figure 4.20 and, once more, the gobal real-time generated power value of the installation for the established conditions was calculated.

| Inverter ID | Current Power | Grid Frequency | Grid Voltage | Temperature | Date |
|---|---|---|---|---|---|
| 404000120768-A | 8 W | 50.0 Hz | 230 V | 37 °C | 2015-11-29 13:31:13 |
| 404000120768-B | 209 W | 50.0 Hz | 230 V | 37 °C | 2015-11-29 13:31:13 |

Figure 4.20: EMA real-time data screen production for experiment 6.

$$\text{Current Power Production} = 217 \text{ W}$$

As happens for experiment 3, on this case it was also not possible to use Simulink model.

### 4.2.6 Remarks on the Outputs of Experiments 3 to 6

From the analysis of experiment 3, it was possible to conclude that there is a small difference between the production value presented on the EMA interface and the one estimated using Simulink. By running a number of similar experiments under the same conditions, it was possible to verify that the output power measured by the micro-inverter tends to be greater than the estimated global power by a percentage of 2% to 8% (where 8% represents the value further from the simulated one). The percentage value was calculated using the Relative Error expression 4.1, expressed below.

$$\text{Relative Error } = 100 \times \frac{\Delta x}{x} \tag{4.1}$$

Taking this error percentage in account an analysis of the production for experiment 4 was made.

For experiment 4, running several experiences showed that the measure displayed on EMA interface is greater than the estimated one, by a small percentage.

For experiments 5 and 6, there was no possibility to compare results with Simulink simulations as these have no option to consider half a shaded module.

Based exclusively on the measurements gathered by the installations' micro-inverter, it was observed that the power production has a drastic decrease on the partly shaded modules compared to the production on a completely soft shaded module. This comparison is very interesting as it demonstrates the overpowering effect partial shades have on the power production of solar panels.

SM255PC8 Photovoltaic Modules are supplied with factory installed bypass diodes that provide a low-resistance current path around shaded cells, thereby minimizing module heating and array current losses. If this wasn't the case, the measured power production for experiments 5 and 6 for the partly shaded module would be even lower than the recorded 20 W and 8 W respectively.

To sum up, with this four experiments it was possible to verify that irregular shading cast on a PV module has a greater effect on the power production than a broader shading evenly affecting the surface of the module.

It was also possible to conclude that the error margin between the power production value measured on by the ECU unit and the one estimated using Simulink is not greater than 8% (real-time production value being always higher), which makes of ECEN2060 model a trustworthy model and therefore a useful photovoltaic projecting tool.

CHAPTER 5

# CONCLUSIONS AND FUTURE WORK

## 5.1 Conclusions

There are still a few aspects in need of improvement when choosing photovoltaic systems as a source of energy supply. As said previously, the work performed in this dissertation intends to develop the accuracy on the estimation of power output production, accounting with shading influence, when projecting photovoltaic installations.

This work started with a survey of all the fundamental concepts and state of the art of the shading influence on photovoltaic systems to help to establish a guideline to the work intended.

In a first approach a Simulink existing model was adapted in order to suit the objectives of the work. Three models were created for different purposes using ECEN2026 as a base model. Those models were used to test theoretic photovoltaic installations as was seen in chapter 3, Implementation.

Using ECEN2026 model, IV and PV characteristic curves were simulated for hypothetical values of irradiation. Comparing those curves with the ones available in the documentation analysed in the previously done survey, it was possible to conclude that the simulated show a good fit in all the studied.

Furthermore, a study that correlates the severity of shading, number of shaded modules and maximum power produced, was realized realized using a model with seven modules connected in series. An equation that models the behaviour of this installation considering the changes in those three variables was developed. The obtained equation showed a 95% goodness of fit, based upon the R-Square statistic, which represents a very good approximation.

To conclude, an estimation of the annual energy production of a single PV module, assuming a previously defined shade was performed. This was done for three different

shading cases considering global and diffuse irradiance as input. To study the accuracy of the results obtained a sun path chart was created, based on the method expressed in the *Guide to the Installation of Photovoltaic Systems* manual and with the help of an online sun chart program provided by the University of Oregon. Results showed good approximation between values an more accuracy in some case than if using the model currently used by the public in general.

In a second approach, a PV installation with two modules linked to a micro inverter was set. Using this installation, two main types of practical experiments were performed, as was summarized in chapter 4, Experimental Results.

The aim of the of first experiment performed in chapter 4 was to draw IV and PV characteristic curves with real data measured using a multimeter. Two situations were chosen to display on the dissertation, the first one shows the current and power values for the measured voltage on a day with almost no irradiance alteration, the other shows the same values for a day with high clouds, which causes a significant change of the incident irradiance in the PV installation. For this type of experiment, it was concluded that the graphs obtained show the expected shape and behaviour for both situations.

A second type of practical experiment was set with the goal to compare the power production of the same installation for different shading for different situations:

- Case A: No shade cast on any of the Modules;
- Case B: Partly soft shaded Module - Soft shade cast in half one of the panels;
- Case C: Entirely soft shaded Module;
- Case D: Partly hard Shaded Module - Hard shade cast in half one of the panels.

Case A was set as a staring comparative point. The measured power output was compared using the previously set Simulink model adapted to the characteristics of the installation. On case B the same comparison was made. As for cases C and D, it is not possible to replicate half shaded situation on the model, so the results were compared with the previous situations and analysed in the light of the theoretical survey resumed on chapter 2, State of the Art.

It was concluded for the four mentioned cases that irregular shading cast on a PV module has a greater effect on the power production than a broader shading evenly affecting the surface of the module. Through the analysis of 20 different cases, it was also possible to conclude that the maximum difference between the Simulink simulations and the values measured by the inverter was 8%, from which it is fair to assume that this is a reliable model.

These experiences with half shaded module cases were also relevant in the sense that they demonstrate the importance of the use of by-pass diodes on PV panels.

## 5.2 Future Work

The improvement in methods and tools to perform photovoltaic systems designing contributes to the evolution of this type of energy sources.

The work performed on this dissertation provides to verify the reliability of an existing public domain model(ECEN2026), which permits good estimates of energy production.

The main objective of the thesis, was the development of a general equation correlating severity of shading and number of shaded panels with power production. This equation has the limitation to have been derived for a specific seven modules serial installation. An opportunity for future work would be to adapt the obtained equation for any number of modules connected in series or in parallel.

Other topic to be considered regarding future work are the suggestions made to the sun chart path presented in *Guide to the Installation of Photovoltaic Systems* manual. It was concluded that for better results, segments sizing on this method should be more strict, which means that, segments closer to noon time should be even smaller and the ones closer to sun rise and down should be slightly bigger, the total number of segments could remain unaltered but each segments sizing should be reviewed.

# BIBLIOGRAPHY


Alonso-García, M. C., J. M. Ruiz, and W. Herrmann (2006). "Computer simulation of shading effects in photovoltaic arrays". In: 31.12, pp. 1986–1993. (Visited on 10/21/2014).

*Archelios PRO*. URL: http://www.archelios.com/ (visited on 06/02/2015).

BBC - GCSE Bitesize (2014). *Sustainable energy resources*. BBC - GCSE Bitesize: Sustainable energy resources. URL: http://www.bbc.co.uk/schools/gcsebitesize/geography/energy_resources/sustainable_energy_rev1.shtml (visited on 10/08/2015).

Canterbury Power Solutions (2012). *Solar Micro-Inverters | Canterbury Power Solutions*. URL: http://canterburypower.co.nz/solar-micro-inverters/ (visited on 03/06/2015).

Chen, S.-M., T.-J. Liang, and K.-R. Hu (2013). "Design, analysis, and implementation of solar power optimizer for DC distribution system". In: *Power Electronics, IEEE Transactions on* 28.4, pp. 1764–1772.

CivicSolar (2015). *APS Energy Communication Unit for Monitoring ECU-3*. URL: http://www.civicsolar.com/product/aps-ecu-3-energy-communication-unit (visited on 01/17/2016).

*Controlling software for photovoltaics - PVCAD* (2015). Program dla fotowoltaiki, PVCAD. URL: http://pvcad.pl/ (visited on 06/02/2015).

Deutsche Gesellschaft für Sonnenenergie (2008). *Planning and Installing Photovoltaic Systems: A Guide for Installers, Architects and Engineers*. Earthscan.

Drif, M., P. Pérez, J. Aguilera, and J. Aguilar (2008). "A new estimation method of irradiance on a partially shaded PV generator in grid-connected photovoltaic systems". In: *Renewable Energy* 33.9, pp. 2048–2056.

ECEE Colorado. *ECEN2060 Renewable Sources and Efficient Electrical Energy Systems*. URL: http://ecee.colorado.edu/~ecen2060/index.html (visited on 03/19/2016).

Frost, J. (2013). *Regression Analysis: How Do I Interpret R-squared and Assess the Goodness-of-Fit?* URL: http://blog.minitab.com/blog/adventures-in-statistics/regression-analysis-how-do-i-interpret-r-squared-and-assess-the-goodness-of-fit (visited on 08/21/2015).

Greenpro (2004). *Energia Fotovoltaica - Manual sobre tecnologias, projecto e instalações*. In collab. with IST, DGS, ALTENER, and Comissão Europeia. URL: http://www.jgduarte.com/download/greenpro_fotovoltaico.pdf (visited on 01/16/2015).

Home Power Inc. (2015). *Solmetric Improves Site Analysis | SolarPro Magazine*. URL: http://solarprofessional.com/articles/products-equipment/product-launches/solmetric-improves-site-analysis (visited on 06/07/2015).

Hong Yang, He Wang, and Minqiang Wang (2012). "Investigation of the Relationship between Reverse Current of Crystalline Silicon Solar Cells and Conduction of Bypass Diode". In: *International Journal of Photoenergy*, pp. 1–5.

Honsberg, C. and S. Bowden (2011). *Hot Spot Heating*. URL: http://pveducation.org/pvcdrom/modules/hot-spot-heating (visited on 11/02/2014).

Images SI Inc. (2007). *How Photovoltaic Cells Generate Electricity*. URL: http://www.imagesco.com/articles/photovoltaic/photovoltaic-pg4.html (visited on 05/08/2015).

JRC's Institute for Energy and Transport (2012a). *PV potential estimation utility*. URL: http://re.jrc.ec.europa.eu/pvgis/apps4/pvest.php# (visited on 08/17/2015).

— (2012b). *PVGIS - European Commission*. URL: http://re.jrc.ec.europa.eu/pvgis/ (visited on 06/02/2015).

Kadri, R., H. Andrei, J.-P. Gaubert, T. Ivanovici, G. Champenois, and P. Andrei (2012). "Modeling of the photovoltaic cell circuit parameters for optimum connection model and real-time emulator with partial shadow conditions". In: *Energy*. 8th World Energy System Conference, WESC 2010 42.1, pp. 57–67.

Karatepe, E., M. Boztepe, and M. Çolak (2007). "Development of a suitable model for characterizing photovoltaic arrays with shaded solar cells". In: *Solar Energy* 81.8, pp. 977–992. (Visited on 01/24/2015).

Kelly, N. A. and T. L. Gibson (2009). "Improved photovoltaic energy output for cloudy conditions with a solar tracking system". In: *Solar Energy* 83.11, pp. 2092–2102.

Krismadinata, N. A. Rahim, H. W. Ping, and J. Selvaraj (2013). "Photovoltaic Module Modeling using Simulink/Matlab". In: *Procedia Environmental Sciences* 17, pp. 537–546.

Lauritzen Inc. (2011). *Lauritzen Solar Tracker Solutions Backtracking*. URL: http://archive.today/b2Pu (visited on 04/13/2015).

Lorenzo, E., L. Narvarte, and J. Muñoz (2011). "Tracking and back-tracking". In: *Progress in Photovoltaics: Research and Applications* 19.6, pp. 747–753. (Visited on 03/24/2015).

Lorenzo, E., M. Pérez, A. Ezpeleta, and J. Acedo (2002). "Design of tracking photovoltaic systems with a single vertical axis". In: *Progress in Photovoltaics: Research and Applications* 10.8, pp. 533–543.

MacAlpine, S., R. Erickson, and M. Brandemuehl (2013). "Characterization of Power Optimizer Potential to Increase Energy Capture in Photovoltaic Systems Operating Under Nonuniform Conditions". In: *IEEE Transactions on Power Electronics* 28.6, pp. 2936–2945.

Marnoto, T., K. Sopian, W. R. W. Daud, M. Algoul, and A. Zaharim (2007). "Mathematical model for determining the performance characteristics of multi-crystalline photovoltaic modules". In: *Proceedings of the 9th WSEAS international conference on Mathematical and computational methods in science and engineering*. World Scientific, Engineering Academy, and Society (WSEAS), pp. 79–84. URL: http://www.researchgate.

net/profile/Kamaruzzaman_Sopian2/publication/228412578_Mathematical_model_for_determining_the_performance_characteristics_of_multi-crystalline_photovoltaic_modules/links/5447adba0cf2d62c305093ac.pdf (visited on 04/28/2015).

Masters, G. M. (2004). *Renewable and efficient electric power systems*. Hoboken, NJ: John Wiley & Sons. 654 pp.

Mathworks, Inc. *Inport*. URL: http://www.mathworks.com/help/simulink/slref/inport.html (visited on 09/02/2015).

— (2015). *MATLAB - The Language of Technical Computing*. URL: http://www.mathworks.com/products/matlab/ (visited on 09/02/2015).

— *Outport*. URL: http://www.mathworks.com/help/simulink/slref/outport.html?searchHighlight=outport (visited on 09/02/2015).

— *To Workspace*. URL: http://www.mathworks.com/help/simulink/slref/toworkspace.html?searchHighlight=simulink%20to%20workspace (visited on 09/02/2015).

— *XY Graph*. URL: http://www.mathworks.com/help/simulink/slref/xygraph.html?searchHighlight=xy%20plot (visited on 09/02/2015).

Maxim Integrated (2016). *Powerline Communications*. URL: https://www.maximintegrated.com/en/products/comms/powerline-communications.html (visited on 01/31/2016).

(MCS), M. C. S. (2012). *Guide to the Installation of Photovoltaic Systems*. Electrical Contractors Association (ECA). URL: www.microgenerationcertification.org.

Meteotest. *Meteonorm: Features*. URL: http://meteonorm.com/en/features (visited on 06/02/2015).

Panico, D., P. Garvison, H. Wenger, and D. Shugar (1991). "Backtracking: a novel strategy for tracking PV systems". In: *, Conference Record of the Twenty Second IEEE Photovoltaic Specialists Conference, 1991.* , Conference Record of the Twenty Second IEEE Photovoltaic Specialists Conference, 1991, 668–673 vol.1.

Passias, D. and B. Källbäck (1984). "Shading effects in rows of solar cell panels". In: *Solar cells* 11.3, pp. 281–291.

Prontes, I. (2013). *What Is a Blocking Diode?* In collab. with eHow. URL: http://www.ehow.com/about_4697360_what-blocking-diode.html (visited on 10/21/2014).

Quaschning, V. and R. Hanitsch (1995). "Shade calculations in photovoltaic systems". In: *ISES Solar World Conference, Harare*. URL: http://www.volker-quaschning.de/downloads/ISES1995.pdf (visited on 01/28/2015).

Queensland Windmill & Solar (2008). *Solar Trackers*. URL: http://www.qldwindmillandsolar.com.au/solar-trackers (visited on 04/13/2015).

Rodríguez, J. D. B., C. A. Ramos-Paja, and E. F. Mejia (2012). "Modeling and parameter calculation of photovoltaic fields in irregular weather conditions". In: *Ingeniería* 17.1, pp. 37–48.

Sargosis Solar & Electric (2014). *How Shade Affects a Solar Array*. URL: http://sargosis.com/articles/science/how-shade-affects-a-solar-array/ (visited on 10/30/2014).

Sera, D. and Y. Baghzouz (2008). "On the impact of partial shading on PV output power". In: *WSEAS/IASME International Conference on Renewable Energy Sources (RES'08)*. URL: http://forskningsbasen.deff.dk/Share.external?sp=S40df9c80-fe53-11dd-83f3-000ea68e967b&sp=Saau (visited on 10/08/2015).

Sher, H. A. and K. E. Addoweesh (2012). "Micro-inverters — Promising solutions in solar photovoltaics". In: *Energy for Sustainable Development* 16.4, pp. 389–400.

Sistemas Digitales de Control 2002, S.L. (2014). *Sistemas de Seguimiento*. URL: http://www.sistemas2002.com/Renovables/Sistemas_Seguimiento/ (visited on 04/20/2015).

Solar-Facts (2012). *Blocking and By-Pass Diodes Used in Solar Panels*. URL: http://www.solar-facts.com/panels/panel-diodes.php (visited on 11/04/2014).

*Solar PV System Shading Calculation with PVSYST - YouTube* (2009). In collab. with Onelecprojects. URL: https://www.youtube.com/watch?v=_YOhElZEiSQ&feature=youtube_gdata_player (visited on 02/26/2015).

Solar Server (2015). *New feature of EasySolar's PV app: design on image*. URL: http://www.solarserver.com/solar-magazine/solar-news/current/2015/kw16/new-feature-of-easysolars-pv-app-design-on-image.html (visited on 06/07/2015).

Solmetric, Inc. (2015). *Solmetric SunEye$^{TM}$*. URL: http://www.solmetric.com/sosu.html (visited on 06/02/2015).

Storr, W. (2014). *Bypass Diodes in Solar Panels and Arrays*. Basic Electronics Tutorials. URL: http://www.electronics-tutorials.ws/diode/bypass-diodes.html (visited on 10/21/2014).

The MathWorks, Inc. (2015). *Simulink - Simulation and Model-Based Design*. URL: http://www.mathworks.com/products/simulink/ (visited on 06/13/2015).

Tsao, P. (2010). "Simulation of PV systems with power optimizers and distributed power electronics". In: *Photovoltaic Specialists Conference (PVSC), 2010 35th IEEE*. IEEE, pp. 389–393. URL: http://ieeexplore.ieee.org/xpls/abs_all.jsp?arnumber=5616814 (visited on 03/05/2015).

UBM Communities (2011). *What is Power Line Communication?* What is Power Line Communication? URL: http://www.eetimes.com/document.asp?doc_id=1279014 (visited on 01/31/2016).

University of Oregon, Solar Radiation Monitoring Laboratory (2007). *Sun path chart program*. URL: http://solardat.uoregon.edu/SunChartProgram.html (visited on 08/16/2015).

Valentin Software GmbH (2015). *PV Software PV*SOL premium | Valentin Software*. URL: http://www.valentin-software.com/en/products/photovoltaics/57/pvsol-premium (visited on 06/02/2015).

Zipp, K. (2014). *Tigo Energy's SMART Module Platform Can Be Modeled In PV*SOL*. Solar Power World. URL: http://www.solarpowerworldonline.com/2014/05/tigo-energys-smart-module-platform-can-modeled-pvsol/ (visited on 06/02/2015).

APPENDIX A

# APPENDIX

**Appendix 1:**

Listing A.1: Initialization code for PV module in Simulink.

```
% PV Module Parameters
% Limitation -> constant temperature

Ns= round(Voc/0.61);        % default number of cells in series
Vt= 26e-3;                  % thermal voltage
G= Isc/1000;                % irradiation to short-circuit current gain
Vmpc= Vr/Ns;                % cell voltage at Pmax
Vocc= Voc/Ns;               % cell open-circuit voltage
Rmpp= Vmpc/Ir;              % cell load resistance at Pmax

Rp= 100*Vocc/Isc;           % initial value for Rp
Vdm= Vocc;                  % initial value for Vdm

% Iterative solution for model parameters: Io, Rs, Rp
for i=1:10
   Idm= Isc-Ir-Vdm/Rp;      % pn-juntion (diode) current at MPP
   Io= (Isc-Vocc/Rp)/(exp(Vocc/Vt)-1);  % pn-juntion reverse saturation
       current
   Vdm= Vt*log(Idm/Io+1); % pn-juntion (diode) voltage at MPP
   Rs= (Vdm-Vmpc)/Ir;       % cell series resistance
   Rd= (Rmpp-Rs)*Rp/(Rp-Rmpp+Rs); % diode incremental resistance at MPP
   Idm= Vt/Rd;              % diode current at MPP based on Rd
   Rsh= Vdm/(Isc-Ir-Idm);  % cell parallel resistance
end
```

**Appendix 2:**

Listing A.2: MATLAB script in-charged of running Simulink seven module design.

```
% Find MPP for PV_Array in different Insolation conditions

clear all
close all

G2 = [750 500 250 0];
Insolation_Initial=1000;

for k = 1:7            %Initializes every module with the value
    Insolation_Initial
     constBlkName = sprintf('PV_Array/Insolation%d', k);
     set_param(constBlkName, 'Value', 'Insolation_Initial');
end

SimOut = sim('PV_Array', 'ReturnWorkspaceOutputs', 'on');
fprintf('\n\nInitialization Complete -> Insolation(1-7) = %d \n\n',
    Insolation_Initial);

P = zeros(4,7);
N_sombreados = zeros(4,7);
Sev_sombreado = zeros(4,7);

Sev_sombreadoC = (1:28)';
Pmax = (1:28)';

Sev_sombreado_var = 100;

volta_num = 0;

 for k = 1:7
     for j = 1:4

         Insolation= G2(j);
         N_sombreados(j,k)= k

         switch k
             case 1
             constBlkName = sprintf('PV_Array/Insolation%d', k);
                      set_param(constBlkName, 'Value', 'Insolation');

             case 2
             constBlkName = sprintf('PV_Array/Insolation%d', k);
```

```
41                  set_param(constBlkName, 'Value', 'Insolation');
42              constBlkName = sprintf('PV_Array/Insolation%d', k-1);
43                  set_param(constBlkName, 'Value', 'Insolation');
44
45              case 3
46              constBlkName = sprintf('PV_Array/Insolation%d', k);
47                  set_param(constBlkName, 'Value', 'Insolation');
48              constBlkName = sprintf('PV_Array/Insolation%d', k-1);
49                  set_param(constBlkName, 'Value', 'Insolation');
50              constBlkName = sprintf('PV_Array/Insolation%d', k-2);
51                  set_param(constBlkName, 'Value', 'Insolation');
52
53              case 4
54              constBlkName = sprintf('PV_Array/Insolation%d', k);
55                  set_param(constBlkName, 'Value', 'Insolation');
56              constBlkName = sprintf('PV_Array/Insolation%d', k-1);
57                  set_param(constBlkName, 'Value', 'Insolation');
58              constBlkName = sprintf('PV_Array/Insolation%d', k-2);
59                  set_param(constBlkName, 'Value', 'Insolation');
60              constBlkName = sprintf('PV_Array/Insolation%d', k-3);
61                  set_param(constBlkName, 'Value', 'Insolation');
62
63              case 5
64              constBlkName = sprintf('PV_Array/Insolation%d', k);
65                  set_param(constBlkName, 'Value', 'Insolation');
66              constBlkName = sprintf('PV_Array/Insolation%d', k-1);
67                  set_param(constBlkName, 'Value', 'Insolation');
68              constBlkName = sprintf('PV_Array/Insolation%d', k-2);
69                  set_param(constBlkName, 'Value', 'Insolation');
70              constBlkName = sprintf('PV_Array/Insolation%d', k-3);
71                  set_param(constBlkName, 'Value', 'Insolation');
72              constBlkName = sprintf('PV_Array/Insolation%d', k-4);
73                  set_param(constBlkName, 'Value', 'Insolation');
74
75              case 6
76              constBlkName = sprintf('PV_Array/Insolation%d', k);
77                  set_param(constBlkName, 'Value', 'Insolation');
78              constBlkName = sprintf('PV_Array/Insolation%d', k-1);
79                  set_param(constBlkName, 'Value', 'Insolation');
80              constBlkName = sprintf('PV_Array/Insolation%d', k-2);
81                  set_param(constBlkName, 'Value', 'Insolation');
82              constBlkName = sprintf('PV_Array/Insolation%d', k-3);
83                  set_param(constBlkName, 'Value', 'Insolation');
84              constBlkName = sprintf('PV_Array/Insolation%d', k-4);
85                  set_param(constBlkName, 'Value', 'Insolation');
86              constBlkName = sprintf('PV_Array/Insolation%d', k-5);
```

```
                    set_param(constBlkName, 'Value', 'Insolation');

            case 7
            constBlkName = sprintf('PV_Array/Insolation%d', k);
                    set_param(constBlkName, 'Value', 'Insolation');
            constBlkName = sprintf('PV_Array/Insolation%d', k-1);
                    set_param(constBlkName, 'Value', 'Insolation');
            constBlkName = sprintf('PV_Array/Insolation%d', k-2);
                    set_param(constBlkName, 'Value', 'Insolation');
            constBlkName = sprintf('PV_Array/Insolation%d', k-3);
                    set_param(constBlkName, 'Value', 'Insolation');
            constBlkName = sprintf('PV_Array/Insolation%d', k-4);
                    set_param(constBlkName, 'Value', 'Insolation');
            constBlkName = sprintf('PV_Array/Insolation%d', k-5);
                    set_param(constBlkName, 'Value', 'Insolation');
            constBlkName = sprintf('PV_Array/Insolation%d', k-6);
                    set_param(constBlkName, 'Value', 'Insolation');
        end

        volta_num= volta_num+1;

        SimOut = sim('PV_Array', 'ReturnWorkspaceOutputs', 'on');
        load('PV.mat')

        P(j,k) = PMPP_sim.Data(end)
        Pmax(volta_num,1) = PMPP_sim.Data(end)

        Sev_sombreado(j,k) = (1000-G2(j))/10 * k *(1/7);
        Sev_sombreadoC(volta_num,1) = (1000-G2(j))/10 * k *(1/7);

    end
```

**Appendix 3:**

Listing A.3: MATLAB script in-charged of running Simulink seven module design.

```
% Find MPP for Module1 for several shading conditions
% Experience #1

clear all
close all

for i=1:12

```

```
9       shade=1;
10
11      Gtotal = load(['Gtotal_' num2str(i) '.mat']);
12      Gdifuse = load(['Gdifuse_' num2str(i) '.mat']);
13      Tamb = load(['Tamb_' num2str(i) '.mat']);
14      Hora = load('Hora.mat');
15      Gzero = zeros(56,1);
16      Insolation = zeros(56,1);
17
18      Gtotal_max = max(Gtotal.Gtotal)
19
20      switch i
21          case {1,11}
22              hora_i = 7; min_i = 38;
23              hora_f = 11; min_f = 02;
24          case {2,10}
25              hora_i = 8; min_i = 05;
26              hora_f = 11; min_f = 10;
27          case {3,9}
28              hora_i = 8; min_i = 55;
29              hora_f = 11; min_f = 45;
30          case 12
31              hora_i = 7; min_i = 20;
32              hora_f = 11; min_f = 00;
33          otherwise
34            shade = 0;
35      end
36
37      ti_objecto = hora_i*60 + min_i;
38      tf_objecto = hora_f*60 + min_f;
39
40      for k = 1:56
41
42          if (shade == 1) && (Hora.Hora.Hora(k) >= ti_objecto) && (Hora.
                Hora.Hora(k) <= tf_objecto)
43              fprintf('\n\nObjecto entre as horas %d:%d e %d:%d\n\n',
                    hora_i, min_i, hora_f, min_f)
44              Insolation(k)= Gdifuse.Gdifuse(k);
45
46          elseif (Hora.Hora.Hora(k) < ti_objecto) || (Hora.Hora.Hora(k) >
                tf_objecto) || (shade == 0)
47              Insolation(k)= Gtotal.Gtotal(k);
48          end
49
50                  constBlkName = sprintf('Modulo1/Insolation1');
51                  set_param(constBlkName, 'Value', 'Insolation(k)');
```

```
52
53                      SimOut = sim('Modulo1', 'ReturnWorkspaceOutputs', 'on'
                            );
54                      load('PV_M1.mat')
55
56                      P(k,i) = PMPP_sim.Data(end)
57
58
59      end
60
61      colorstring = [0 0 1 % blue
62      64/255 0 128/255 % purple
63      0 1 0  % light green
64      128/255 128/255 1 %light purple
65      0 1 1 %cyan
66      1 128/255 128/255 % pinkish
67      1 0 1  %red
68      .61 .51 .74   % azul sujo
69      0 64/255 0 % verde escuro
70      240/255 120/255 0 % orange
71      128/255 128/255 128/255 % gray
72      0 128/255 128/255 ]; %bordoux
73
74      figure(1)
75      hold all
76      x= plot(Hora.Hora.Hora/60,P(:,i), 'Color', colorstring(i,:));
77      plot(Hora.Hora.Hora/60,P(:,i),'*', 'Color', colorstring(i,:));
78      xlabel('Solar Time (h)')
79      ylabel('Produced Power (W)')
80      hold off
81
82      legend('January', '', 'February', '','March', '','April', '','May',
            '','June', '','July', '','August', '','September', '','October
            ', '','November', '','December', '')
83      title('Monthly Power Production Affected by Shade')
84
85          P_total = sum(sum(P))
86  end
87
88  Mes = sum(P,1)*0.25    % yearly power prodcution
89
90  E = Mes(1)*31 + Mes(2)*28 + Mes(3)*31 + Mes(4)*30 + Mes(5)*31 + Mes(6)
        *30 + Mes(7)*30 + Mes(8)*31 + Mes(9)*30 + Mes(10)*31 + Mes(9)*30 +
        Mes(12)*31
```

# HIT PHOTOVOLTAIC MODULE

# HIP-215NHE5, HIP-210NHE5, HIP-205NHE5

The SANYO HIT (**H**eterojunction with **I**ntrinsic **T**hin layer) solar cell is made of a thin mono crystalline silicon wafer surrounded by ultra-thin amorphous silicon layers. This product provides the industry's leading performance and value using state-of-the-art manufacturing techniques.


## Benefit in Terms of Performance

High efficiency cell

| Model | Cell Efficency | Module Efficency |
|---|---|---|
| HIP-215NHE5 | 19.3% | 17.2% |
| HIP-210NHE5 | 18.7% | 16.8% |
| HIP-205NHE5 | 18.2% | 16.4% |

The HIT cell and module have the world's highest level of conversion efficiency in mass production.

**High performance at high temperatures**
Even at high temperatures, the HIT solar cell can maintain higher efficiency than a conventional crystalline silicon solar cell.

**[Changes in generated power daytime]**

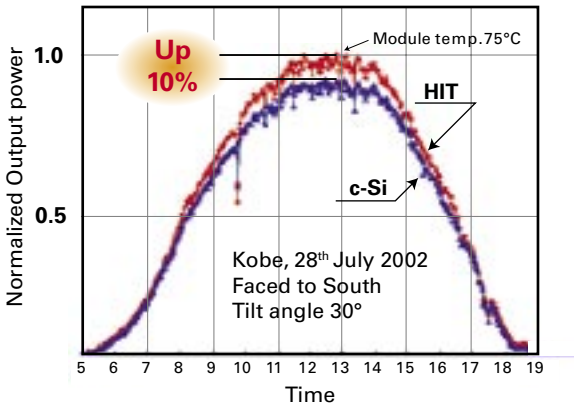


## HIT Solar Cell Structure

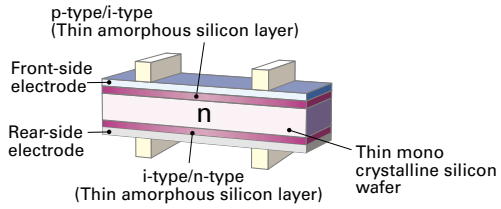


Development of HIT solar cell was supported in part by the New Energy and Industrial Technology Development Organization (NEDO).

## Environmental Friendly Solar Cell

**More Clean Energy**
HIT can generate more annual power output per unit area than other conventional crystalline silicon solar cells.

**Special Features**
SANYO HIT solar modules are 100% emission free, have no moving parts and produce no noise.
The dimensions of the HIT modules allow space-saving installation and achievement of maximum output power possible on given roof area.

## Benefit in Terms of Quality

**High quality in accordance with ISO 9001 and 14001 standards**
HIT solar cell and modules are subject to strict inspections and measurements to ensure compliance with electrical, mechanical and visual criteria.

# Electrical and Mechanical Characteristics

# HIP-215NHE5, HIP-210NHE5, HIP-205NHE5

| | | Models HIP-xxxNHE5 | | |
|---|---|---|---|---|
| **Electrical data** | | **215** | **210** | **205** |
| Maximum power (Pmax) | [W] | 215 | 210 | 205 |
| Max. power voltage (Vpm) | [V] | 42.0 | 41.3 | 40.7 |
| Max. power current (Ipm) | [A] | 5.13 | 5.09 | 5.05 |
| Open circuit voltage (Voc) | [V] | 51.6 | 50.9 | 50.3 |
| Short circuit current (Isc) | [A] | 5.61 | 5.57 | 5.54 |
| Warranted minimum power (Pmin) | [W] | 204.3 | 199.5 | 194.8 |
| Output power tolerance | [%] | +10/-5 | | |
| Maximum system voltage | [Vdc] | 1000 | | |
| Temperature coefficient of Pmax | [%/°C] | -0.3 | | |
| Voc | [V/°C] | -0.129 | -0.127 | -0.126 |
| Isc | [mA/°C] | 1.68 | 1.67 | 1.66 |

Note 1: Standard test conditions: Air mass 1.5, Irradiance = 1000W/m$^2$, Cell temperature = 25°C
Note 2: The values in the above table are nominal.

## Dimensions and weight

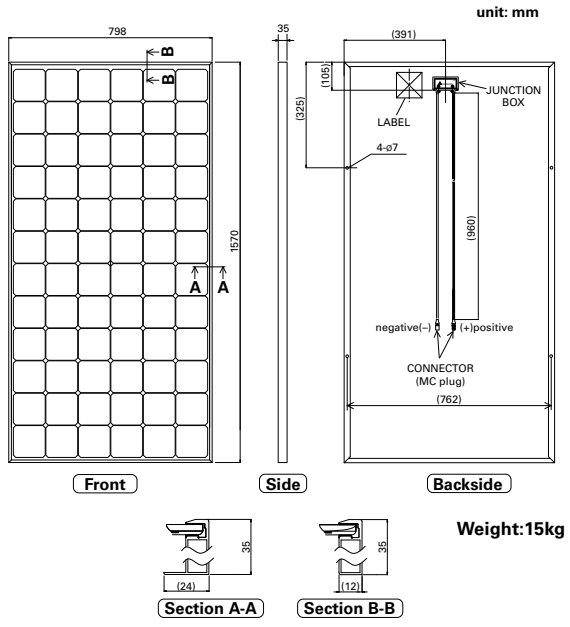


Reference data for model HIP-215NHE5

## Dependence on irradiance

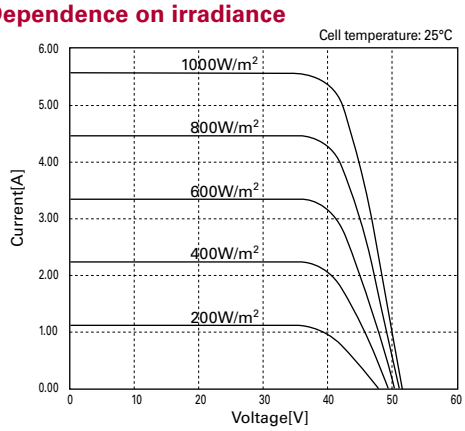


Reference data for model HIP-215NHE5

## Dependence on temperature

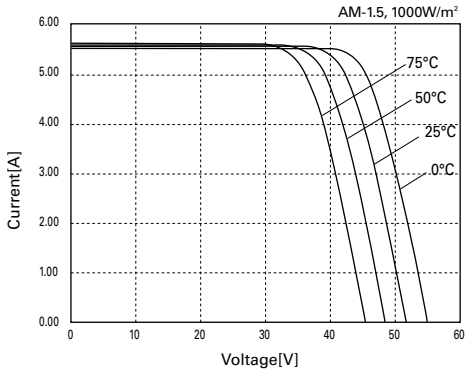


## Certificates

IEC 61215

Electrical Protection Class II

Please consult your local dealer for more information.

## Warranty

Power output: 20 years (80% of minimum output power (Pmin))
Product workmanship: 2 years
(Based on contract terms)

⚠ **CAUTION!** Please read the operating instructions carefully before using the products.

Due to our policy of continual improvement the products covered by this brochure may be changed without notice.


**SANYO Component Europe GmbH**
**Clean Energy Division**

Stahlgruberring 4
81829 Munich, Germany
TEL: +49-(0)89-46 00 95-0
FAX: +49-(0)89-46 00 95-170
http://www.sanyo-component.com
email: info.solar@sanyo-component.com

**SANYO Electric Co., Ltd.**
**Clean Energy Company**

http://www.sanyo.co.jp/clean/solar/hit_e/index_e.html
email: sola1011115@sanyo.co.jp


2006/06

# SM-255PC8 60 cell-series
## Polycrystalline PV Module

S-ENERGY

# 240 ~ 255 Watt

### New story creator, S-Energy

As the first company for PV industry in Korea, S-Energy has always been marking its name in every milestone of Korean PV history. Since 1992, we have been manufacturing PV modules and providing system integration service to our customers, and now we are proud to boast our world-wide recognition based on unbeatable quality standards and reliability. S-Energy's PC8 series is designed with our accumulated experience and cutting edge technology, and it will be the perfect choice for you which can be used in any environment and any installation conditions.

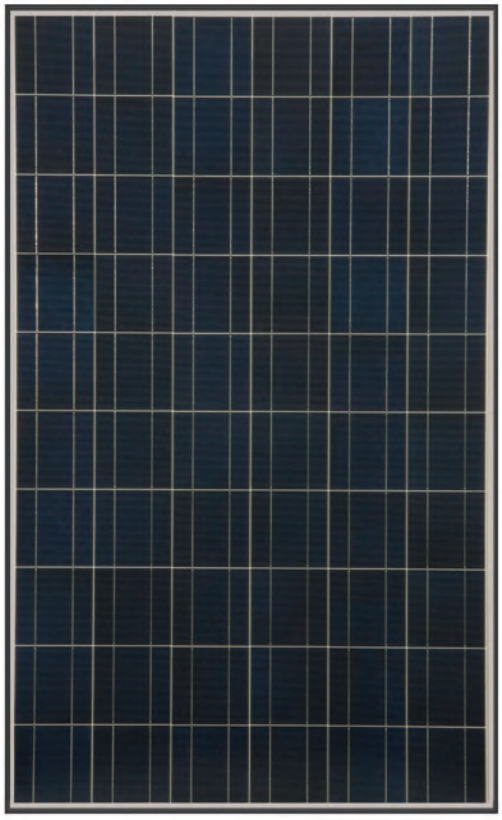

## Features


### Positive tolerance

0~+5W positive power sorting

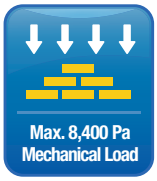


### Mechanical load

8,400 Pa (857kg/m$^2$)
(IEC Standards: 245kg/m$^2$)


### Hail impact test

30.7m/s speed ball
(IEC Standards: 23m/s)


### Ammonia corrosion resistance test

Applicable in agricultural
and stock breeding environment


### Salt mist corrosion test

Applicable in marine environment


### Linear warranty

Max annual power decline 0.7%

## Qualifications & Certifications

IEC 61215 & 61730, CE, UL1703, MCS, JET
ISO 9001, ISO 14001, OHSAS 18001, PV Cycle

### Mechanical Characteristics

| | |
|---|---|
| Solar cell | Polycrystalline 156mm x 156mm (6 inches) |
| No. of cells | 60 cells 6 x 10 matrix |
| Dimensions | 1665mm x 999mm x 50mm |
| Weight | 20 kg (44.09 lbs) |
| Front glass | 3.2mm High-transmittance low iron tempered glass |
| Frame | Anodized aluminum silver frame<br>Option : black color / rail type |
| Output cables | RHW-2, 12AWG (4mm$^2$) / Cable length:1000mm |
| Connectors | MC4 connectable |

### Warranty

| | |
|---|---|
| Product warranty | 10 years limited product warranty |
| Performance warranty | 1$^{st}$ year minimum peak power output : 97% |
| | 2$^{nd}$ year to 24$^{th}$ year peak power output<br>: max annual power decline 0.7% |
| | 25 years peak power output : 80.2% |

# SM-255PC8 60 cell-series

## Polycrystalline PV Module

### Electrical Characteristics

| STC (Irradiance 1000W/m², module temperature 25°C, AM=1.5) | SM-240PC8 | SM-245PC8 | SM-250PC8 | SM-255PC8 |
|---|---|---|---|---|
| Rated power ($P_{max}$) | 240W | 245W | 250W | 255W |
| Voltage at Pmax ($V_{mp}$) | 30.0V | 30.4V | 30.8V | 30.8V |
| Current at Pmax ($I_{mp}$) | 8.02A | 8.08A | 8.14A | 8.28A |
| Warranted minimum $P_{max}$ | 240W | 245W | 250W | 255W |
| Short-circuit current ($I_{sc}$) | 8.58A | 8.63A | 8.67A | 8.82A |
| Open-circuit voltage ($V_{oc}$) | 37.3V | 37.4V | 37.5V | 37.9V |
| Module efficiency | 14.42% | 14.72% | 15.03% | 15.33% |
| Operating module temperature | -40℃ to + 85℃ | | | |
| Maximum system voltage | 600VDC (UL) / 1000VDC (IEC) | | | |
| Maximum series fuse rating | 15A | | | |
| Maximum reverse current | 20.25A | | | |
| Power tolerance | 0 ~ +5 W | | | |

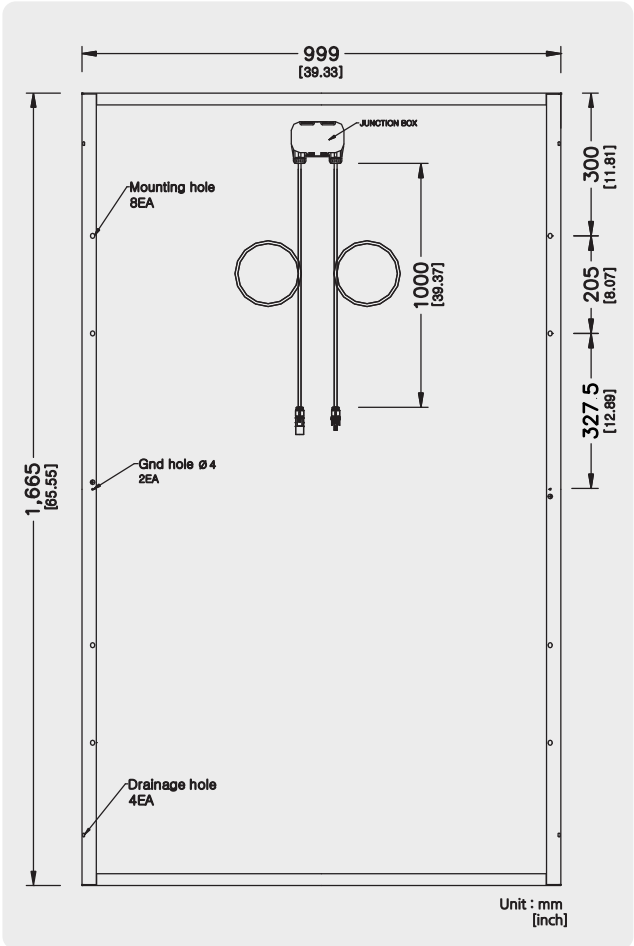


### Temperature Characteristics

| | |
|---|---|
| Temperature coefficient of $I_{sc}$ | 0.052%/℃ |
| Temperature coefficient of $V_{oc}$ | -0.312%/℃ |
| Temperature coefficient of power | -0.429%/℃ |
| NOCT (Air 20℃; Sun 0.8kW/m²; Wind 1m/s) | 45±3℃ |

### Packing Configuration

| Container | 40' H/C |
|---|---|
| Modules per pallet | 20 pcs |
| Pallets per container | 26 pallets |
| Modules per container | 520 pcs |

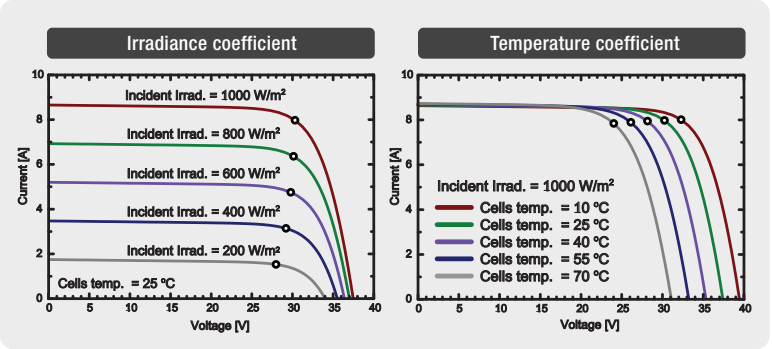


### Remarks :

Pmax measurement tolerance : ±3%
S-Energy uses triple A class simulator.
Specification subject to change without prior notice. S-Energy reserves the rights of final interpretation.
Document : SE-Datasheet_255PC8_60_Black_2013_V01


S-Energy Co., Ltd.
Address. 3rd Fl., Miraeasset Tower, 685, Sampyeong-dong, Bundang-gu, Seongnam-si, Gyeonggi-do 463-400, Republic of KOREA
Tel. +82-70-4339-7100 Fax. +82-70-4339-7199 E-mail. inquiry@s-energy.com

SENA International (dba S-Energy Europe)
Address. Ludwig-Erhard-Str. 30-34, 65760 Eschborn, Germany
Tel. +49-6196-9540-111~3 Fax. +49-6196-9985-778 E-mail. info.europe@s-energy.com

SEAI America, Inc.(dba S-Energy America)
Address. 18881 Von Karman Ave, Suite 760 Irvine, CA 92612, U.S.A
Tel. +1-949-281-7897 Fax. + 1-949-281-7893 E-mail. bizdev@s-energy.com